Brain Imaging and Behavior
DOI 10.1007/s11682-017-9770-3

REVIEW ARTICLE

Mouse models of neurodegenerative disease: preclinical imaging and neurovascular component

Sandra Albanese[1,2,3] · Adelaide Greco[1,2,3] · Luigi Auletta[4] · Marcello Mancini[2]

Abstract Neurodegenerative diseases represent great challenges for basic science and clinical medicine because of their prevalence, pathologies, lack of mechanism-based treatments, and impacts on individuals. Translational research might contribute to the study of neurodegenerative diseases. The mouse has become a key model for studying disease mechanisms that might recapitulate in part some aspects of the corresponding human diseases. Neurodegenerative disorders are very complicated and multifactorial. This has to be taken in account when testing drugs. Most of the drugs screening in mice are very difficult to be interpretated and often useless. Mouse models could be condiderated a 'pathway models', rather than as models for the whole complicated construct that makes a human disease. Non-invasive in vivo imaging in mice has gained increasing interest in preclinical research in the last years thanks to the availability of high-resolution single-photon emission computed tomography (SPECT), positron emission tomography (PET), high field Magnetic resonance, Optical Imaging scanners and of highly specific contrast agents. Behavioral test are useful tool to characterize different animal models of neurodegenerative pathology. Furthermore, many authors have observed vascular pathological features associated to the different neurodegenerative disorders. Aim of this review is to focus on the different existing animal models of neurodegenerative disorders, describe behavioral tests and preclinical imaging techniques used for diagnose and describe the vascular pathological features associated to these diseases.

Keywords Neurodegenerative diseases · Behavoiural test · Preclinical imaging · Mice · Neurovascular pathological features

Abbreviations

ALS	Amyotrophic lateral sclerosis
AD	Alzheimer's disease
PD	Parkinson's disease
HD	Huntington's disease
Iba1	Ionized calcium binding adapter molecule 1
PET	Positron emission tomography
CT	Computed tomography
MRI	Magnetic resonance imaging
BBB	Blood–brain barrier
SPECT	Single photon emission computed tomography
CBF	Cerebral blood flow
fMRI	Functional magnetic resonance imaging
CBV	Cerebral blood volume
BOLD fMRI	Blood oxygenation level dependent fMRI
MRA	Magnetic resonance angiography
TOF	Time-of-flight MRA
CE	Contrast enhanced
OI	Optical imaging
WR	Wobbler
pmn	Progressive motor neuronopathy
SOD	SuperOxide dismutase
VEGF	Vascular endothelial growth factor

✉ Adelaide Greco
adegreco@unina.it

[1] Dipartimento di Scienze Biomediche Avanzate, Università degli Studi di Napoli Federico II, Via Pansini 5, 80131 Napoli, Italy

[2] IBB, CNR, Via T. De Amicis 95, 80145 Napoli, Italy

[3] CEINGE Biotecnologie Avanzate, Scarl, Via G. Salvatore 486, 80145 Napoli, Italy

[4] IRCCS SDN, Via E. Gianturco 113, 80143 Napoli, Italy

Published online: 26 October 2017

VEGFR2	VEGF receptor 2
SN	*Substantia Nigra*
FMU	Flow metabolism uncoupling
ADC	Apparent diffusion coefficient
TSPO	18 kDa translocator protein
Aβ	Beta amyloid
APP	Amyloid precursor protein
MWM	Morris water maze
CAA	Celebral amyloid angiopathy
NIRF	Near infrared fluorescence
6-OHDA	6-hydroxydopamine
MPTP	1-methyl-4-phenyl-1,2,3,6-tetrahydropyridine
PQ	Paraquat
DAT	Dopamine transporter
SNpc	SN *pars compacta*
VMAT2	Vesicular monoamine transporter 2
MRE	Magnetic resonance elastography
GABA	Gamma amino butirric acid
^{18}F-DOPA	6-^{18}fluoro-L-3,4-dihydroxyphenylalanine
MSNs	Medium spiny neurons
QA	Quinolinic acid
3-NP	3-Nitropropionic acid
YAC	Yeast artificial chromosomes
NO	Nitric oxide
$O2^{-}$	Superoxide
mGluR	Metabotropic glutamate receptor
CEST	Chemical exchange saturation transfer
PDE10A	Phosphodiesterase 10A

Introduction

Neurodegenerative diseases are among the main causes of mental and physical disabilities in humans (for review, see Kreiner 2015). Although there is no substitute for studying real human biology, animal models provide opportunities for experimentation that are often not possible in human patients and represent a critical platform upon which translational efforts for treating human neurodegenerative diseases are built (Arora et al. 2011). Indeed, transgenic animals carrying human mutations provide a unique opportunity to understand the pathogenetic mechanisms underlying human disease (Luo et al. 2016; Southwell et al. 2017). The quality or utility of a model often depends on its validity, and the assessment of cognitive abilities is an important aspect of the validation and experimental use of models for neurocognitive disorders, as well as to evaluate cerebral microvascular aberrations that are recognized as playing a role in neurodegenerative disorders (Dorr et al. 2012; Miyazaki et al. 2012; Sarkar et al. 2014). The most used animal models of neurological disorders, with the related characteristic lesions, are summarized in Table 1. Exploring the relationship between neuromuscular degeneration and behavioral/motor tests is a useful and important step in identifying the clinical characteristics of mice models (Grant et al. 2014). The most commonly used behavioral tests, divided according to the different neurodegenerative mice models of disease, are summarized in Table 2.

Preclinical imaging allows the evaluation of neurodegenerative aspects and of vascular alterations at different time points, the study of neuropathological evolution even before the onset of the symptoms, and the evaluation of pre- and post-symptomatic therapies. Preclinical imaging approaches related to the different animal models of neurological diseases are summarized in Table 1.

Clinical brain computed tomography (CT) and magnetic resonance imaging (MRI) scans routinely demonstrate impaired regions of the blood–brain barrier (BBB) as focal areas of "contrast enhancement." Brain tumors and abscesses, sub-acute strokes, and active multiple sclerosis lesions are recognized by local contrast enhancement. In these instances, the signal-to-noise ratio for the contrast agent in the region of localized BBB impairment is very high (Bowman and Quinn 2008).

Functional imaging modalities, such as single photon emission computerized tomography (SPECT), positron emission tomography (PET) and MRI, are useful in assessing the early phases of disease (Fig. 1). Both PET and SPECT are sensitive methods for measuring in vivo neurochemistry; PET cameras has spatial resolution of about 1–2 mm, while SPECT can get a submillimeter spatial resolution using dedicated multipinhole geometry (for review, see Khalil et al. 2011).

The most suitable method to detect abnormalities in mouse models of cerebrovascular disorders is MRI because the reduction of the T2 relaxation time has been shown to be associated with reduced cerebral blood flow (CBF) (Helpern et al. 2004). Preclinical MRI is used to highlight the presence of plaques in the brain or areas of atrophy typical of neurodegenerative disorders (Wadghiri et al. 2012; Li et al. 2016; Santin et al. 2016). Functional MRI (fMRI) allows the non-invasive analysis of brain function in humans and animals, evaluating the cerebral blood volume (CBV), CBF and blood oxygenation level (blood oxygenation level dependent – BOLD – fMRI) and is also used to assess hemodynamic changes in response to therapies. Moreover, magnetic resonance angiography (MRA) comprises different techniques applied to evaluating vascular architecture, e.g., time-of-flight (TOF) MRA is used to study the major cerebral arteries (Fig. 2). Signal voids in TOF-MRA may indicate an absence of flow, low flow velocity, or turbulent flow. Contrast-enhanced (CE) MRA is used to analyze brain vessel architecture with fewer flow and motion artifacts than TOF-MRA (Mellin et al. 1994; Lin et al. 1997).

Table 1 Animal models of neurological disorders, with related genetic lesion, neurological lesion and vascular lesion

Pathology	Mouse model	Neurological lesion	Vascular lesions	Neuro-imaging	Vascular imaging	References
ALS	Wobbler	Neuroinflammation Spinal cord, brainstem, motor cortex, hippocampus		MRI - T2 weighted		(Bose et al. 1998; Tovar-y-Romo et al. 2009; Bigini et al. 2012; Moser et al. 2013; Thielsen et al. 2013)
	pmn	Caudo-cranial degeneration of motor axons Distal axonopathy with minor alterations of neuronal somas				(Kennel et al. 2000; Tovar-y-Romo et al. 2009)
	Wasted	Motor neurons in the spinal cord and neuromuscular junctions				(Woloschak et al. 1987; Newbery et al. 2005)
	SOD1	Increased astrogliosis, activation of microglia, and loss of spinal cord motor neurons	Decreased diameter and density of capillary vessels VEGF and VEGFR2 reduction in the spinal cord	MRI - T2 weighted ADC MRI Optical imaging	In vivo two-photon microscope imaging	(Bruijn et al. 2004; Zang and Cheema 2002; Lunn et al. 2009; Tovar-y-Romo et al. 2009; Knippenberg et al. 2010; Miyazaki et al. 2012; Evans et al. 2014; Patterson et al. 2014; Brownell et al. 2015; Oliván et al. 2015)
	hAPP	Amyloid pathology	Hypo-perfusion	MRI	3D MRI	(Hall and Roberson 2012; Hébert et al. 2013; Iascone et al. 2013; Klohs et al. 2014)
AD	PSAPP	Aβ plaque deposition	Micro-vascular abnormalities	[18F]-FDG PET		(Kumar-Singh et al. 2005; Bryan et al. 2009; Platt et al. 2011)
	5XFAD	Amyloid pathology Neuron loss	Micro-vascular abnormalities	[18F]-Florbetapir [11C]-methylaminophenyl- hydroxybenzothiazole [18F] -FDG PET/CT MRI T1 and T2 Relaxation Times		(Oakley et al. 2006; Teipel et al. 2011; Hall and Roberson 2012; Rojas et al. 2013; Spencer et al. 2013; Girard et al. 2014; Macdonald et al. 2014; Xu et al. 2014)
	3xTg-AD	White matter pathology Dendritic spine loss	Inflammation	MRI	Spatial frequency domain imaging Diffuse optical imaging Near infrared fluorescence	(Oddo et al. 2003a, b; Giménez-Llort et al. 2007; Klohs et al. 2014)
	TgCRND8	Amyloid pathology Cortical and hippocampal atrophy	CAA Increased tortuosity / decreased caliber of cortical penetrating arterioles	[64Cu] PET/CT MRI - T2 weighted	Two photon microscopy Laser Doppler fowmetry	(Romberg et al. 2013; Lai et al. 2015; Bellucci et al. 2006; McLean et al. 2013; Burgess et al. 2014)
	Tg2576	Increased cortical and hippocampal soluble Aβ levels	CAA	MRI - T2 weighted	MRA Multiphoton microscopy	(Deacon et al. 2009; Hall and Roberson 2012; Kara et al. 2012; Kishimoto et al. 2013; Cheng et al. 2015; Milner et al. 2014)

Table 1 (continued)

Pathology	Mouse model	Neurological lesion	Vascular lesions	Neuro-imaging	Vascular imaging	References
AD	APP 23	Amyloid pathology	Alterations of CBF alterations in cerebro-vascular angiogenesis	[11C]PIB [11C]PIB / T2*-weighted MRI	MRA Fluorescence imaging	(Beckmann et al. 2003; Thomason et al. 2013; Van Dam et al. 2003)
	APP dutch	β oligomer pathology	CAA	fMRI		(Teipel et al. 2011; Brautigam et al. 2012; Li et al. 2014)
	arcAß	Amyloid pathology and impairment of brain functional connectivity	CAA	fMRI MRI	CE-MRA CBV-MRI	(Knobloch et al. 2007; Thomason et al. 2013; Grandjean et al. 2014)
	Thy-APP751	Amyloid pathology	CAA			(Rockenstein et al. 2001; Klohs et al. 2014)
	Tg SWDI	Amyloid pathology	CAA	Two-photon imaging	Laser-Doppler flowmetry Near infrared fluorescence	(Van Vickle et al. 2008; Montgomery et al. 2016)
	PDAPP	Amyloid pathology	CAA	MRI T2-weighted [18F]-FDG PET	fMRI	(Elder et al. 2010; Klohs et al. 2014)
	APP/London	Amyloid pathology	CAA	MRI T2-weighted		(Dewachter et al. 2000; Van Dorpe et al. 2000)
	TgAPParc	Amyloid pathology	CAA			(George et al. 2014; Klohs et al. 2014)
AD	APP/PS1	Amyloid pathology	CAA	[18F]-7B PET/CT [11C]-C-PIB PET T2-relaxation time-contrast MRI [11C]PK11195 PET [18F]-FDG-PET	TOF-MRA CE-MRA	(Webster et al. 2013; Klohs et al. 2014)
PD	6-OHDA	Lesion to the nigro-striatal pathway		[18F]-FDG [18F]-FECT [18F]-FP-CIT [11C]methylphenidate PET/CT [123I]-FP-CIT SPECT		(Andringa et al. 2005; Boix et al. 2015)
	MPTP	Lesion to *substantia nigra pars compacta*	Microvessels Vessel density reduced	[123I]-FP-CIT SPECT [18F]- DTBZ PET/CT [1H]-[13C]-NMR spectroscopy Fluorescence imaging		(Andringa et al. 2005; Meredith et al. 2008; Luchtman et al. 2009; Taylor et al. 2010; Blandini and Armentero 2012; Toomey et al. 2012; Bagga et al. 2013; Lee et al. 2013; Sarkar et al. 2014)
	Parkin deficient	Dopamine transporter and vesicular monoamine transporter 2 reduced				(Rial et al. 2014)
	DJ-1	Alteration nigro-striatal dopaminergic function				(Chen et al. 2005)
	α-synucleine model	Synucleinopathies				(Fleming et al. 2004)

Table 1 (continued)

Pathology	Mouse model	Neurological lesion	Vascular lesions	Neuro-imaging	Vascular imaging	References
PD	Rotenone	Reduced dopamine levels in the *striatum* Massive loss of dopamine neurons No aggregate formation		MRI MR spectroscopy [^{18}F]-DOPA PET		(Sharma et al. 2006; Moussa et al. 2008; Terzioglu and Galter 2008; Liu et al. 2015)
	Paraquat	Reduced dopamine levels in the *striatum* Loss of dopamine neurons in the *substantia nigra* No aggregate formation				(Brooks et al. 1999; Fernagut et al. 2007; Terzioglu and Galter 2008; Taylor et al. 2009; Litteljohn et al. 2011)
HD	Quinolinic acid	Striatal neurodegeneration		[^{18}F]-FDG PET		(Ramaswamy et al. 2007)
	3-Nitropropionic acid	Degeneration of GABAergic medium spiny neurons in the *striatum*		MRI		(Beal et al. 1993; Fernagut et al. 2002; Lee and Chang 2004; Kudo et al. 2014)
	R6/2	Enlargement of the lateral ventricles Shrinkage of the *striatum* and cortex	Increased striatal blood vessel density Abnormalities in striatal vascular network	MRI - rapid acquisition with relaxation enhancement		(Ramaswamy et al. 2007; Sawiak et al. 2009; Drouin-Ouellet et al. 2015)
HD	YAC 128	Atrophy *striatum, globus pallidus*, cortex	Increased vascualr density and lenght in *striatum*	MRI - T_2 weighted		(Van Raamsdonk et al. 2005; Ramaswamy et al. 2007; Lerch et al. 2008; Franciosi et al. 2012)
	N171-82Q	Brain atrophy in the *striatum* and neocortex		MRI - T_2 weighted		(Ramaswamy et al. 2007; Cheng et al. 2011)
	CAG140	Loss in *striatal* volume Striatal neuronal loss				(Hickey et al. 2012)
	CAG150	Decrease in *striatal* dopamine receptors Diminished striatal neuron number				(Ramaswamy et al. 2007; Heng et al. 2008)
MS	EAE	Demyelination, axonal loss and gliosis	Inflammation, vessel denity increased	MRI -T1- and T2-weighted Two photon microscopy	MPO-Gd MRI SWI- MRI T2* MRI PET-[^{18}F]FDG PET-[^{18}F]PBR111 Near infrared fluorescence	(Miller et al. 2007; Boroujerdi et al. 2013)
	TMEV- induced	Demyelination	Inflammation	MRI -T1- and T2-weighted	MRI - T2 weighted	(Oleszak et al. 2004; Procaccini et al. 2015)
	Toxin-induced demyelination	Demyelination		T2-weighted MRI MTR PET- [^{11}C]CIC PET- [^{11}C]MeDAS		(Procaccini et al. 2015; Dehghan et al. 2016)

Table 2 Behavioral tests of most common alterated function in animal models of neurodegenerative diseases

Behavioral test	Neuro-sensory-motor-function	Models	References
Grid walking	Voluntary motor control Coordination and accurate paw placement	Wobbler MPTP	(Starkey et al. 2005; Meredith et al. 2008; Taylor et al. 2010; Moser et al. 2013)
Grip	Muscle strength Motor performance	*pmn* TgCRND8	(Kennel et al. 2000; Bellucci et al. 2006)
Rotarod Stride length	Motor coordination Motor function	Wasted SOD1 Thy1-APP751 TgCRND8 APP 23 arcAß MPTP Parkin deficient DJ-1 Rotenone 3-Nitropropionic acid YAC 128 N171-82Q CAG150 EAE TMEV- induced Toxin-induced demyelination	(Fernagut et al. 2002; Van Dam et al. 2003; Chen et al. 2005; Newbery et al. 2005; Van Raamsdonk et al. 2005; Bellucci et al. 2006; Liebetanz and Merkler 2006; Wang and Qin 2006; Knobloch et al. 2007; Ramaswamy et al. 2007; Heng et al. 2008; Lynch et al. 2008; Gorton et al. 2010; Knippenberg et al. 2010; Taylor et al. 2010; Cheng et al. 2011; Havas et al. 2012; Franciosi et al. 2012; Miyazaki et al. 2012; Acharjee et al. 2013; Lee et al. 2013; Takemiya and Takeuchi 2013; Evans et al. 2014; Rial et al. 2014; Abakumova et al. 2015; Liu et al. 2015; Oliván et al. 2015; Stover et al. 2015; Gilli et al. 2016; Paz Soldán et al. 2015)
Hanging wire	Muscular strength of the limbs	SOD1 CAG150	(Heng et al. 2007; Günther et al. 2012; Oliván et al. 2015)
Morris water maze	Spatial learning and memory	hAPP Thy1-APP751 Tg-SWDI APP/London PSAPP 3xTg-AD APP 23 arcAß APP/PS1 Paraquat Quinolinic acid R6/2 EAE	(D'Hooge and De Deyn 2001; Van Dam et al. 2003; Kumar-Singh et al. 2005; Giménez-Llort et al. 2007; Knobloch et al. 2007; Ramaswamy et al. 2007; Busche et al. 2008; Bryan et al. 2009; Philipson et al. 2010; Havas et al. 2012; Litteljohn et al. 2011; Gu et al. 2012; Hall and Roberson 2012; Acharjee et al. 2013; Iascone et al. 2013; Passos et al. 2013; Thomason et al. 2013; Li et al. 2014)
Y maze T maze Novel object recognition test	Reference and working memory	PSAPP PDAPP APP Dutch 5XFAD TgCRND8 Tg-SWDI arcAß Parkin deficient Quinolinic acid R6/2 YAC 128	(Van Raamsdonk et al. 2005; Oakley et al. 2006; Knobloch et al. 2007; Ramaswamy et al. 2007; Bryan et al. 2009, Hall and Roberson 2012; Passos et al. 2013; Romberg et al. 2013; Webster et al. 2013; Beauquis et al. 2014; Burgess et al. 2014; Girard et al. 2014; Rial et al. 2014; Knight et al. 2015)
Olfactory tubing maze	Learning and memory	5XFAD	(Roman et al. 2002; Girard et al. 2014)
Barnes maze	Spatial learning and memory	TgAPParc 5XFAD	(Rönnbäck et al. 2011; Xu et al. 2014)
Righting reflex	Defects of neuromuscular junction Synapse maturation and vestibulo-spinal input	Wobbler	(Bose et al. 1998; Moser et al. 2013)
Hole board	Exploratory activity Neuromuscular functions	TgCRND8 Thy1-APP751	(Bellucci et al. 2006; Havas et al. 2012)

Table 2 (continued)

Behavioral test	Neuro-sensory-motor-function	Models	References
Radial arm water maze	Reference and working memory	Quinolinic acid N171-82Q	(Ramaswamy et al. 2007; Webster et al. 2013)
Pole	Coordination	MPTP Parkin deficient α-synuclein Rotenone Paraquat 3-Nitropropionic acid	(Fernagut et al. 2002, 2007; Fleming et al. 2004; Luchtman et al. 2009; Taylor et al. 2009, 2010; Rekha and Selvakumar 2014; Rial et al. 2014; Liu et al. 2015)
Open field Bar test	Locomotor and spontaneous activity	R6/2 YAC 128 CAG140 PDAPP TgAPParc 3xTg-AD Tg2576 APP 23 arcAß MPTP DJ-1 α-synuclein Rotenone Paraquat 3-Nitropropionic acid Thy1-APP751	(Fernagut et al. 2002; Van Dam et al. 2003; Fleming et al. 2004; Chen et al. 2005; Van Raamsdonk et al. 2005; Giménez-Llort et al. 2007; Knobloch et al. 2007; Ramaswamy et al. 2007; Deacon et al. 2009; Luchtman et al. 2009; Taylor et al. 2009, 2010; Havas et al. 2012; Litteljohn et al. 2011; Rönnbäck et al. 2011; Hickey et al. 2012; Kishimoto et al. 2013; Lee et al. 2013; Beauquis et al. 2014; Kudo et al. 2014; Rekha and Selvakumar 2014; Liu et al. 2015)
Footprint analysis	Gait abnormalities	SOD1 CAG150 EAE	(Buddeberg et al. 2004; Heng et al. 2008; Knippenberg et al. 2010; Oliván et al. 2015)
Climbing	Coordination	CAG150	(Hickey et al. 2012; Rattray et al. 2012)
Wheel running	Motor deficits	CAG150 Toxin-induced demyelination	(Liebetanz and Merkler 2006, Hickey et al. 2012; Switonski et al. 2012)
Tail suspension	Depressive behavior	CAG150 Parkin deficient	(Heng et al. 2007; Iascone et al. 2013; Rial et al. 2014)
Balance beam	Motor coordination and balance	CAG150	(Heng et al. 2008; Luong et al. 2011)
Elevated plus maze Light–dark exploration Marble burying	Anxiety	3xTg-AD APP Dutch MPTP Parkin deficient Toxin-induced demyelination	(Giménez-Llort et al. 2007; Gorton et al. 2010; Taylor et al. 2010; Li et al. 2014; Rial et al. 2014; Abakumova et al. 2015; Knight et al. 2015)
Forced swimming	Depressive behavior	Parkin deficient	(Rial et al. 2014)
Grasping strength	Motor function	Parkin deficient	(Rial et al. 2014)
Adhesive tape removal von Frey filament	Motor response to sensory stimuli	DJ-1 α-synuclein TMEV- induced	(Fleming et al. 2004; Chen et al. 2005; Lynch et al. 2008; Taylor et al. 2010)
Challenging beam traversal	Motor performance and coordination	Paraquat α-synuclein	(Brooks et al. 1999; Fleming et al. 2004; Fernagut et al. 2007; Taylor et al. 2010)
Inverted grid	Motor coordination	α-synuclein	(Fleming et al. 2004; Taylor et al. 2010)
Bin cotton use	Motor performance and coordination	α-synuclein	(Fleming et al. 2004)
Solid gastric emptying Stool collection	Gastrointestial disfunction	Rotenone	(Taylor et al. 2010; Liu et al. 2015)
Water & food finding	Social memory	Tg2576	(Deacon et al. 2009; Kishimoto et al. 2013)
Buried pellet Olfactory discrimination	Olfactory function	MPTP α-synuclein Parkin deficient	(Taylor et al. 2010; Rial et al. 2014)

Table 2 (continued)

Behavioral test	Neuro-sensory-motor-function	Models	References
Cylinder Stepping	Forelimb akinesia	6-OHDA	(Andringa et al. 2005; Boix et al. 2015)
Corridor Rotation test	Sensory-motor function	6-OHDA	(Boix et al. 2015)
Touch-screen automated tests battery	Visual, memory, attention, cognitive	TgCRND8	(Romberg et al. 2013)

Another approach to studying neurodegenerative disorders is in vivo optical imaging (OI) using transgenic mouse models, which express a reporter gene, e.g., green fluorescent protein, under a promoter that has the ability to be activated, which should represent a disease biomarker. This imaging approach has the advantages that it avoids radiation and radiolabeled tracers/agents, does not require complex surgical techniques and is cheaper than other imaging techniques (for review, see Patterson et al. 2014).

This review summarizes the most common mouse models of neurodegenerative diseases, describing the neurovascular component involved in these pathologies and presenting the diagnosis and grading methods adopted to evaluate these animal models accurately, such as behavioral tests and in vivo imaging techniques.

Mouse models of amyotrophic lateral sclerosis

ALS is a fatal neurodegenerative disease characterized by the selective and progressive death of both upper and lower motor neurons, leading to progressive paralysis (for review, see Tovar-y-Romo et al. 2009). In mouse models of ALS, specific motor tasks are indispensable for the detection of disease onset and early progression (Knippenberg et al. 2010). Although body weight has been indicated as a useful additional parameter, in particular to monitor disease progression during later stages (Knippenberg et al. 2010),

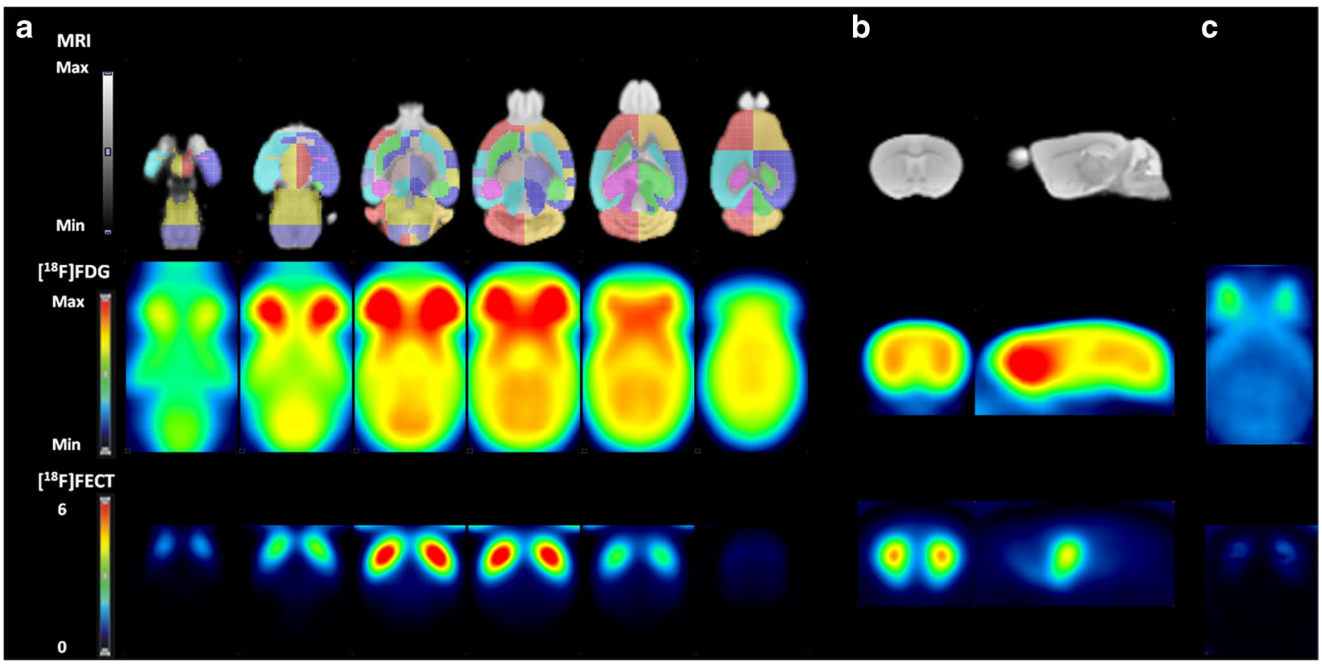

Fig. 1 [^{18}F]FDG and [^{18}F]FECT probabilistic atlases. **a** Series of axial sections (ventral to dorsal, slice interval 1.2 mm, radiological orientated) through the mouse brain MRM atlas (top row) and co-registered [^{18}F]FDG (middle row) and [^{18}F]FECT (bottom row) small-animal PET template. **b** One representative coronal (radiological orientation) and sagittal slice through caudate-putamen. **c** Horizontal section through variance map at level $z = 22.8$ (relative to bregma). The mouse brain MRM atlas shows the pre-defined VOI map overlayed. Color bars indicate relative intensities for [^{18}F]FDG; binding potential for [^{18}F]FECT. (Casteels et al. 2013)

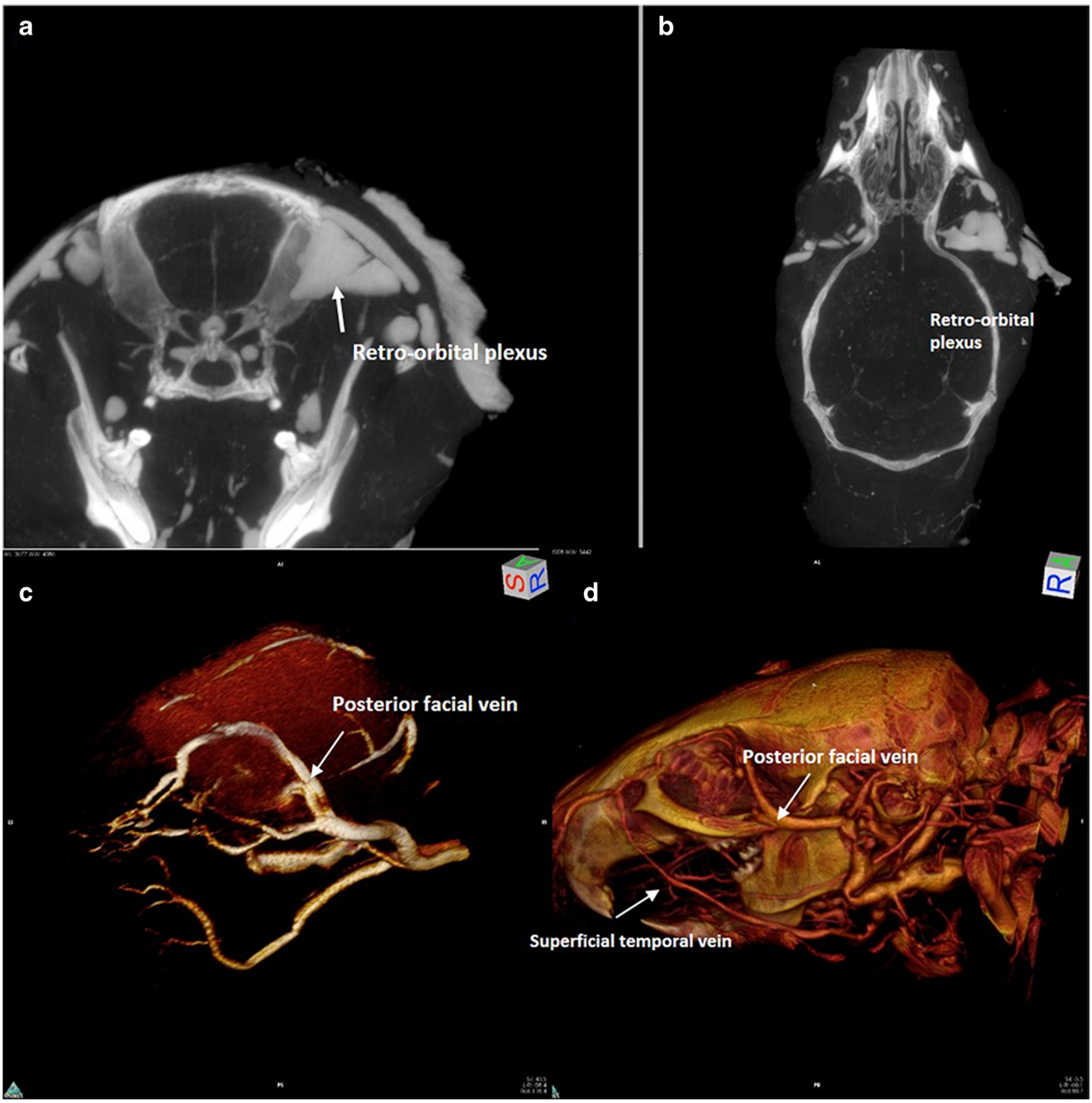

Fig. 2 Magnetic resonance angiography with 3D rendering acquisition of the orbital region. Upper row: (**a**) axial and (**b**) coronal computed tomography slice. Lower row: 3D rendering of magnetic resonance angiography acquisition of the left orbital region ((**c**) antero-lateral view). 3D rendering of silicon-enhanced computed tomography angiography ((**d**) lateral view). (**a**), (**b**), The large retro-orbital venous plexus (white arrow) is clearly visible as well its drainage into the posterior facial vein ((**c**), (**d**) white arrow). (**d**) The superficial temporal vein is also shown in (Mancini et al. 2015)

weight loss is a symptom that cannot be attributed exclusively to a neurodegenerative disease.

The oldest known model that shows similarities with human ALS is the wobbler (WR) mouse, in which neurons of the spinal cord, brainstem and motor cortex are affected (Moser et al. 2013). The severity of motor neuron defects is assessed by evaluating the mouse performance in the grid walking and righting reflex tests (Bose et al. 1998), indeed, WR mice develop severe problems in grabbing and climbing the grid due to their progressive muscle weakness, and rapidly lose the righting reflex (Bose et al. 1998; Ott et al. 2015).

Another ALS model is the mouse progressive motor neuronopathy (*pmn*) mutant, developing from a spontaneous autosomal recessive mutation that maps to mouse chromosome 13 (Schmalbruch et al. 1991). Clinical signs in *pmn* homozygotes are identifiable 2–3 weeks after birth, including profound paralysis of the hind limbs and atrophy of the pelvic girdle, as displayed by grip test, and almost all distal axons disappear 4–5 weeks after birth (Kennel et al. 2000).

Mice bearing the autosomal recessive gene "wasted" (*wst*/*wst*), mimic the sporadic ALS form. The wst/wst mouse develops low or absent secretory immune responses, abnormal DNA repair mechanisms, and uncoordinated body movements (Woloschak et al. 1987). The *wst*/*wst* mice is characterized by prominent vascular degeneration of neurons within the anterior horns of the spinal cord and the motor nuclei of the brain stem, and neuropathologic studies showed deficit with rotarod test (Newbery et al. 2005).

Both familial ALS and 5% of apparently sporadic ALS seem to be associated with the gene encoding the enzyme Cu^{2+}/Zn^{2+} superoxide dismutase (SOD1). Indeed, the most similar mouse model is $SOD1^{G93A}$, which develops a progressive paralysis starting from the hind limbs via denervation of the neuromuscular junctions. In contrast to the variable pattern of weakness recorded in humans, in the SOD1 mutant mice, weakness typically starts in the hind limbs between 3 and 12 months of age, depending on both the mutation ($SOD1^{G85R}$, $SOD1^{G37R}$, and $SOD1^{G93A}$) and the level to which it is expressed. Hindlimb weakness coincides with increased astrogliosis, the activation of microglia, and the loss of spinal cord motor neurons. The pathology in these mice closely mimics many aspects of the human disease (Evans et al. 2014). In humans, ALS predominantly affects males, probably due to differences between men and women in the nervous system or in its response mechanisms to environmental stimuli. Gender differences in the motor impairment in $SOD1^{G93A}$ mice have recently been demonstrated through behavioral tests; in particular, female mice endured the disease progression better (Choi et al. 2008). However, the gender effect on survival is an open debate (Kirkinezos et al. 2003; Choi et al. 2008; Knippenberg et al. 2010). The clinical phenotype, detection and monitoring of motor symptoms in $SOD1^{G93A}$ mice have been perfectly characterized by the conventional behavioral tests: rotarod, footprint analysis and hanging-wire, which represent the most accurate tests to monitor the disease progression in this transgenic model (Knippenberg et al. 2010; Oliván et al. 2015). Furthermore, to classify disease stages, a scoring system was developed by Vercelli et al. (2008). The $SOD1^{G93A\ G1H}$ transgenic mouse is a widely used animal model of familial human ALS (Zang et al. 2004). In this model, the primary pathology is linked to the degeneration of lower motor neurons (LMNs) in the lumbar spinal cord and brainstem (Lowry et al. 2001).

Evidence of vascular changes in ALS

Vascular endothelial growth factor (VEGF) and the expression of the VEGF receptor 2 (VEGFR2) are essential in angiogenesis during embryonic development as well as in pathological conditions such as stroke, acute ischemia, ischemic neuropathy and many cancer histotypes (Oosthuyse et al. 2001; Zhao and Adjei 2015). The potential role of VEGF in ALS has been illustrated in several studies utilizing different variants of SOD1 mutation models, e.g., cell culture models and knock-in and knock-out mouse models (for review, see Keifer Jr et al. 2014). The majority of these studies have focused on the VEGF-A and VEGF-B isoforms, considering the larger literature establishing their neurotrophic role (Oosthuyse et al. 2001; Poesen et al. 2008). The first study to evaluate the therapeutic potential of VEGF for the treatment of ALS was conducted by Azzouz et al. (2004), who showed that a single injection of a VEGF-expressing lentiviral vector into various muscles slowed the progression of ALS in $SOD1^{G93A}$ mice, even when treatment was initiated at the onset of paralysis. The VEGF treatment increased the life expectancy of ALS mice by 30% without causing toxic side effects, and the intraperitoneal injection of VEGF has been shown to delay disease progression and increase survival in $SOD1^{G93A}$ transgenic mice (Azzouz et al. 2004). Mice homozygous for the deletion of VEGF suffer severe muscle weakness in adulthood due to degeneration of the lower motor neurons innervating skeletal muscle fibers, reminiscent of the clinical symptoms and neuropathological signs of ALS. In these mice, the neuropathy may be due to chronic ischemia resulting from neurovascular perfusion deficits but may also be exacerbated by insufficient VEGF-dependent neuroprotection, and thus the abnormal expression of VEGF may constitute a previously unknown risk factor for motor neuron degeneration (Oosthuyse et al. 2001). Within the $SOD1^{G93A}$ mouse spinal cord, a reduction in VEGF and VEGFR2 expression, with loss of large motor neurons, has been observed (Lunn et al. 2009). Similar reductions are evident in human patients with ALS (Brockington et al. 2006). Another confirmation of the role of VEGF in the pathogenesis of ALS is given by exposure to low doses of environmental lead (Pb) (Barbeito et al. 2016). Although Pb is a well-known risk factor for ALS, sub-toxic Pb concentrations up-regulate VEGF expression (Barbeito et al. 2016). Chronic exposure to sub-toxic Pb concentration did not affect disease onset but significantly increased life expectancy (by 12 days) in $SOD1^{G93A}$ mice. This result suggests that Pb might be involved in a novel pathway that can reduce neuroinflammation and slow neurodegeneration in ALS.

Damage to the vasculature is one of the earliest pathological events in the toxic cascade initiated by both dismutase-active and -inactive SOD1 mutants, and such changes at the

vascular level probably make an important contribution to the degeneration of the large motor neurons in models of familial ALS (Zhong et al. 2008). Targeted deletion of the hypoxia-response element in the VEGF gene resulted in mice with a normal baseline expression of VEGF but a pronounced deficit in the ability to induce VEGF up-regulation in response to hypoxia. Motor neuron deficits first appear in mice between 5 and 7 months of age and then gradually progress. All the classic features of ALS are observed: accumulation of neurofilaments in spinal and brainstem motor neurons, degeneration of motor axons, and the characteristic denervation-induced muscle atrophy (Lunn et al. 2009).

Among the vascular-related pathophysiological mechanisms underlying ALS, flow metabolism uncoupling (FMU), which is characterized by an initial blood flow reduction and local glucose utilization increase in the spinal cord of ALS mice, has recently been considered to precede the sequential changes of the disease (Miyazaki et al. 2012).

FMU has been shown to be strongly correlated to decreasing capillary diameter and density, as well as to neurovascular unit disruption within the anatomical regions affected by ALS. Although the reason for the presence of FMU in SOD1 mice is unclear, it might be profoundly involved in the overall disease process, as suggested by the aforementioned correlations, and should be explored as a potential target for therapeutic intervention (Miyazaki et al. 2012).

Preclinical imaging in ALS

A recent clinical study revealed neuronal loss and reduced axonal density in the primary motor cortex in ALS patients through MRI analysis (Meadowcroft et al. 2014). MRI is a valid tool even in characterizing animal models of ALS, as it has been demonstrated to allow evaluation of the pre-symptomatic period (Evans et al. 2014). Neuronal degeneration of the brainstem motor nuclei was visualized in T2-weighted MRI acquisitions: hyperintense areas visualized regions of cerebral neurodegeneration, which were found primarily in the brainstem (Zang et al. 2004). Stronger hyperintense regions were discovered primarily in three cranial nerve nuclei: the *nucleus ambiguus*, the facial nerve nucleus and the motor trigeminal nucleus. Such hyperintense areas in the brainstem indicate areas of neurodegeneration. On the other hand, hypointensities, indicative of diffuse atrophy, were detected in the brain and cerebellum (Zang et al. 2004). Moreover, the T2 MRI sequence showed a reduction in the number of neurons in the *substantia nigra* (SN) in SOD1. The MRI results allowed the prediction of deficits in vocalization, mastication and swallowing in the SOD1$^{G93A\ G1H}$ transgenic mice, in which the clinical evaluation of such symptoms is not easy. These symptoms occur similarly in bulbar onset patients, who show voice and/or swallowing difficulties in the first phase of the disease; hence, preclinical MRI has proven useful in detecting thie analogy between human and mice (Zang et al. 2004).

Although the signal strength was correlated with disease progression, T2-weighted MRI does not provide an absolute quantification, and it is useless for studying damage to the spinal cord. A useful tool to complement the T2 data is the apparent diffusion coefficient (ADC), which provides information regarding brain tissue integrity based on measuring water mobility (Niessen et al. 2006). In contrast to the T2 measurements, the ADC values are generally influenced by the animals' age, leading to increases in *nucleus V, nucleus VII*, and *nucleus XII*, in the motor cortex, and in the thalamus of SOD1^{G93A} compared to wild-type mice (Niessen et al. 2006). The combination of ADC and T2 mapping enable the longitudinal non-invasive evaluation of disease progression in the SOD1^{G93A}. The MRI signal alterations appear in different critical brain regions, e.g., the brainstem and spinal cord, early in the course of the disease, when the animals are still clinically unremarkable (Niessen et al. 2006).

To date, preclinical MRI allowed only the identification of structural/anatomical damages, and no vascular alterations have been documented yet. Ex vivo transmission electron microscopy, immunihistochemical and immunofluorescence studies of murine models of ALS have highlighted the presence of various alterations in the neurovascular unit in the spinal chord (Zhong et al. 2008; Miyazaki et al. 2011). Anyway, the T1 CE-MRI of SOD1^{G93A} mice did not show any increase in vascular permeability, as confirmed by immunohistochemistry, in any of the cerebral regions studied (Evans et al. 2014).

In addition to its diagnostic usefulness, MRI was used in tracking stem cells injected into mice with ALS. The administration of stem cells is a promising novel approach for the treatment of neurodegenerative diseases, seeking to replace lost or dysfunctional neurons. The intraspinal injection of adult stem cells from human umbilical cord blood into the spinal cord prolongs survival, delays the deterioration of motor function and prevents motor neuron loss and astrocytosis in SOD1 transgenic mice (Knippenberg et al. 2012). Thus, clinical trials to confirm the same effects in human beings would be desirable.

In vivo two-photon microscope imaging of spinal capillary vessels showed decreases in both the diameter and density of capillary vessels, which resulted in a progressive decrease in flow volume in SOD1 mice (Miyazaki et al. 2012). Nonetheless, the impact of abnormal vascularity as well as neuroinflammatory processes on axonal degeneration in the peripheral nervous system remains elusive.

Time-lapse 2-photon laser-scanning microscopy is a useful imaging approach, which allows analysis of the role of macrophage-related neuroinflammation and reactive microglia. The increase in microglia presence, the ameboid transformation, the loss of tissue surveillance and the decrease in

the injury-directed movement process, all of which prominently occur during the human clinical course, emphasize the contribution of microglia to disease progression in SOD1 animals in the late phase of the disease (Dibaj et al. 2011).

In vivo OI in bi-genic mice ($SOD1^{G93A}$:GFAP-*luciferase*) showed several successive stages of repeated increases in the expression of GFAP. The pre-symptomatic stage is characterized by an increase in GFAP-*luciferase*, with prominent signaling emitted by the lumbar spinal cord projections and peripheral neurons. The clinical onset is characterized by distinct behavioral deficits and hind-limb paralysis. The fluorescence peak signal at 113 days corresponded precisely to the onset of hind-limb paralysis. These results suggest that populations of non-neuronal cells, perhaps glial cells, can affect the viability of motor neurons (Keller et al. 2009). Moreover, an increased signal contribution from the corticospinal tract and upper motor neurons was shown by OI, with the approach of the end stages of the disease. Microtubule associated protein 1 light chain 3 is a marker of autophagy, which, fused to green fluorescent protein, might be used to study in vivo autophagy in $SOD1^{G93A}$ mice (Wei 2014).

The PET/CT approach is useful in evaluating the pathological and inflammatory processes in ALS mice, including the modulation of glutamatergic function (Brownell et al. 2015). Imaging of the inflammatory response was performed using translocator protein 18 kDa (TSPO) ligand [^{11}C]-PBR28, an imaging ligand for the translocator protein, which is a biomarker for inflammation and activated microglia: the most significant enhancement was detected in the brain and spinal cord, during progression of the disease in $SOD1^{G93A}$ (Brownell et al. 2015). Recently, an increased [^{18}F]-DPA-714 uptake in cerebellum and brainstem was demonstrated in vivo, proving the feasibility and sensitivity of [^{18}F]-DPA-714 for the study of 18 kDa translocator protein (TSPO) expression and of microglial activation in the brain and spinal cord of transgenic $SOD1^{G93A}$ with PET/CT, probably linked to the ionized calcium binding adapter molecule 1 (Iba1) microglial overexpression (Gargiulo et al. 2016). The brainstem is known to be a site of degeneration and gliosis in ALS patients, consistent with the increased TSPO expression in the brainstem nuclei, as shown by immunostaining (Gargiulo et al. 2016). The TSPO, also known as peripheral benzodiazepine receptor, is a protein of the outer mitochondrial membrane associated to nucleoside transport and steroids and neurosteroids synthesis (for review, see Jacobs et al. 2012). In the normal brain, the TSPO is globally low expressed, and its up-regulation is a biomarker of activated microglia (Diorio et al. 1991, for review, see; Jacobs et al. 2012). Its diagnostic importance in neurological diseases is linked to the possibility to bind it specifically with several radioligands, both for PET and SPECT imaging, i.e. [^{11}C]-DAA1106, [^{18}F]-FE-DAA1106, [^{11}C]-DPA-713, [^{18}F]-DPA-714, [^{18}F]-PBR28, [^{18}F]-PBR111, [^{11}C]-SSR18075, [^{11}C]-CLINME, [^{123}I]-CLINDE, and [^{11}C]-vinpocetine (Diorio et al. 1991).

Mouse models of Alzheimer's disease

The AD is a neurodegenerative disease accounting for 50–75% of dementia cases. As of 2015, approximately 44 million people worldwide were estimated to have AD or related dementia (for review, see Van Cauwenberghe et al. 2015). The disease is clinically characterized by progressive deterioration of the memory and cognitive functions, leading to loss of autonomy and ultimately requiring full-time medical care (Cheng et al. 2015). To date, there are no known viable treatments for this condition, but an appropriate lifestyle can help to prevent this disease. To understand the biological mechanisms underlying this disease, several mouse models have been developed, although no existing model exhibits all the features of AD.

The first and the most widely used mouse models of AD are based on the transgenic expression of human amyloid precursor protein (hAPP). In general, these strains develop robust amyloid pathology, show memory deficits, and exhibit depressive behavior at the tail suspension test (Iascone et al. 2013). However, the mice also exhibit deficits in spatial memory, as observed in the Morris water maze (MWM) test for hippocampus-dependent memory (Iascone et al. 2013). They resemble the synaptotoxicity of AD but do not typically exhibit significant neuron loss, since beta-amyloid (Aβ) oligomers are known to act as a potent CNS neurotoxins, via specific disruption of neuronal signal transduction, without loss of cell bodies, as demonstrated by array tomography (for review, see Klein 2002; Lacor et al. 2004; for review, see; Mucke and Selkoe 2012). Moreover, the synaptotoxic role of Aβ is furtherly supported by the Aβ-immunotherapy favorable effects on memory and neurite architecture in AD mouse models (for review, see Spires-Jones and Knafo 2012). The promoters driving hAPP expression, the hAPP isoform(s) and mutation(s) expressed, and the background strain are among the differences between hAPP lines (Hall and Roberson 2012).

The Thy1-APP751 model express high levels of mutant hAPP751 under the control of the mThy1 promoter. This mouse model is characterized by plaques onset at 3 months of age, when dense amyloid deposits appear in the frontal cortex, while extensive amyloid deposits in most of the neocortex, hippocampus, thalamus, and cerebellum are developed by 9 to 11 months of age (Rockenstein et al. 2001). The early plaques onset makes this model ideal for the study of anti-amyloidogenic drugs.

The Tg-SwDI mouse is obtained by a triple mutation of the hAPP gene, i.e. Swedish K670N/M671L, Dutch E693Q,

and Iowa D694N mutations (Montgomery et al. 2016), and it develops amyloid plaques by 2 to 3 months of age, which are extensive by 12 months of age (Gu et al. 2012; Van Vickle et al. 2008). The Tg-SwDI mouse develops extensive fibrillar Aβ deposits primarily in cerebral micro vessels, whereas non-fibrillar plaques are predominantly diffuse in the brain parenchyma (Van Vickle et al. 2008). These features make the model useful for studying the progression of plaque formation and the predisposing factors (Gu et al. 2012).

The TgCRND8 mice carry the Swedish KM670/671NL and Indiana V717F mutations in the Aβ precursor encoding gene. The brain areas mainly affected are those rich in cholinergic fibers, i.e. the *stratum radiatum* of the hippocampus and the *corpus callosum*. The cholinergic damage is closely linked to the spread of amyloid plaques, which are detected by 7 months of age, and mirrors AD pathology in patients (Bellucci et al. 2006).

The Tg2576 mice express the human 695-amino acid isoform of AβPP bearing the double Swedish mutation (Lu et al. 2016). By 12 months of age, the Tg2576 mice develop progressively β amyloid plaques, gliosis and astrocytosis, with decreased glucose utilization and oxidative stress in the cerebral cortex (Apelt et al. 2002).

The PDAPP model mirrors the early onset AD form and it is characterized by the expression of human V717F mutation in the APP gene under the control of the PDGF promoter (Redwine et al. 2003). These mice show parenchymal amyloid plaques spreading by 6 to 9 months of age, and this diffusion progresses between 12 and 25 months of age, without any neuronal loss (Reilly et al. 2003). Furthermore, amyloid plaques have a structure that resembles those of AD patients, making this model useful for deeply studying amyloid plaques (Reilly et al. 2003).

The APP Dutch model with E693Q mutation under the Thy-1 promoter develops CAA, neuroinflammation and hemorrages, but it is not suitable to study amylioid depositions; indeed, Aβ levels are to low for amyloid precipitation and deposits formation (Kumar-Singh et al. 2000). The APP London model is characterized by hAPP London mutant overexpression exclusively in neurons, and mice bearing such mutation develop amyloid plaques at 12–15 months of age and vascular amyloid between 13 and 24 months of age (Dewachter et al. 2000). The amyloid vascular diffusion increases with age, and this feature allows studying new therapies to prevent vascular amyloid deposits (Van Dorpe et al. 2000).

The APP23 mouse, carrying the hAPP with the Swedish double mutation, develops plaques predominantly in the neocortex and the hippocampus, and it displays activated microglia, hypertrophic astrocytes, axonal sprouting and dystrophic neurites. Furthermore, by 14 months of age, this model develops hippocampal neuronal loss and vascular amyloid deposition (Van Dam et al. 2003; Mahler et al. 2015).

The TgAPParc is a mouse model that expresses APP with Arctic mutation (E693G). The Aβ-neuropathology onset in the subiculum and after spreads to interconnected limbic brain regions over 3–15 months. The TgAPParc is useful in order to understanding the spread and progression of Aβ neuropathology mechanism in AD (George et al. 2014).

The arcAb mouse develops age-dependent Aβ accumulation both in cerebral parenchyma and vessels. Six months old arcAβ mice show the first intracellular punctate deposits Aβ deposits in the cortex and hippocampus, later between 9 and 15 months of age, β amyloid plaques are prominent. The development of Aβ deposits in this model is used to evaluate amyloids deposition mechanism in AD (Knobloch et al. 2007; Klohs et al. 2013).

Presenilin mutations have also been used to develop mouse models of AD. Presenilin mutant mice crossed with hAPP transgenic mice exhibit extensive plaque deposition and behavioral deficits. A prototype is the PSAPP line, derived from a cross between transgenic mice expressing the M146L presenilin mutation and the hAPP transgenic mouse line Tg2576. This line develops Aβ plaque deposition earlier than Tg2576 and has increased Aβ42 levels. The PSAPP mice have deficits in the Y-maze even before plaque deposition, a finding that separates cognitive deficits from plaque burden (Holcomb et al. 1998). Today, the combined injection of the presenilin and hAPP transgenes as a single transgene is a more commonly used approach than breeding the presenilin and the hAPP mutant mice. The combined introduction of transgenes can be achieved either with two constructs, each with its own promoter element, coinjected into the pronucleus, or with transgenes cloned into one vector, separated by an internal ribosomal entry site and placed under the control of a single promoter (Jankowsky et al. 2004). The 5XFAD mice express high levels of Aβ42 and develop amyloid pathology and cognitive deficits by 4 months, and they show impaired memory in the Y-maze. In addition, the 5XFAD line develops neuron loss, unlike most other hAPP and hAPP/PS1 models. Thus, 5XFAD mice rapidly recapitulate major features of AD amyloid pathology and may be useful models of neurodegeneration and amyloid plaque formation (Oakley et al. 2006). On the other hand, an age-dependent increase in Aβ deposition has been documented in AβPP/PS1 mice, and these animals display cognitive deficits at the age of 6 months (Zhang et al. 2012).

The most commonly used behavioral tests to evaluate AD deficits are the MWM test, which evaluates spatial memory in rodents, and the Y- and T-maze tests, often used to test working memory. In AD mouse models, the recognition test has also been evaluated. The latter test is an easier and potentially more sensitive method to evaluate compound effects (Zhang et al. 2012). In addition to memory impairment, this disease causes additional symptoms, and therefore, other tests, such as a touch screen-based automated test battery, have been studied to evaluate attention deficits, which have been confirmed in both TgCRND8 mice and 3xTgAD mice (Romberg et al. 2013).

Evidence of vascular changes in AD

Epidemiological and clinico-pathological data suggest overlaps between AD and cerebrovascular lesions. Such lesions may magnify the effect of mild AD and promote the progression of cognitive decline, or may even precede neuronal damage and dementia. Vascular pathology in AD, as well as in the aging brain, includes cerebral amyloid angiopathy (CAA) and microvascular changes (for review, see Jellinger 2002). CAA is the most common pathological finding, present in up to 90% of AD patients (for review, see Jellinger 2002; Vinters 1987). Both AD and CAA can lead to pronounced cerebrovascular dysfunction, characterized by the impaired neurovascular and metabolic regulation of CBF and aberrations in vascular morphology and density. Mouse models that better represent CAA are Thy1-APP751, Tg-SwDI, and TgCRND8, whereas late-onset CAA, i.e., after 9 months of age, is usually detected in mice expressing mutated APP restricted to one familiar mutation, as in Tg2576, PDAPP, APPDutch, APP/London, APP23, or TgAPPArc animals.

Tg2576 mice represent an optimal model to mimic cerebrovascular conditions that commonly occur in AD patients, allowing the visualization with MRA of blood flow abnormalities in the middle cerebral artery (Kara et al. 2012), and amyloid plaques, which might play a role in the cerebrovascular alterations observed in AD (Kara et al. 2012). Tg2576 mice develop age-dependent cerebrovascular dysfunction, with the most severe deficits noted in aged mice having extensive CAA, and the impairment is directly correlated with the extent of CAA (Fig. 3) (Milner et al. 2014). The APP model shows varying degrees of CAA, which appears in aged animals and can be used to determine the inter-relationship between CAA, parenchymal amyloid pathology and vascular deterioration associated with aging (Li et al. 2014). The TgCRND8 model develops Aβ plaques in the parenchyma by 3 months of age, and by 7–10 months of age, both the number of vessels with CAA and the extent of Aβ deposition along the vessel walls increase significantly (Hawkes and McLaurin 2009).

The APP23 model shows alterations in cerebrovascular angiogenesis, and by 20 months of age, it shows vascular rearrangement and replacement in the posterior cerebral arteries. In the latter model, an increase in the number of cerebral vessels expressing markers of angiogenesis was detected. This mechanism is probably triggered by blood vessel damage (Thomason et al. 2013). The arcAβ mice develop intracellular Aβ deposits by 3 months of age and develop dense cored Aβ plaques starting at 7 months old, coinciding with the development of severe CAA (Knobloch et al. 2007). By 24 months of age, fibrinogen accumulation in vessels, indicating neurovascular damage, was detected. Furthermore, this mouse model shows a progressive decrease in endothelial glucose transporter 1, mainly in vessels with CAA (Thomason et al. 2013). The APP Dutch model is characterized by Aβ deposits predominantly located in the vasculature, with rare parenchymal plaques. Cerebral blood vessels show a thickened basement membrane, due to amyloid fibril deposition, and a loss of vascular smooth muscle cells (Thomason et al. 2013).

The CAA is often associated with cerebral microhemorrhages, which occur as a result of weakened vessel walls due to amyloid pathology. For increased understanding of cerebral microhemorrhages, there are some mouse models, such as Tg2576, that develop cerebral microhemorrhages

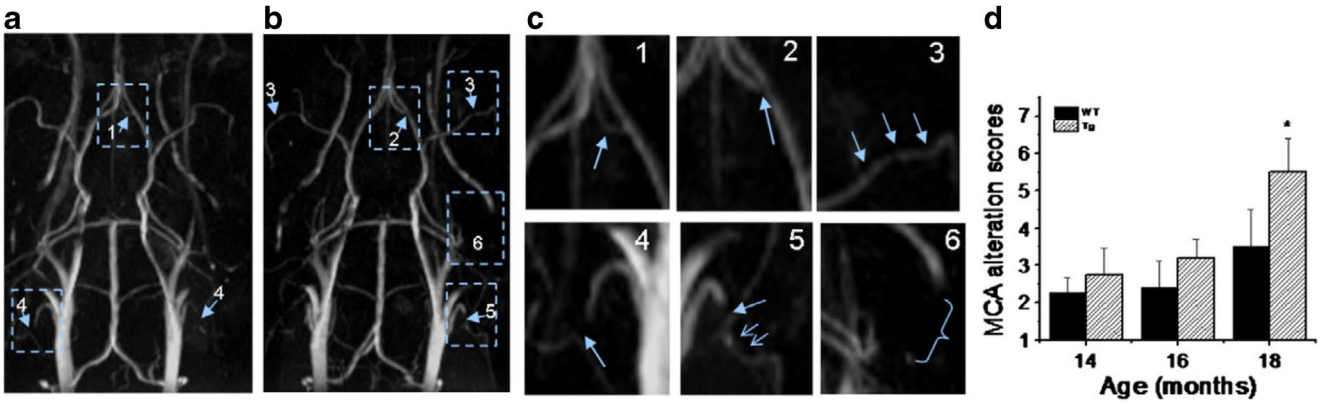

Fig. 3 Angiograms collected at 17.6 T magnet of 18-month-old transgenic mice showing various level of severities of morphological changes appointed in 3D MIP. The number indicates the appointed score to the level of severity of alterations. For example: 1 = a flow disturbance (as seen in AComA in image **a**); 2 = a small signal void (as observed at the origin of AComA in image **b**); 3 = more than two small voids in same artery (as observed on the MCA on both sides in image **b**); 4 = an extended void (as observed in the external carotid artery on both sides in image **a**); 5 = a combination of an extended void and several small signal voids (as observed in the external carotid artery on both sides in image **b**); 6 = the signal is no longer visible (as shown at the pterygo portion of the pterygopalatine artery in image **a** and **b**). The enlarge view of alterations is shown in (**c**). (**d**) MCA alteration mean score in control and Tg2576 mice with age. Values are mean ± SE (error bars); one-tail student T test; *Pb0.05; $n = 4$ (Kara et al. 2012)

between 15 and 24 months of age, in addition to CAA. The APP23 model also shows cerebral hemorrhages between 14 and 27 months of age, whereas in arcAβ mice, hemorrhages are infrequent (Thomason et al. 2013).

Preclinical imaging in AD

Transgenic mouse models of AD have become essential bio-systems for developing and defining optimal imaging approaches to visualize AD pathology in vivo, as well as for understanding the genotype–phenotype interaction in this disease (for review, see Benveniste et al. 2007). Most in vivo experiments have focused on the role of amyloid plaques, which are insoluble protein aggregates occupying the interneuronal spaces in brain tissue (Bigot et al. 2013).

Numerous imaging methodologies have been applied to evaluate the effect of plaques on the vascular system. Luo et al. showed for the first time, using fMRI, a correlation between the presence of Aβ40 and the decrease in CBV (Luo et al. 2008). The MRI studies performed in vivo using mouse models of AD proved to be a useful tool to visualize Aβ plaques using a T2-weighted sequence, and the contrast between plaques and normal-appearing adjacent brain tissue, defined as "local magnetic susceptibility," is presumably related to the iron that resides within most plaques (Chamberlain et al. 2009). Bigot et al. reported magnetization transfer contrast MRI, a technique derived from MR spectroscopy, as a novel approach to detect amyloid plaques in vivo (Bigot et al. 2013). Another approach to imaging Aβ plaques has been to target the plaques with specific MRI contrast agents that cross the BBB (Martins et al. 2013). The ideal MRI contrast agent for visualizing and quantifying the pathological burden of Aβ plaque should have four properties: (1) high in vivo stability, (2) ability to cross the BBB nondestructively following intravenous injection, (3) specific binding to plaques with high affinity, and (4) ability to produce local changes in tissue contrast that are detectable by MRI (Poduslo et al. 2002). The best mouse model for studying Aβ plaques is the APP/PS1 mouse, with plaque formation beginning at 3 months of age. The systemic injection of Aβ40 peptide chelated to gadolinium (Gd), after intravascular co-injection with mannitol to transiently open the BBB, can be used to detect Aβ plaques by μMRI in the brains of AD transgenic mice (Wadghiri et al. 2013). The T2-weighted and T2-star-weighted μMRI protocols have been used because they allow the clear identification of hypointense lesions, corresponding to Aβ plaques identified at histology, with relatively short acquisition times, i.e., 1 to 2 h. However, this method detected the plaques at an advanced stage and thus does not allow diagnosis of the disease at an early stage. To overcome mannitol pre-injection or the administration of any other agent to induce specific BBB permeation, ultrasmall superparamagnetic iron oxide nanoparticles chelated to polyethylene glycol linked to Aβ42 contrast agent can be used to image amyloid plaques and are therefore more suitable for longitudinal studies in the AD model, as well as for its ability to distinguish the plaques from the blood vessels (Wadghiri et al. 2013).

Although in vivo microscopic techniques are a valid tool for differentiating CAA from neuritic deposits, such techniques are invasive and therefore confined to yielding mechanistic information in animals (for review, see Klohs et al. 2014). Nonetheless, they constitute an important complement for macroscopic imaging approaches such as PET and MRI, which can also be used in humans. Even with high field MRI, it is difficult to analyze deposits less than 35 μm, which is critical for the early diagnosis of CAA (Jaruszewski et al. 2014). Monocrystalline iron oxide nanoparticles have been used to detect CAA, but not for its treatment, and such nanoparticles cannot be used as PET or SPECT contrast agents. To avoid these problems, specific nanovehicles have been designed and labeled with the novel amyloid antibody IgG4.1, which can target CAA and can serve as both an early diagnostic and therapeutic agent. These nanovehicles were chelated with Gd-based MRI contrast agents, or SPECT agents, such as ^{125}iodine (I). In addition, they could be used for drug delivery and anti-inflammatory therapy (Kandimalla et al. 2007). In particular, the F(ab′)24.1 fragment of IgG4.1 is grafted onto the polymeric core of nanovehicles to aid the targeting to cerebrovascular amyloid (Agyare et al. 2008). Although MRI is a useful tool to assess brain atrophy, alterations in perfusion, and various brain networks in AD, it is not the imaging modality of choice for visualizing microglia activation (James et al. 2015).

The [^{11}C]-PIB compound readily passes the BBB and rapidly clears from normal brain tissue, and it is useful for the imaging of β-amyloid plaques in transgenic mice, even if its specificity is highly dependent on the model and the plaque structure (for review, see Waerzeggers et al. 2010; Manook et al. 2012; Snellman et al. 2013). Indeed, it binds not only to classical and diffuse β-amyloid plaques, but also to CAA lesions (Lockhart et al. 2007).

The cerebral glucose metabolism, measured by [^{18}F]-FDG PET, is one of the most sensitive functional biomarkers of AD (Poisnel et al. 2012). AD patients display early and progressive reductions of glucose metabolism in cortical and hippocampal regions (Poisnel et al. 2012). The 3xTG mouse model is a useful model, as it mimics the brain glucose uptake abnormalities of AD patients (Nicholson et al. 2010). In contrast, in APP/PS1, the [^{18}F]-FDG PET showed an age-related increase of uptake in the cortex in the hippocampus and in the *striatum* (Poisnel et al. 2012). Imaging with FDG PET showed hypermetabolism associated with elevated taurine concentrations, revealed by proton MRS, in

Tg2576 mice. Using fMRI for CBV calculation, the integrity of the cerebral vascular compliance in 7-month-old Tg2576 versus WT was confirmed. The Tg2576 mouse brain hypermetabolism seems to be unrelated to changes in vascular compliance, but it may be due to a primary central nervous system process related to amyloid hyperproduction. Taken together, these data suggest that the utility of the Tg2576 model may be limited to studying production and clearance mechanisms, rather than neuronal metabolism (Luo et al. 2012).

Light-based microscopy methods allow collecting information at very high resolution, but they are restricted to superficial cerebral areas, i.e. the cortex, during in vivo microscopy. These techniques are also limited by the presence of the skull, hence they need an optical window, such as thinned bone areas or craniotomy. On the other hand, near-infrared fluorescence (NIRF) allows three-dimensional study of deeper brain structures, at the expenses of spatial resolution (for review, see Klohs et al. 2014). In Tg2576 mice, the CAA evolution has been studied through multiphoton microscopy, and it has been shown to start by 9 months of age and to progress linearly between 9 and 16 months (Robbins et al. 2006). Amyloid specific dyes, typically used for histopathological evaluation, can be chemically modified to obtain imaging probes for amyloid deposition detection in vivo (for review, see Klohs et al. 2014). Fluorescent dyes transit time was prolonged in TgCRND8 mice compared to wildtype littermates, suggesting impaired cerebral perfusion, which can be studied with two-photon microscopy as well as with laser Doppler flowmetry (Dorr et al. 2012). Spatial frequency domain imaging and diffuse optical imaging allowed quantitative measurement of oxy- and deoxyhemoglobin concentrations in 3xTg-AD mice, showing that even if normal aging produce a significant decrease of such parameters in the brain of control mice, their reduction is always superior in AD mice (Lin et al. 2014).

An example of NIRF application was the study of the drug efflux transporter ATP-binding cassette sub-family G member 2 (AbcG2), a transmembrane protein that seems to operate as a controller at the BBB level preventing Aβ entering the brain parenchyma from bloodstream. In fact, it has been demonstrated that knock-out AbcG2 mice accumulate significantly more Aβ compared to control mice. On the other hand, both Tg-SwDI and 3XTg-AD mouse models displayed an increased expression of the AbcG2, suggesting that Aβ accumulation might be due to an impaired clearance as well as to an over deposition (Xiong et al. 2009). Microglial cells and blood vessels staining was obtained in vivo by high pressure injection of tomato lectin conjugated with a fluorescent dye into the cortex of an APP23 cross transgenic model, as well (Busche et al. 2008; Schwendele et al. 2012).

Mouse models of Parkinson's disease

Parkinson's disease (PD) is the second most common neurodegenerative disorder, affecting approximately 0.3% of the entire population, 1% of people over 60 years of age and up to 4% of people over 80 years of age (for review, see Mao et al. 2015). PD is caused by progressive degeneration of the nigrostriatal dopaminergic pathway, leading to dopamine deficiency. When the deficit reaches 80%, clinical symptoms appear. There are 2 principal mouse models of PD. The first requires the use of neurotoxins and replicates most of the pathological and/or phenotypic features of PD in mammals; the second is genetic and models monogenic forms of familial PD (for review, see Bogaerts et al. 2008).

The toxic models of PD are developed using the toxins 6-hydroxydopamine (6-OHDA), 1-methyl-4-phenyl-1,2,3,6-tetrahydropyridine (MPTP), rotenone, paraquat (PQ) or epoxomicin. The toxin 6-OHDA shares some structural similarities with dopamine and norepinephrine, exhibiting a high affinity for several catecholaminergic plasma membrane transporters such as the dopamine transporter (DAT) and norepinephrine transporter. Its administration causes nigrostriatal depletion and gliosis when stereotactically injected into the SN, median forebrain bundle or striatum (for review, see Waerzeggers et al. 2010). Following 6-OHDA injections into the nigrostriatal tract, dopaminergic neurons start degenerating within 24 h, and striatal dopamine is depleted 2 to 3 days later (Faull and Laverty 1969). Although the 6-OHDA model is a valid tool for the development of new therapeutic strategies, it does not mimic all the clinical and pathological features characteristic of PD, such as the formation of Lewy bodies and cytoplasmic inclusions. Furthermore, the acute nature of the experimental model differs from the progressive degeneration of the dopaminergic nigral neurons (for review, see Betarbet et al. 2002).

The most common animal model for studying PD is the MPTP mouse model. MPTP is a potent and irreversible mitochondrial complex I inhibitor whose toxic metabolite MPP + is selectively transported by the DAT and whose administration results in Parkinsonism (for review, see Waerzeggers et al. 2010). The MPTP model is a valid tool for studying the mechanism of dopaminergic neuronal death and testing neuroprotective agents, but its major limitation, which is shared by the toxic models in general, is that the SN *pars compacta* (SNpc) lesion is not accompanied by the formation of Lewy body-like cytoplasmic inclusions (Muñoz-Manchado et al. 2016). Meredith et al. developed a chronic MPTP model with the concomitant administration of probenecid, in which a significant reduction in the number of neurons in the SNpc, the loss of 50% of dopamine neurons and the reduction of striatal dopamine levels by 90 – 95% were demonstrated (for review, see Meredith et al. 2008).

The PQ and rotenone administration in mouse produce specific feature of human PD, due to oxidative stress (Sharma et al. 2006; Fernagut et al. 2007). The PQ model shown a reduction in ambulatory movement, and Rotenone induce a progressive and chronic degeneration of the nigrostriatal pathway similar to what is observed in humans due to systemic complex I inhibition (Liu et al. 2015).

The genetic PD models are α-synuclein mice, parkin knockout mice, DJ-1 knockout mice, Nurr1 and PITX3-aphakia mice. The α-synuclein transgenic mouse shows variable neuropathological and behavioral phenotypes. The main feature of this model is the manifestation of the typical motor dysfunction of PD, although the dopaminergic and behavioral defects depend on the level of expression of the transgene in both the neuronal and glial populations (Fernagut and Chesselet 2004).

The "*parkin*" mutation causes the most common autosomal recessive form of PD (for review, see Blandini and Armentero 2012). As several studies have shown that the knockout mouse models for the *parkin* gene showed impairment of the short-term spatial memory and hippocampal synaptic plasticity, the *parkin* mouse model could be a useful tool for further investigations of hippocampal functioning (Hanson et al. 2010; Rial et al. 2014).

The DJ-1 knockout mice are more sensitive to toxins and oxidative stress, but they do not display major neuronal abnormalities. Furthermore, the loss of DJ-1 function in mice can lead to motor deficits as well as to alterations in nigrostriatal dopaminergic function (Chen et al. 2005).

Behavioral tests to assess neurological status and the response to pharmacological treatments have been developed for these models. The activity test in the open field and the rotarod test for coordination are the most commonly used to assess motor function, although they lack the sensitivity to detect subtle alterations in the nigrostriatal dopamine system (Fleming et al. 2013). Other common tests are the sucrose preference, the tail-suspension and the forced swimming tests, which allow detection of signs of depression, and the elevated plus maze and marble burying tests, which highlight signs of anxiety (Bonito-Oliva et al. 2014; Gorton et al. 2010). A battery of tests more sensitive to different aspects of sensory and motor function and to subtle changes in basal ganglia function are the challenging beam traversal, which evaluates motor performance and coordination; the pole test, to assess basal ganglia-related movement disorders; the spontaneous activity in a cylinder; the inverted grid; the bin cotton use; the gait analysis; and the adhesive removal tests (Fleming et al. 2004, 2013).

Other behavioral assessments have been developed to evaluate the efficacy of therapies for non-motor symptoms. The identification of these non-motor symptoms is very important because some mouse models do not present motor deficits at all. As olfactory disturbances are the first non-motor symptoms observed in PD, behavioral testing, such as the buried pellet test, can be used to study this function and can facilitate early detection (Fleming et al. 2008). Both α-synuclein and MPTP mice took longer to find a buried pellet than their wild-type littermates (Fleming et al. 2008; Baranyi et al. 2016). Sleep dysfunction is another important non-motor sign of PD in humans. During sleep, mice exhibit a distinctive posture and breathing pattern that allows the observer to determine the onset of the sleep. Thus, the time of latency before the mice begin this behavior is easily recordable and comparable between strains (for review, see Taylor et al. 2010). Furthermore, some authors describe gastrointestinal dysfunctions similar to the ones reported in PD patients. Screening for such dysfunctions in mice can be performed using the solid gastric emptying test, which evaluates stomach motility, and the stool collection test, to examine colon motility (Taylor et al. 2009). Other non-motor signs are anxiety and depression, which could be evaluated using the elevated plus maze, open field testing, and light–dark exploration, whereas cognitive deficits can be evaluated using the radial arm maze functions and the modified water maze (for review, see Taylor et al. 2010).

Parkin-deficient mice display normal performance on behavioral tests evaluating olfactory function, anxiety, depressive-like behavior tested with forced swimming and tail suspension, and motor function verified by the rotarod, grasping strength and pole tests. However, *Parkin*-deficient mice show poor performances in the open field habituation, object location and modified Y-maze tasks, suggesting procedural and short-term spatial memory deficits (Rial et al. 2014). Hence, this model is useful for studying new therapeutic strategies to restore the learning, memory and synaptic plasticity impairments that are characteristic of PD (Rial et al. 2014).

The MPTP/p model shows impaired ambulatory behavioral in the open field test and the pole test, due to an irreversible state of bradykinesia, and increased immobility in the bar test, compatible with catatonia (Rekha and Selvakumar 2014). Furthermore, increased anxiety has been measured by the marble burying test in this model (Gorton et al. 2010). A partial bilateral lesion of the dorsal striatum with 6-OHDA results in a subtle impairment of gait dynamics, accompanied by olfactory deficit and depression- and anxiety-like behavior. The mild motor impairment indicates that this model reproduces a relatively early stage of PD (Bonito-Oliva et al. 2014). Unlike the MPTP model, the 6-OHDA mice do not display any reduction in horizontal motor activity and show normal stride length and frequency. Nonetheless, bilateral injection of 6-OHDA into the striatum increases the immobility time in the forced swimming and tail suspension tests (Bonito-Oliva et al. 2014). In this model, subtle impairments of gait dynamics and reduced olfactory discrimination, reminiscent of early stage PD,

are accompanied by depressive and anxiety-like behaviors (Bonito-Oliva et al. 2014). However, the unilateral injection of 6-OHDA into the medial forebrain bundle results in total denervation of the dopaminergic nigrostriatal pathway. This partial lesion model is assessed by a battery of tests that are specific for this model, i.e., the cylinder, stepping, corridor and rotation tests (Boix et al. 2015).

The α-synuclein models display progressive sensorimotor anomalies, altered response to dopaminergic drugs, alterations in striatal dopamine receptor function, and olfactory deficits (Fleming et al. 2004). The Thy1-aSYN mice made significantly more errors per step than their wild-type counterparts in the beam traversal task, and they also showed a significant deficit on the pole test (Fernagut et al. 2007).

The PQ-intoxicated mice displays signs of increased hippocampal oxidative stress and impaired memory function in the MWM, as well as reduced exploration of a novel open field arena, with females apparently less susceptible than male mice (Litteljohn et al. 2011).

Evidence of vascular changes in PD

In humans, both BBB and vascular damage have been reported in PD. Studies with PET have shown decreased regional CBF and oxygen utilization (Sarkar et al. 2014). Examinations with SPECT displayed a reduction of regional CBF in the temporal and parietal cortices in PD patients with or without dementia, as well as cortical blood flow alterations in PD patients with dementia (Sarkar et al. 2014; Varma et al. 1997). Immunohistochemical studies on microvasculature changes in MPTP mice showed reductions in length and number, sclerosis and ischemia. Moreover, vessel density was also dramatically reduced in the *striatum* and SN (Fig. 4) (Sarkar et al. 2014).

There is growing interest in the evaluation of VEGF in neurodegenerative disorders, and generally in neuroprotection (Storkebaum et al. 2004). The intrastriatal implantation of encapsulated VEGF-secreting cells has been reported to exert beneficial effects in a PD model, effects that persisted for at least 8 weeks (Yasuhara et al. 2004). VEGF itself may have a direct neuroprotective effect on dopaminergic neurons. The rescue of dopaminergic neurons from 6-OHDA lesions in the *striatum* and in the SN of VEGF-treated animals has been demonstrated by immunohistochemistry (Yasuhara et al. 2004). However, once the dose of VEGF exceeds the limit, its adverse effects might exceed the neuroprotective effects, causing deterioration in dopaminergic neuronal survival and function (Yasuhara et al. 2004).

The inflammatory process involved in microglia triggering is one of the key processes in PD. The peptide angiotensin II, via type 1 receptors, is among the most important inflammation and oxidative stress inducers and produces reactive oxygen species. The brain possesses a local angiotensin system that modulates striatal dopamine release. Angiotensin II may normally be involved in the modulation of dopaminergic neurotransmission and may enhance the microglial/inflammatory response after an initial lesion induced by neurotoxins such as MPTP. This response is amplified by angiotensin II and inhibited by angiotensin type 1 receptor antagonists, both in vivo and in vitro (Joglar et al. 2009).

Preclinical imaging in PD

In vivo imaging, especially MRI and nuclear imaging techniques, are a useful tool to evaluate PD progression and response to therapy. MPTP administration is not only known to cause disturbances in neural cell proliferation and differentiation, due to dopamine depletion but also to evoke an inflammatory reaction, such as the accumulation of microglia, lymphocytic infiltration and an increase in cytokine production, in the affected brain areas (Klein et al. 2014). These inflammatory responses might also be correlated to the transient increase in brain elasticity (Klein et al. 2014). In fact, a correlation between the steep transient rise in elasticity within the hippocampal region of up to over 50%, 6 days after MPTP treatment, and an increased neuronal density in the dentate gyrus, which could not be detected in healthy controls, was demonstrated by magnetic resonance elastography (MRE) (Klein et al. 2014). This technique has proven to be useful in analyzing the correlation between morphological brain changes and dopamine depletion (Klein et al. 2014).

While BOLD fMRI is used to map the neurological substrate of motor and cognitive symptoms in PD, activation-induced, manganese-enhanced MRI can also be used for the non-invasive investigation of whole brain activity, independently from blood hemodynamics and direct study of the neuronal activity. It can be used to diagnose PD but potentially also for the study and diagnosis of various other neurological disorders (Kikuta et al. 2015). With this method, it was possible to identify elevated striatal activity in MPTP mice (Kikuta et al. 2015).

To obtain a biomarker of brain function in PD, MRI spectroscopy is the method of choice to evaluate brain metabolism with quantitative measurements. Spectroscopy revealed a decreased N-acetyl-aspartate to creatine ratio in the striatum of PD patients (Bagga et al. 2013). A novel spectroscopic approach, with the infusion of [1,6-$^{13}C_2$]-glucose or [2-^{13}C]-acetate, was used to assess the glutamatergic, gamma-aminobutyric-acid-(GABA)-ergic and astroglial function in different brain regions of mice exposed to MPTP (Bagga et al. 2013). This technique allowed the identification of dysfunction in the

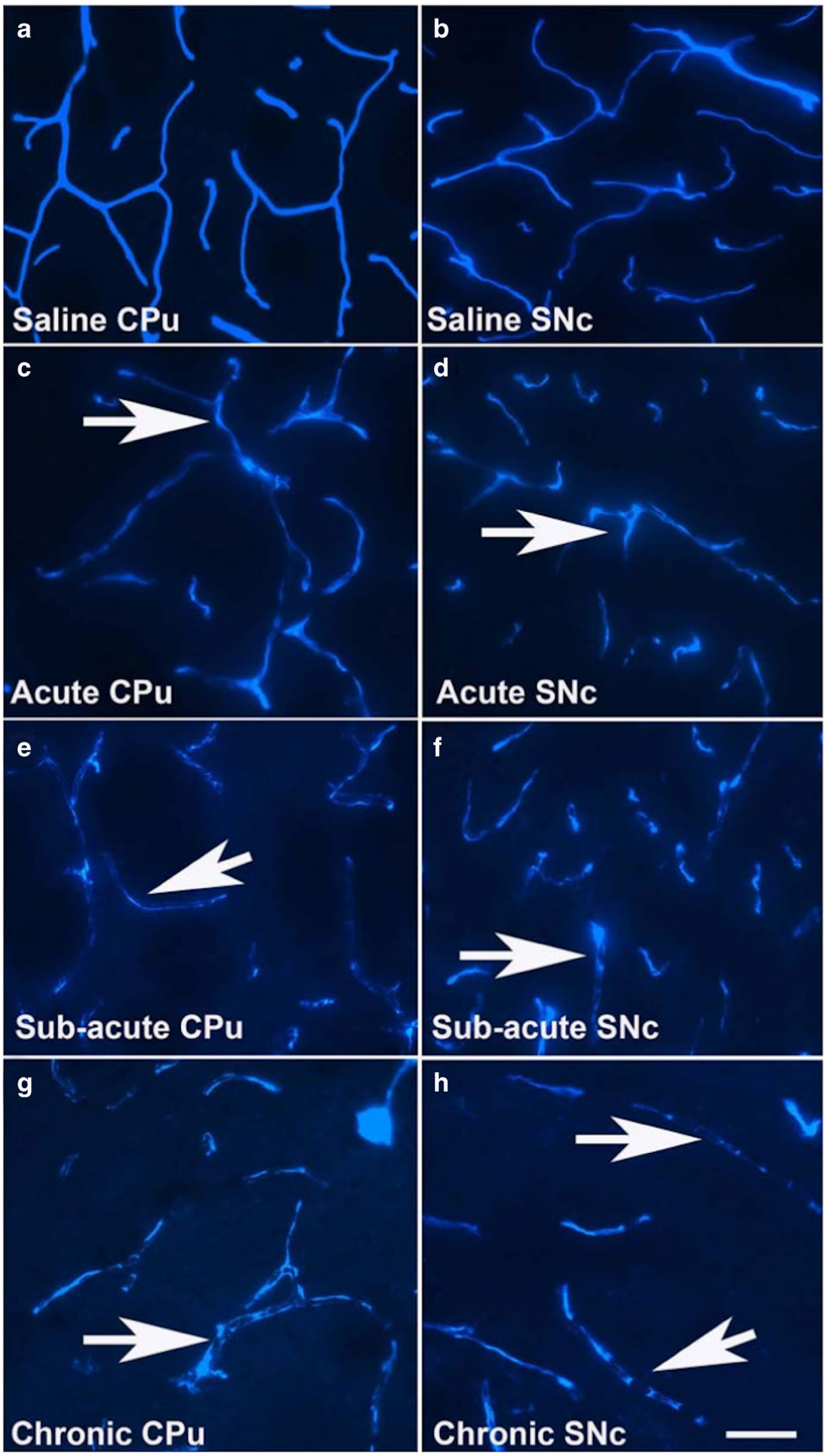

Fig. 4 Series of coronal sections at the level of CPu putamen and SNc from control and MPTP treated mice brain. Morphologically, FT-gel labeling in the saline treated animals was uniformly distributed within the capillaries in CPu (**a**) SNc (**b**). In acutely treated animals, both in CPu (**c**) and SNc (**d**) blood vessels were shorter, regressed, fainter in appearance and ischemic (arrows). In the sub-acute treated animals, both in CPu (**e**) and SNc (**f**), the capillaries was dense in some parts forming the 'clusters' of various shapes and sizes with little or no staining between the 'clusters' (arrows). In the CPu (**g**) and SNc (**h**) of chronic treated mice, blood vessels were more regressed, more pronounced endothelial cell clusters (arrows) were apparent as compared to their saline treated counterparts (**a** and **b**). Scale bar: 100 μm. Structural abbreviations: CPu: striatum. (Sarkar et al. 2014)

glutamatergic and GABAergic neuronal activities in the olfactory bulb in MPTP mice, as well as impairment of the excitatory and inhibitory pathways in brain regions that are involved in regulating movement and in the olfactory bulb and cerebellum (Bagga et al. 2013).

The PET- and SPECT-based methods of imaging DAT-binding radiotracers are widely used to assess the integrity of the nigrostriatal projection in vivo (Fig. 5) (Alvarez-Fischer et al. 2007). The DAT SPECT tracers are used frequently in routine clinical studies to confirm or exclude the loss of nigrostriatal dopaminergic neurons in patients suspected to suffer from PD (Ziebell et al. 2012) This technique represents the main tool to determine DAT density in rodents, to test the effects of potential neuroprotective drugs (for review, see Suwijn et al. 2014).

The striatal [^{123}I]-FP-CIT SPECT signal in vivo correlates with the DAT level, in both MPTP and 6-OHDA mice, but the main limitation of this method is that the number of nigral dopaminergic cells cannot be evaluated. However, [^{123}I]-FP-CIT pinhole SPECT allows more accurate detection of relatively large striatal DAT deficits in mice, i.e., losses of approximately 60–80% (Andringa et al. 2005). This approach may be useful for analyzing neuroprotective treatments (Andringa et al. 2005).

Although 6-^{18}fluoro-L-3,4-dihydroxyphenylalanine ([^{18}F]-DOPA) PET is considered the gold standard for the assessment of presynaptic dopaminergic integrity in vivo and is widely used in both patients and animal models, it is rapidly metabolized (Waerzeggers et al. 2010). To overcome this issue, ^{18}F-dihydrotetrabenazine, a VMAT2 ligand with a prolonged half-life, has been used to examine changes in the dopaminergic system in MPTP mice. This tracer correlates positively with the loss of dopaminergic neurons (Toomey et al. 2012). In addition, 2β-carbomethoxy-3β-(4-chlorophenyl)-8-(2-[^{18}F]-fluoroethyl)-nortropane is an established PET tracer for the DAT that has been successfully used in humans and monkeys. This tracer has clearly superior imaging characteristics compared with previously published ligands for the DAT (Honer et al. 2006). It displays very high accumulation in the right and left *striatum*, yielding PET images of high target-to-background ratios. Furthermore, its uptake in the *striatum* of MPTP mice was significantly reduced by 60% (Honer et al. 2006).

Neuroinflammation is another process involved in PD. Microglia activation, in response to pathological stimuli such as MPP+, 6-OHDA, or rotenone, has been studied in animal models of PD (Zhou et al. 2005). Imaging with appropriate radiotracers, e.g., radiolabeled isoquinolone PK11195, can track the in vivo distribution of activated microglia (Venneti et al. 2009). In MPTP and 6-OHDA models studied with PET, an immediate inflammatory reaction to the toxic insult and a later stage reaction consistent with the ongoing neurodegenerative process were shown. Thus, this PET technique offers a tool for the location and characterization of disease activity.

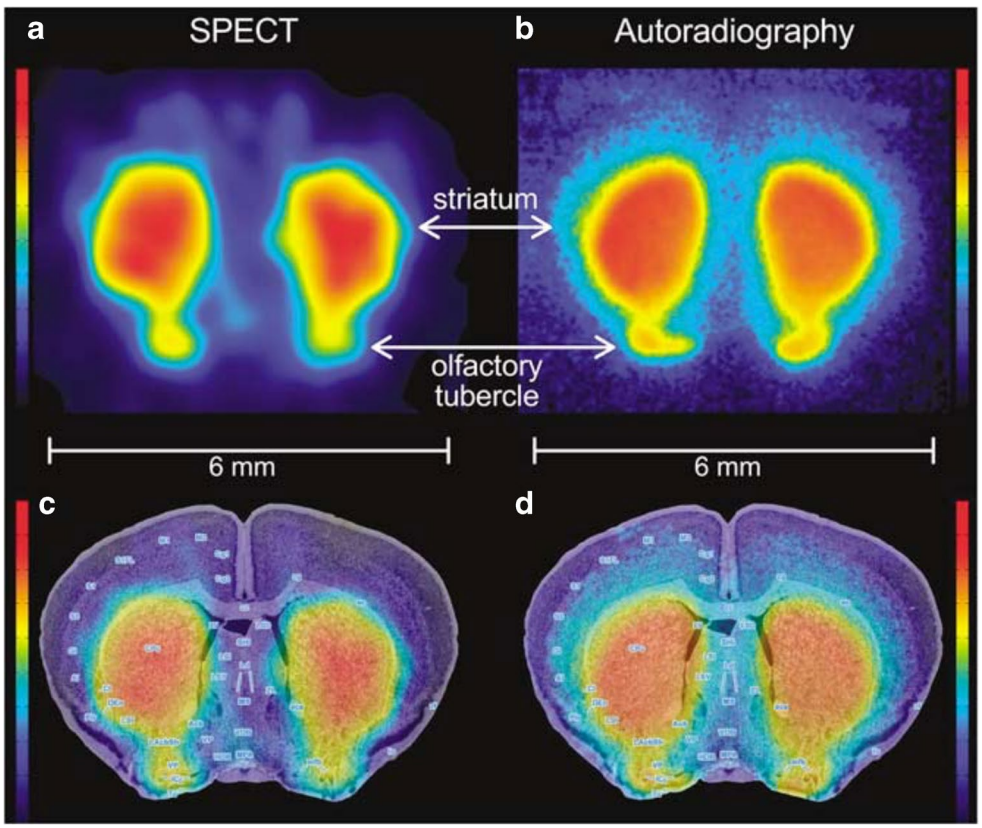

Fig. 5 High resolution in vivo imaging of striatal DAT (left) compared with DAT autoradiography (right). **a** Horizontal SPECT slice of the striatum, showing the possibility to distinguish sub-striatial structures through DAT binding of [^{123}I] FP-CIT. **b** Autoradiogram at the level of the striatum and olfactory tubercle of a mouse brain post mortem. Please note, that the autoradiography and SPECT images look similar, suggesting that pinhole SPECT is able to delineate DAT binding within a sub-millimeter range **c** SPECT slice overlaid on an anatomic brain atlas of the mouse. **d** Autoradiogram overlaid on anatomic brain atlas. DAT, dopamine transporter; [^{123}I] FP-CIT, [^{123}I]N-o-fluoropropyl-2b-carbomethoxy-3b-(4-iodophenyl)- nortropane; SPECT, single photon emission computed tomography. (Vastenhouw et al. 2007)

Moreover, in MPTP mice, a specific apoptosis-targeting peptide, linked to fluorescent dye, was used to study in vivo dopaminergic neurons death. It was demonstrated the feasibility of these approach, evaluated by a fluorescence molecular imaging system, even in the assessment of drugs efiiciency (Lee et al. 2012).

Mouse models of Huntington's disease

Huntington's Disease (HD) is a neurodegenerative disorder characterized mainly by the loss of medium spiny neurons (MSNs) in the *striatum, caudate nucleus* and *putamen* of the basal ganglia and by the degeneration of the cortex and hippocampus, resulting in chorea, dystonia, psychiatric and cognitive abnormalities (Glorioso et al. 2015). As observed in other neurodegenerative diseases, there is no single mouse model that summarizes all the characteristics of HD. In particular, chorea is a symptom restricted to primates (for review, see Heng et al. 2008). Mouse models are classified into two categories: toxin-induced and genetic models; the latter category is further divided into transgenic and knock-in models.

The two most common toxin-induced models are produced by the administration of quinolinic acid (QA) and 3-nitropropionic acid (3-NP). The QA administration mimics the early stage of HD, reproducing hyperactivity. The cognitive deficits are detectable by the MWM, the radial arm water maze, and the T-maze (Furtado and Mazurek 1996; Shear et al. 1998).

The 3-NP model is a mitochondrial dysfunction model and resembles the later stage of HD, characterized by motor disorders and related striatal damage, which are tested using the pole, the rotarod, the stride length, and the open-field spontaneous activity tests (Fernagut et al. 2002).

Among the transgenic models, R6/2 is the most used. As the onset of symptoms is at 5 to 6 weeks of age, R6/2 is considered a model of juvenile disease (Parievsky et al. 2012; Chang et al. 2015). In contrast to human HD, the R6/2 brains do not show a massive neuronal loss (for review, see Wang and Qin 2006). The mice display a severe phenotype with low weight, diabetes, clasping, tremor and convulsions (Wang et al. 2005). The main behavioral signs are motor deficits, occurring as early as 40 days of age, and hyperactivity, verified using the open-field test for locomotion and exploratory behavior. Cognitive deficits appear before the motor symptoms and can be confirmed by the MWM and the T-maze tasks. Both tests require the subjects to replace a previously learned strategy using their intact fronto-striatal circuitry (for review, see Ramaswamy et al. 2007).

The R6/1 model is less common than the R6/2 model and shows a mild behavioral phenotype. Aberrant synaptic plasticity has been described in these mice (for review, see Cepeda et al. 2010). The behavioral tests used to evaluate R6/1 deficits include footprint analysis, which evaluates gait abnormalities, decreased anxiety, and hindlimb clasping behavior (Denny et al. 2010). Even though the R6/2 and R6/1 models are not the most genetically accurate, thus far, they represent the most feasible models for therapeutics research, as the outcomes are more prevalent and definable (for review, see Wang and Qin 2006).

Mouse models expressing yeast artificial chromosome (YAC) *htt* are more genetically accurate but have a more variable and subtle phenotype. They are characterized by atrophy and neuronal loss in the *striatum* (Berggren et al. 2016).

The most used among YAC models is YAC128, which shows hyperkinetic abnormalities at 3 months of age and hypokinesia at 6 months of age in the open field and rotarod tests. Furthermore, examining YAC128 mice with the swimming T-maze reveals difficulties in forming new strategies (Van Raamsdonk et al. 2005).

The N171-82Q mouse model expresses a human *htt* gene and represents a good model for adult HD. At the onset, the mice display resting tremor, hypokinesia, hindlimb and forelimb clasping, and abnormal gait. At 14 weeks of age, they show deficits of working and reference memory in the radial arm water maze test (for review, see Ramaswamy et al. 2007). At 4 to 6 weeks before death, they show tremor, hypokinesis, and clasping (Heng et al. 2008). The later onset of behavioral symptoms and the protracted time course make this model ideal for the study of presymptomatic therapies.

Knock-in mouse models are generated by replacing a portion of the murine *htt* gene with the human mutant copy, which contains an expansion of the CAG region. Such expansion is directly proportional to the precocity of symptoms onset, in both rodents and humans (Fernandes and Raymond 2009). The knock-in models are the most representative of genetic and protein alterations, although they are not appropriate for behavioral studies. For example, knock-in HdhQ111 mice do not show behavioral deficiencies compared to the controls when subjected to specific tasks (for review, see Ramaswamy et al. 2007). Nonetheless, they recapitulate an important pathological change observed in the HD human brain, i.e., the preferential accumulation of mutant *htt* in the striatal neurons (for review, see Chang et al. 2015). However, homozygous knock-in mice show very early behavioral anomalies, prior to any detectable neuropathology. Behavioral abnormalities can be evaluated in the knock-in CAG140 and CAG150 models. The first was rotarod deficit at 9 months, the latter at 4 months (for review, see Ramaswamy et al. 2007).

Evidence of vascular changes in HD

Changes in the morphology of microglia, when activated by any brain insult, are accompanied by vascular changes due

to the persistent secretion of pro-inflammatory factors. This activation may be involved in the pathogenesis of HD, as confirmed by microglia activation in the R6/2 and YAC128 models (Franciosi et al. 2012). The progression of HD may be studied by evaluating pro-inflammatory markers in the plasma in R6/2 mice, but most of the studies showed some limitations, such as small sample size and differences in baseline characteristics between the study groups, so the correlation between disease progression and inflammation has not yet been confirmed (for review, see Chang et al. 2015).

Cerebral hyperperfusion has been reported in HD patients and mice and is observed as increased vessel density, CBV and/or CBF (Hua et al. 2014). Longitudinal studies using fMRI showed functional and morphological changes in the cerebral blood vessels and alteration in the BBB in R6/2 mice. In particular, a decrease in blood vessels size and atrophy of the *putamen* have been detected. Hence, the reduction in oxygen supply triggers a compensatory mechanism, which leads to the increase in vascularization and in arterial CBV, particularly in the grey matter of HD patients and R6/2 mice (Drouin-Ouellet et al. 2015). The evaluation of microvessels and BBB using μMRA and dynamic CE MRI showed significant increases in vessel density and CBV, but not in vessel size, in R6/2 mice as early as 7 weeks of age. These changes in vessel density in the cortex and *striatum* preceded any behavioral aberrations and worsened with disease progression, with no apparent concomitant disruption of the BBB (Lin et al. 2013). These studies underline a correlation between vascular impairment and neurodegeneration. If these phenomena are confirmed in the early stages of the clinical HD, they can be considered as targets for future therapies (Waldvogel et al. 2015).

Vascular impairment has also been studied in the R6/1 model by myography. The R6/1 model presented reduced contractility in arteries from several different vascular beds, probably due to altered calcium fluctuations in the arterial smooth muscle cells (Rahman et al. 2013). This mouse model displayed alterations in peripheral arterial resistance form 12 weeks of age due to an impairment of nitric oxide (NO) -dependent mechanisms. Moreover these mice did not exhibit endothelial relaxation between 12 and 16 weeks, and they showed significant enhancement of endothelial-dependent dilation and impaired vasoconstrictor responses (Kane et al. 2016). It should be remembered the importance of the equilibrium between superoxide ($O2^-$) and NO in maintaining the physiologic vascular tone: a NO increase would lead to vasodilation; on the other hand, the $O2^-$ increase is linked to vasoconstriction and increased peripheral vascular resistance (Kane et al. 2016) The production of $O2^-$ may be due to several factors, including huntingtin effects and mitochondrial damage (Rahman et al. 2013; Kane et al. 2016). Finally, the impaired vascular reactivity, i.e. the ability of the blood vessel to control the CBV in response to hemodynamic changes detected in R6/2 mice with MRI, seems to be induced by aberrant HD astrocytes via an increased VEGF-A production (Hsiao et al. 2015).

Preclinical imaging in HD

The technique most commonly used for the study of HD mouse models is MRI. MRI allows the characterization of several neuroanatomical features in the brains of YAC128 mice, including the striatal volume decrease as of 8 months of life and an asymmetric atrophy, similar to observations in HD patients (Lerch et al. 2008). To the best of our knowledge, R6/2 mice are the most commonly used to characterize MRI in HD. The ex vivo MRI analysis of R6/2 brains showed morphological changes, such as reduced striatal and increased ventricular volumes, and demonstrated a good correlation between the MRI results and traditional histology (Sawiak et al. 2009).

In vivo MRI studies have been demonstrated to be more accurate than ex vivo, although the scanning time, contrasts and image resolution are the main limitations of the technique (Zhang et al. 2010). The first results of in vivo MRI in HD models revealed the opportunity to detect atrophy before the onset of motor symptoms (Zhang et al. 2010). In vivo MRI performed in HdhQ150 showed global brain atrophy before the onset of motor signs, although, unlike HD patients, alteration in white matter region have not been showed in corpus callosum (Steventon et al. 2016). The R6/2 mouse models showed atrophy of the cortex and the *striatum*. Such lesions can be visualized from the third week of age, and significant progressive atrophy in the R6/2 cortex was observed mainly in the early postnatal phase, becoming less evident in later stages, up to 5 weeks of age (Fig. 6) (Aggarwal et al. 2012). Measuring the brain volume by T2 MRI, it is possible to evaluate the effect of therapy. The R6/2 model is not adequate for this purpose, since brain atrophy is evident from 3 to 5 weeks of age, and hence the time is too short to assess the therapy effectiveness (Aggarwal et al. 2012). The N171-82Q model represents a less severe phenotype compared to R6/2. This model allows evaluating brain atrophy using MRI in response to Sertraline, a neuroprotective agent, from 6 weeks of age. These results confirm that MRI is useful not only to test the effectiveness of therapy, but also in the selection of the murine model, which possesses the most adequate characteristics, e.g. time of onset, to study drug efficiency or specific pathological processes (Cheng et al. 2011).

The detection of cerebral functional alterations using MRI proved to be useful in studying HD progression, as these alterations are detectable before structural changes become apparent. Relative CBV alterations in the *striatum*, temporal cortex, primary motor cortex, and prefrontal motor

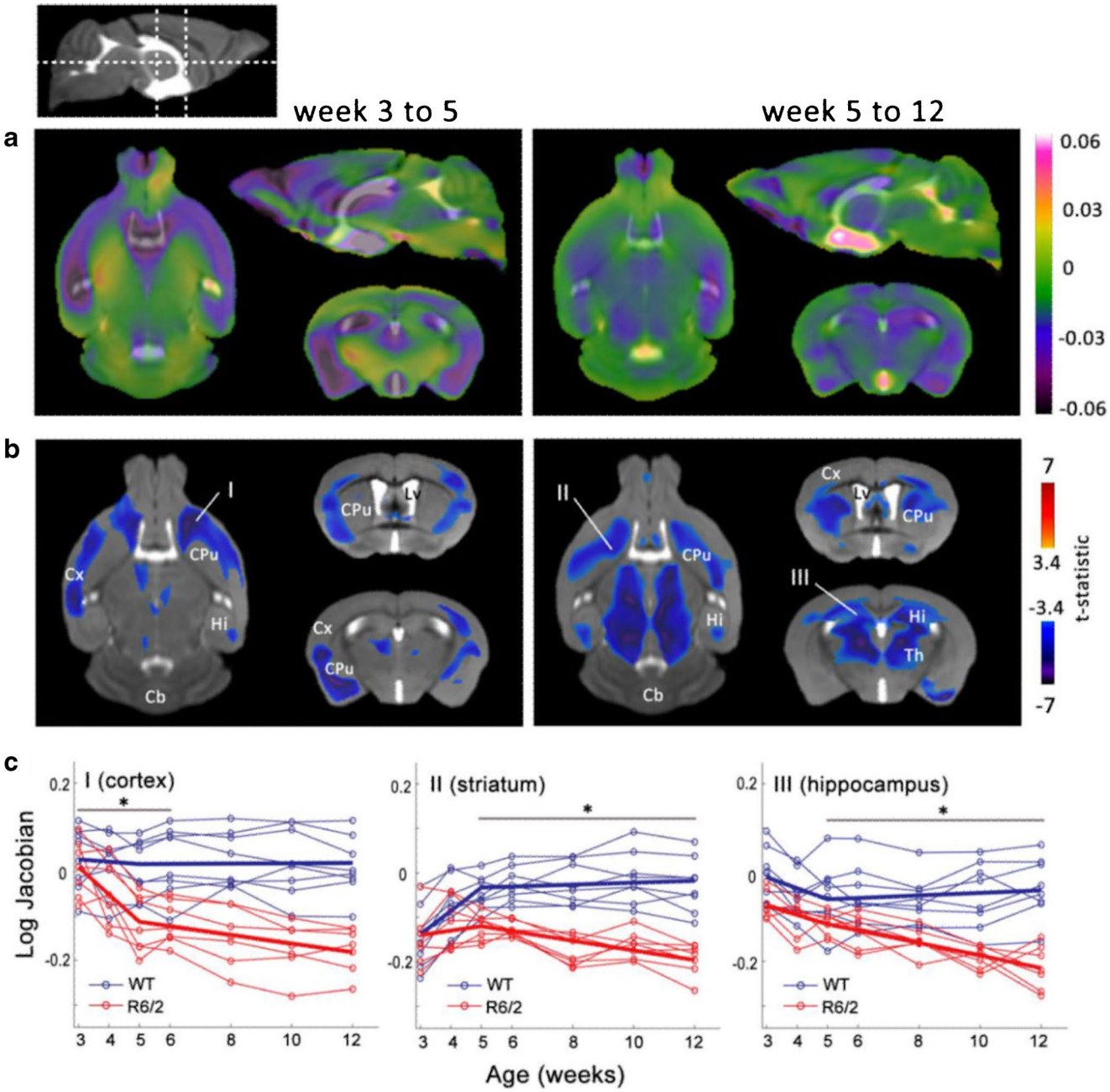

Fig. 6 Spatiotemporally-varying rate of atrophy in the R6/2 mouse model of HD. **a** Color-coded maps showing the average rate of atrophy in the week 3 to 5 and week 5 to 12 age spans are overlaid on orthogonal sections from the reference atlas. The color bar represents the difference in fitted slopes of log-Jacobian between the R6/2 and wild-type control cohorts, with negative values indicating progressive atrophy in the R6/2 brain compared to controls. **b** Statistical maps (false discovery rate = 0.05) showing regions with significant differences in the fitted slopes of log-Jacobian between the R6/2 and control brains overlaid on the reference atlas. The log-Jacobian profiles at selected voxel locations are plotted in (**c**), showing the individual trajectories (open circles) and the overall LME model fit (bold lines) for the wild-type (WT) and R6/2 cohorts. Structural abbreviations are: Cx: cerebral cortex, Cb: cerebellum, CPu: striatum, Hi: hippocampus, LV: lateral ventricle, Th: thalamus. (Aggarwal et al. 2012)

cortex can all be detected in early symptomatic R6/2 mice. Therefore, relative CBV measurements may serve as a biomarker of HD and can be used to evaluate the effects of therapies (Parievsky et al. 2012). The CBV alteration has been found also in YAC 128 mouse, in the dorsal striatum and in a region homologous to the posterior caudate in humans, confirming human data (Lewandowski et al. 2013). The "energy deficit," a decrease in metabolism displayed by HD patients, has been confirmed in HD models by a reduction of the signal from brown adipose tissue in MRI

(Lindenberg et al. 2014). Moreover, the glutamate plays an essential role in synaptic transmission and neuronal excitability, through the interaction with metabotropic receptors as metabotropic glutamate receptor (mGluR) 1 and mGluR5. In fact, the HD resulted to be characterized by a decrease of mGluR1 (Yamasaki et al. 2014). To better understand the role of glutamate in HD, Chemical Exchange Saturation Transfer imaging of glutamate (gluCEST) was developed to map glutamate distribution in the brain of a knock-in mouse model of HD. The T2 weghited MRI with gluCEST contrast have showed altered metabolic profile in *striatum* and *corpus callosum* in knock-in CAG140 model (Pépin et al. 2016).

In vivo PET/CT has been used with [^{11}C]-methylbenzamide to quantify the mGluR 1 decline in HD models, leading to a better understanding of its action in the pathophysiology of neuorodegenerative disorders (Yamasaki et al. 2014). The PET/CT technique also allowed the specific evaluation of the striatal MSNs' expression of phosphodiesterase 10A (PDE10A), a regulator of *striatum* signaling, using a novel [^{11}C]-radioligand (Tóth et al. 2015). The radioligand [^{11}C] T-773, has showed high affinity for PDE10A, with higher uptake in the striatum of PDE10A knock-out mice compared to control mice. Further studies will allow identifying other targets of PDE10A, reducing the activity of medium spiny neurons (Tóth et al. 2015).

Mouse models of multiple sclerosis

Multiple Sclerosis (MS) is a chronic inflammatory disease characterized by demyelination and axonal damage, leading to motor and cognitive dysfunction (Peruga et al. 2011). The MS is a complex disease that can manifests different symptoms and clinical signs. However, it is categorized into three classes based on the clinical course: the relapsing-remitting (RR), the Secondary Progressive, and the Primary progressive forms (for review, see Procaccini et al. 2015). To date, effective treatments for MS are unavailable, and for this reason different mouse models have been developed to study the different aspects of this complex pathology, such as immunological aspects and motor symptoms, as well as the de-re-myelination processes. The three mouse models of MS are: the experimental autoimmune/allergic encephalomyelitis (EAE); the virally induced chronic demyelinating disease, induced by Theiler's murine encephalomyelitis virus (TMEV) infection, and the toxin-induced demyelination.

The EAE mouse model is the most commonly used to study MS, as it enclose all the pathological features of MS, i.e. inflammation, demyelination, axonal loss and gliosis. This model is induced by the administration of antigens like the myelin basic protein (MBP) or the proteolipid protein (PLP), emulsified with complete Freund's adjuvant (CFA) or incomplete Freund's adjuvant (ICF), and followed by pertussis toxin administration, which allows efficient induction of active disease (Miller et al. 2007). The EAE model can reproduce both the RR than the primary progressive forms of MS depending on the mice genetic background, the antigen used for immunization and the immunization protocol itself (Berard et al. 2010; Dehghan et al. 2016). The RR form is reproduced with the subcutaneous injection of the immunodominant epitope of the PLP ($PLP_{139-151}$) in SJL/J mice; this model is used to study the pathogenesis and immune-regulation of T cell–mediated demyelination. On the other hand, the disease induced by the immunodominant MOG_{35-55} peptide in C57BL6/J mice is of chronic nature, and it represents a good approximation of the primary progressive human disease. The latter model is used to clarify the role of the immune system in the pathogenesis of MS, and the specific contribution of B cells, monocytes, $CD8^+$ and $CD4^+$ T cells (Berard et al. 2010).

Following the EAE immunization, mice develop an ascending flaccid paralysis, which is classified by a clinical score (Miller et al. 2007).

Among motor test, Rotarod test and Foot print analysis are the most useful in EAE, since they allow detecting disabilities earlier compared to the clinical score. Indeed, the EAE mice showed motor skills impairment in rotaroad test and footprint analysis, when the clinical score was still "normal" (Takemiya and Takeuchi 2013; Van den Berg et al. 2016). Behavioral investigation about anxiety and depression in EAE showed some conflicting results. Rodrigues and coll. analyzed memory and anxiety in animals using the elevated plus maze, the step inhibitory avoidance task and the object recognition test, and no differences were detectable between controls and EAE mice in any of the tests. In contrast, some studies showed deficit in memory using the MWM, as well as increased anxiety, measured by the elevated plus maze and the light/dark box, and depression-like behavior when performing forced swim and tail suspension tests (Acharjee et al. 2013). These cognitive alterations are associated to the neuroinflammatory process, which induces an increased level of IL-1b and TNF-a in the hypothalamus accompanied by increased corticosterone levels and hence changes in emotional and cognitive behavior (Acharjee et al. 2013).

The TMEV is a pathogen that infects only mice and induces chronic progressive inflammatory demyelinating disease. Different TMEV types are used: the GDVII type is highly virulent and it induces death within 1 to 2 weeks, whereas the TO type, which include the Daniels (DA) and the BeAn8386 (BeAn) strains, induces an acute polyencephalomyelitis (for review, see Procaccini et al. 2015). Two to 3 weeks post infection with the DA strain, mice develop a spastic paresis of the hind limbs, progressing in a severe spastic paralysis. In contrast, infection of SJL/J mice with the culture-adapted BeAn 8386 strain does not produce clinical evidence of a first-phase disease. Infected mice

begin to show clinical signs between 30 and 40 days post infection and they develop a chronic, progressive paralysis with no recovery or remitting episodes, similar to the primary progressive MS (McCarthy et al. 2012). The rotarod revealed to be effective in the evaluation of motor disabilities also in this model, beginning from the third month post-infection (Gilli et al. 2016). Furthermore, TMEV models suffer of thermal hyperalgesia and mechanical allodynia similarly to MS patients, evaluated by von Frey filament (Lynch et al. 2008).

The toxin-induced mouse model of demyelination is reproduce with the administration of toxic substances that cause demyelination, which can be reversed when the toxic substance is removed, allowing re-myelination (Abakumova et al. 2015). The most common agents used are cuprizone and lysolecithin. Cuprizone induces widespread demyelination in white and gray matter, affecting in particular oligodendrocytes, which die by apoptosis due to metabolic failure triggered by the chelating properties of cuprizone itself.

Behavioral tests for toxin model must be enough sensitive to reveal the de- and re-myelination effect. The modified wheel running test has been performed to reveals latent motor deficit in the cuprizone model, both during demyelination than remyelination. In this test, mice are first trained to run on a wheels composed of regularly spaced crossbars till maximal wheel-running performance is achieved. Subsequently, mice are exposed to wheels with irregularly spaced crossbars (complex wheel) demanding high-level motor coordination. Interestingly, mice fed with cuprizone diet showed motor impairment as compared to control mice both in simple than complex wheel. In contrast the remyelinated mice showed normal performance in simple wheel, but motor impairment in the complex wheel, indicating a latent motor skill deficit (Liebetanz and Merkler 2006). Elevated plus maze, as well as rotarod, did not show any symptoms recovery after 2 weeks of cuprizone deprivation, probably due a delayed remyelination after chronic demyelination (Abakumova et al. 2015).

Evidence of vascular changes in MS

The demyelinating lesions both in MS and in EAE are associated with an increased VEGF expression (Roscoe et al. 2009). In the EAE, the VEGF is expressed by astrocytes, monocytes and activated Th1 lymphocytes, all contributing to BBB breakdown. The inflammatory cells infiltrating the CNS trigger the pathophysiological processes behind MS, and promote and stimulate the angiogenesis. Some studies reported that angiogenesis in EAE is detectable in gray matter and the leptomeninges (Macmillan et al. 2011); more recently, an increase in vessels number and size has been showed in the area surrounding the demyelinating plaques (for review, see Lengfeld et al. 2014). Several factors contribute to the angiogenetic process, e.g. ipoxia, which induce releasing of VEGF, and macrophages of M2 phenotype, which are expressed in EAE mice during acute phase and remission. The M2 macrophages promote angiogenesis by producing Fibroblast growth factor (FGF), VEGF, platelet-derived growth factor (PDGF) and metalloproteinase, which are able to digest components of the extracellular matrix, facilitating immune cell infiltration into the CNS in the context of both MS and EAE (for review, see Lengfeld et al. 2014).

During EAE progression, an increased neuronal VEGF expression has been described in the early phase, correlated to the clinical score, while there are reductions in angiopoietin-1 and angiopoietin receptor Tie-2. By day 21 post induction, VEGF was markedly reduced, levels of angiopoietin-1 and angiopoietin-2 were augmented, this event corresponds with angiogenesis peak in gray matter and adjacent to the leptomeninges. These vascular changes suggest the angiogenesis implication in MS and EAE (Macmillan et al. 2011).

Recently, cerebrovascular remodeling has been demonstrated during the pre-symptomatic phase of EAE in regions not yet demyelinated, while increased blood vessels density has been assessed at later stages. Although angiogenesis precedes the demyelination, and hence the clinical symptoms of EAE, it has not yet determined if it has an advantageous or a detrimental effect (Boroujerdi et al. 2013).

Some studies showed that the administration of anti-angiogenic therapies during the acute phase of EAE produced a significant reduction of the process of demyelination and improved the clinical score (Roscoe et al. 2009). On the other hand, the increase in vessel number and size during EAE supports the release of trophic factor that enhances axonal remodeling and functional recovery (Muramatsu et al. 2012). Further studies are needed to evaluate the role played by angiogenesis in the progression of the disease. The inflammatory process affects cerebral and spinal cord gray matter in the early acute phase of TMEV models, while in the chronic phase the inflammatory infiltration is widespread to the spinal leptomeninges (for review, see Oleszak et al. 2004).

Preclinical imaging in MS

The MRI is considered the gold standard for the diagnosis of MS. On the other hand, lesions revealed by MRI do not always correlate with the level of patients' disability, thus the need for preclinical imaging studies (for review, see Nathoo et al. 2014). Thanks to MRI studies on EAE mice, it might be possible to find out if a correlation exists between imaging and cerebral lesions, i.e. demyelination,

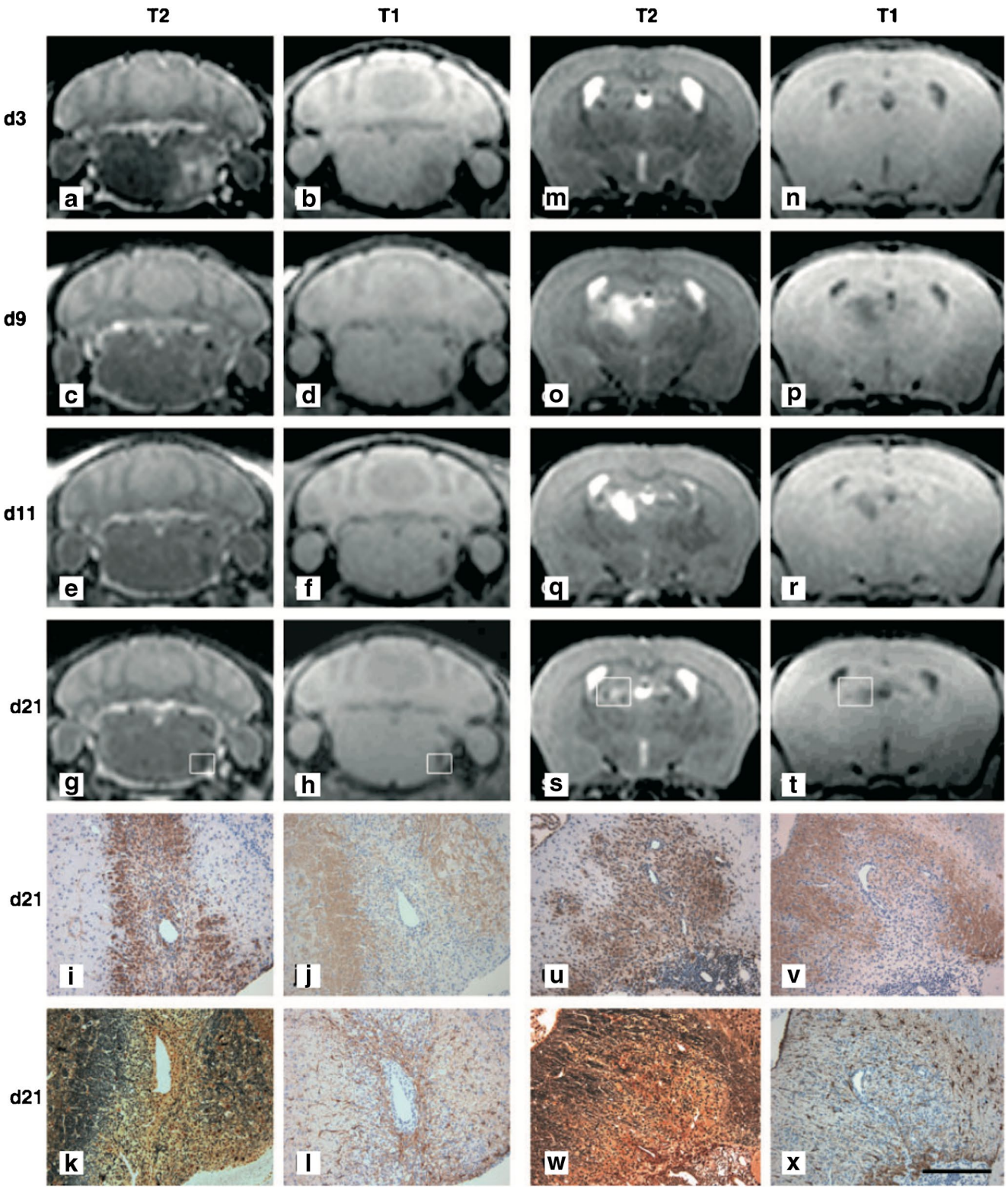

BBB breakdown, level of inflammation and vascular defects (Fig. 7).

In the acute phase, two types of lesion are identified by 2.35 T: strongly hypointense lesions on T1- and T2-weighted images, and isointense or slightly hypointense lesions on T1-weighted images, which result hyperintense on the corresponding T2-weighted images. Histopatological results confirmed that hypointense lesions on T1- and T2-weighted

◂**Fig. 7** Serial MRI of two distinct EAE lesions in one animal at days 3, 9, 11 and 21 after disease onset. A typical evolution of a type A brainstem lesion with a persistent hypointense centre on both T1- and T2-weighted MRI and a fading hyperintense rim on T2-weighted MRI is depicted in A^H (left columns). Final histological examination demonstrates infiltration by foamy macrophages/microglia (I; Mac-3), myelin loss (J; MBP), marked reduction in axonal density (K; Bielschowsky) and perivascularly accentuated gliosis in the area of most prominent tissue damage (L; GFAP). The atypical lesion adjacent to the lateral ventricle (right columns, M ^T) is first seen at day 9 (O, P). Part of the signal intensity changes may be related to CSF leakage (O ^R). Histopathology reveals infiltration with macrophages/microglia at day 21. Perivascular lymphocytic infiltrates are visible at the right lower image border (U; Mac-3). A circumscribed area of myelin loss is apparent (V; MBP). Axon density is reduced (W; Bielschowsky), and astrocytic gliosis is prominent around the lesion (X; GFAP). Rectangles in G, H, S and T indicate the respective areas depicted in histology (I^L and U^X). Original magnifications: I^L, U^X: 100; scale bar: X: 200 mm

correspond to axonal and myelin loss (Nessler et al. 2007). Axonal loss, characterized by hypointense areas, is observed in TMEV with T1 sequence. Brain atrophy has been demonstrated in TMEV mouse by ventricular enlargement, assessed with T2- weighted imaging, which correlates with progression of disease and motor impairment (Paz Soldán et al. 2015). The MRI revealed the reduction of the corpus callosum volume and the presence of hyperintense foci in the cuprizone model (Abakumova et al. 2015). The remyelination process in the pathological foci, studied with T2-weighted MRI, was detectable 2 weeks after cuprizone withdrawal (Abakumova et al. 2015). Magnetization transfer ratio (MTR) has been used to evaluate myelin loss in MS lesion in the cuprizone model, whereas in the EAE model it does not correlate with demyelination (Fjær et al. 2015).

In order to study BBB breakdown, the administration of Gd-DTPA, is useful to reveals areas of cerebral enhancement, which reflect the BBB disruption and thus early inflammation (Nessler et al. 2007). The Gd-based contrast agent, gadofluorine M (Gf) is more sensitive than other Gd chelates in detecting cerebral and spinal cord lesions BBB lesions, not seen with other contrast agents or in T2-weighted sequences (for review, see Nathoo et al. 2014).

The conjugate-nanoparticles for MRI is a useful tool for inflammatory lesions study. The vascular cell adhesion molecule (VCAM) is upregulated in MS and EAE, so that VCAM-Micrometer-sized iron oxide particles (MPIO) binding, is a good tool to study inflammation, as it is observed in the hindbrain and in the caudal part of the forebrain before both clinical signs and BBB breakdown appear (Serres et al. 2011). Recently, the efficacy of myeloperoxidase (MPO)-Gd contrast agent has been assessed to evaluate anti-inflammatory effect of the recombinant human form of gelsolin (rhp-GSN) in the EAE brain. The group of mice treated with rhp-GSN showed decreasing both in MPO activity and in neuroinflammation. The MPO-Gd MRI performed during peak acute inflammation demonstrated larger lesions and stronger signal enhancement in the control group compared to the rhp-GSN treatment group (Li-Chun et al. 2015). Imaging inflammation in TMEV has been carried out using T2 weighted imaging and USPIO, tracking inflammation and migration of specific cell types, including CD8 + and CD4 + T-cells.

Vascular alterations in EAE have been observed with T2* MRI as large hypointense vessels. Susceptibility-weighted imaging (SWI) is an MRI method that is very sensitive in analyzing venous vasculature, and in EAE mice it has been used to identify hypointensities due to intravascular deoxyhemoglobin (Nathoo et al. 2015).

Although MRI is the technique of choice to study MS and EAE, the PET imaging provides useful biological information at the molecular level, before anatomical changes occur (Mattner et al. 2013). The PET allows the quantification of cerebral myelin taking advantage of the binding capacity with the beta-sheet structure of MBP of tracers, such as the Thioflavine-T derivative 2-(40-methylaminophenyl)-6-hydroxybenzothiazole (PIB). This tracer has been already used to detect the plaques in AD, and it was able to detect demyelinated lesions in MS patients (Stankoff et al. 2011). The [^{11}C]-CIC and [^{11}C]-MeDAS, containing stilbene moiety which bind beta-sheet structure as well, and are promising tracer for monitoring demyelination and remyelination processes. During the demyelination process, the beta sheet structure is lost, and consequently the link with the contrast decreases, resulting in reduced uptake. Interestingly, only the [^{11}C]-MeDAS was able to detect remyelination in the cuprizone mouse model (De Paula Faria et al. 2014).

The PET/CT has proved useful also for the detection of inflammation in EAE models, thanks to the use of [^{18}F]-FDG tracer. It allows the quantification of glycolysis in the spinal cord, which correlates with the onset of EAE neurological symptoms and with the presence of inflammatory infiltrates detected by histological analysis (Radu et al. 2007). The neuroinflammatory processes have been studied with several tracers binding TSPO. Recently, The imidazopyridine [^{18}F]-PBR111 has been developed a sensitive radioligand of TSPO able to quantify the TSPO in the different RR phases of EAE, showing an increasing TSPO level in the first phase of disease correlated to mild to moderate clinical scores (Mattner et al. 2013).

Two-photon microscopy of EAE mice allowed observing axonal transport abnormalities evolution (for review, see Rougon et al. 2016). The NIRF vascular imaging agent AngioSense demonstrated vascular leaks in the BBB in EAE mice by elevated cerebral fluorescence even in pre-symptomatic mice, as well as an elevated spinal signal. Similarly, an increased protease activity was detected both in the brain and in the spinal chord of EAE mice (Eaton et al. 2013).

Open questions in neurodegeneration

The cerebral parenchyma is completely separated from circulating particles by the BBB, which prevents the leakage of molecules as well as of blood cells in the CNS. Hence, the CNS has a separate immune system, and microglial cells represent the equivalent of macrophages (for review, see Rougon et al. 2016). Among the etiopathogenetical theories on neuroinflammation and neurodegeneration, the escape of fibrinogen or the presence of micro-hemorrhages, due to BBB disruption, are advocated to play a key role as the primum movens in neuroinflammation (for review, see Zamboni 2006, for review, see; Hare et al. 2013; Onida and Davies 2014, for review, see; Rougon et al. 2016). Fibrinogen has been demonstrated to sustain CNS inflammation by recruiting myelin antigen-specific Th1 lymphocytes, which lead to secondary demyelination, in different reporter fluorescent mouse strains studied with two photon in vivo imaging (for review, see Ryu et al. 2015, for review, see; Rougon et al. 2016).

On the other hand, disturbances of cerebral venous outflow seem to lead to hemosiderin and excessive iron deposition and consequently to neuroinflammation, in accordance to the pathogenetic model of chronic venous disease of lower extremities (for review, see Zamboni 2006; for review, see; Hare et al. 2013; Onida and Davies 2014). Excess iron deposition and inflammatory lesions in the brain has been found in Alzheimer's and Parkinson's disease and in multiple sclerosis, as well as in the ageing brain (Onida and Davies 2014). To test the latter hypothesis, after the study of Atkinson and coll. who failed to demonstrate a correlation between cerebral venous outflow disruption and neuroinflammation/demyelination (Atkinson et al. 2012), our group recently set up a new and more aggressive surgical model of cerebral venous outflow occlusion (Auletta et al. 2017).

Iron oxide-labeled stem cells have been used in MS as well as ALS patients, but their tracking with MRI failed to allow a long term monitoring. In mouse models of ALS, an alternative tracking methods has been used, whit the aid of OI (bioluminescence) to non-invasively and longitudinally observe the fate of stem cells. In this case, stem cells were attacked by the host immune system, which is probably enhanced by the ALS hostile microenvironment (Srivastava et al. 2017).

In any case, efforts in developing new mouse models and new imaging technologies should continue to test etiopathogenetical theories as well as new therapies.

Compliance with ethical standards

Funding This study was funded by a research grant from the Italian Ministry for Education, University and Research in the framework of PRIN (2010XE5L2R_004). The funders had no role in study design, data collection and analysis, decision to publish, or preparation of the manuscript.

Conflict of interest No conflict exist. All authors of the manuscript declare they have no conflict of interest.

Ethical approval This article does not contain any studies with animals performed by any of the authors.

References

Abakumova, T. O., Kuz'kina, A. A., Zharova, M. E., Pozdeeva, D. A., Gubskii, I. L., Shepeleva, I. I., et al. (2015). Cuprizone model as a tool for preclinical studies of the efficacy of multiple sclerosis diagnosis and therapy. *Bullettin of Experimental Biology and Medicine, 159*(1), 111–115.

Acharjee, S., Nayani, N., Tsutsui, M., Hill, M. N., Ousman, S. S., & Pittman, Q. J. (2013). Altered cognitive-emotional behavior in early experimental autoimmune encephalitis–cytokine and hormonal correlates. *Brain, Behavior and Immunity, 33*, 164–172.

Aggarwal, M., Duan, W., Hou, Z., Rakesh, N., Peng, Q., Ross, C. A., et al. (2012). Spatiotemporal mapping of brain atrophy in mouse models of Huntington's disease using longitudinal in vivo magnetic resonance imaging. *NeuroImage, 60*(4), 2086–2095.

Agyare, E. K., Curran, G. L., Ramakrishnan, M., Yu, C. C., Poduslo, J. F., & Kandimalla, K. K. (2008). Development of a smart nano-vehicle to target cerebrovascular amyloid deposits and brain parenchymal plaques observed in Alzheimer's disease and cerebral amyloid angiopathy. *Pharmaceutical Research, 25*(11), 2674–2684.

Alvarez-Fischer, D., Blessmann, G., Trosowski, C., Béhé, M., Schurrat, T., Hartmann, A., et al. (2007). Quantitative [(123)I]-FP-CIT pinhole SPECT imaging predicts striatal dopamine levels, but not number of nigral neurons in different mouse models of Parkinson's disease. *NeuroImage, 38*(1), 5–12, 2007.

Andringa, G., Drukarch, B., Bol, J. G., de Bruin, K., Sorman, K., Habraken, J. B., et al. (2005). Pinhole SPECT imaging of dopamine transporters correlates with dopamine transporter immunohistochemical analysis in the MPTP mouse model of Parkinson's disease. *NeuroImage, 26*(4), 1150–1158.

Apelt, J., Kumar, A., & Schliebs, R. (2002). Impairment of cholinergic neurotransmission in adult and aged transgenic Tg2576 mouse brain expressing the Swedish mutation of human beta-amyloid precursor protein. *Brain Research, 953*(1–2), 17–30.

Arora, T., Mehta, A. K., Joshi, V., Mehta, K. D., Rathor, N., Mediratta, P. K., et al. (2011). Substitute of animals in drug research: an approach towards fulfillment of 4R's. *Indian Journal of Pharmaceutical Sciences, 73*(1), 1–6.

Atkinson, W., Forghani, R., Wojtkiewicz, G. R., Pulli, B., Iwamoto, Y., Ueno, T., et al. (2012). Ligation of the jugular veins does not result in brain inflammation or demyelination in mice. *PLoS ONE, 7*(3), e33671. https://doi.org/10.1371/journal.pone.0033671.

Auletta, L., Greco, A., Albanese, S., Meomartino, L., Salvatore, M., & Mancini, M. (2017). Feasibility and safety of two surgical techniques for the development of an animal model of jugular vein occlusion. *Experimental Bioliogy and Medicine (Maywood), 242*(1), 22–28.

Azzouz, M., Ralph, G. S., Storkebaum, E., Walmsley, L. E., Mitrophanous, K. A., & Kingsman, S. M. (2004). VEGF delivery with

retrogradely transported lentivector prolongs survival in a mouse ALS model. *Nature, 429*(6990), 413–417.

Bagga, P., Chugani, A. N., Varadarajan, K. S., & Patel, A. B. (2013). In vivo NMR studies of regional cerebral energetics in MPTP model of Parkinson's disease: recovery of cerebral metabolism with acute levodopa treatment. *Journal of Neurochemistry, 127*(3), 365–377.

Baranyi, M., Porceddu, P. F., Gölöncsér, F., Kulcsár, S., Otrokocsi, L., Kittel, Á., et al. (2016). Novel (Hetero)arylalkenyl propargylamine compounds are protective in toxin-induced models of Parkinson's disease. *Molecular Neurodegeneratio, 11*, 6.

Barbeito, A. G., Martinez-Palma, L., Vargas, M. R., Pehar, M., Mañay, N., Beckman, J. S., et al. (2016). Lead exposure stimulates VEGF expression in the spinal cord and extends survival in a mouse model of ALS. *Neurobiology of Disease, 37*(3), 574–580.

Beal, M. F., Brouillet, E., Jenkins, B. G., Ferrante, R. J., Kowall, N. W., Miller, J. M., et al. (1993). Neurochemical and histologic characterization of striatal excitotoxic lesions produced by the mitochondrial toxin 3-nitropropionic acid. *The Journal of Neuroscience, 13*(10), 4181–4192.

Beauquis, J., Vinuesa, A., Pomilio, C., Pavía, P., Galván, V., & Saravia, F. (2014). Neuronal and glial alterations, increased anxiety, and cognitive impairment before hippocampal amyloid deposition in PDAPP mice, model of Alzheimer's disease. *Hippocampus, 24*(3), 257–269.

Beckmann, N., Schuler, A., Mueggler, T., Meyer, E. P., Wiederhold, K. H., Staufenbiel, M., et al. (2003). Age-dependent cerebrovascular abnormalities and blood flow disturbances in APP23 mice modeling Alzheimer's disease. *Journal of Neuroscience, 23*(24), 8453–8459.

Bellucci, A., Luccarini, I., Scali, C., Prosperi, C., Giovannini, M. G., Pepeu, G., et al. (2006). Cholinergic dysfunction, neuronal damage and axonal loss in TgCRND8 mice. *Neurobiology of Disease, 32*(2), 260–272.

Benveniste, H., Ma, Y., Dhawan, J., Gifford, A., Smith, S. D., Feinstein, I., et al. (2007). Anatomical and functional phenotyping of mice models of Alzheimer's disease by MR microscopy. *Annals of the New York Academy of Sciences, 1097*, 12–29.

Berard, J. L., Wolak, K., Fournier, S., & David, S. (2010). Characterization of relapsing-remitting and chronic forms of experimental autoimmune encephalomyelitis in C57BL/6 mice. *Glia, 58*(4), 434–445.

Berggren, K. L., Lu, Z., Fox, J. A., Dudenhoeffer, M., Agrawal, S., & Fox, J. H. (2016). Neonatal iron supplementation induces striatal atrophy in female YAC128 Huntington's disease mice. *Journal of Huntingtons Disease, 5*(1), 53–63.

Betarbet, R., Sherer, T. B., & Greenamyre, J. T. (2002). Animal models of Parkinson's disease. *BioEssays, 24*(4), 308–318.

Bigini, P., Diana, V., Barbera, S., Fumagalli, E., Micotti, E., Sitia, L., et al. (2012). Longitudinal tracking of human fetal cells labeled with super paramagnetic iron oxide nanoparticles in the brain of mice with motor neuron disease. *PLoS One, 7*(2).

Bigot, C., Vanhoutte, G., Verhoye, M., & Van der Linden, A. (2013). Magnetization transfer contrast imaging reveals amyloid pathology in Alzheimer's disease transgenic mice. *NeuroImage, 87*, 111–119.

Blandini, F., & Armentero, M. T. (2012). Animal models of Parkinson's disease. *The FEBS Journal, 279*(7), 1156–1166.

Bogaerts, V., Theuns, J., & van Broeckhoven, C. (2008). Genetic findings in Parkinson's disease and translation into treatment: a leading role for mitochondria? *Genes, Brain Behaviour, 7*(2), 129–151.

Boix, J., Padel, T., & Paul, G. (2015). A partial lesion model of Parkinson's disease in mice–characterization of a 6-OHDA-induced medial forebrain bundle lesion. *Behavioural Brain Research, 284*, 196–206.

Bonito-Oliva, A., Masini, D., & Fisone, G. (2014). A mouse model of non-motor symptoms in Parkinson's disease: focus on pharmacological interventions targeting affective dysfunctions. *Frontiers in Behavioral Neuroscience*. https://doi.org/10.3389/fnbeh.2014.00290.

Boroujerdi, A., Welser-Alves, J. V., & Milner, R. (2013). Extensive vascular remodeling in the spinal cord of pre-symptomatic experimental autoimmune encephalomyelitis mice; increased vessel expression of fibronectin and the α5β1 integrin. *Experimentale Neurolology, 250*, 43–51.

Bose, P., Fielding, R., Ameis, K. M., & Vacca-Galloway, L. L. (1998). A novel behavioral method to detect motoneuron disease in Wobbler mice aged three to seven days old. *Brain Research, 813*(2), 334–342.

Bowman, G. L., & Quinn, J. F. (2008). Alzheimer's disease and the blood-brain barrier: past, present and future. *Aging Health, 4*(1), 47–55.

Brautigam, H., Steele, J. W., Westaway, D., Fraser, P. E., St George-Hyslop, P. H., Gandy, S., et al (2012). The isotropic fractionator provides evidence for differential loss of hippocampal neurons in two mouse models of Alzheimer's disease. *Molecular Neurodegeneration*. https://doi.org/10.1186/1750-1326-7-58.

Brockington, A., Wharton, S. B., Fernando, M., Gelsthorpe, C. H., Baxter, L., Ince, P. G., et al. (2006). Expression of vascular endothelial growth factor and its receptors in the central nervous system in amyotrophic lateral sclerosis. *Journal of Neuropathology and Experimental Neurology, 65*, 26–36.

Brooks, A. I., Chadwick, C. A., Gelbard, H. A., Cory-Slechta, D. A., & Federoff, H. J. (1999). Paraquat elicited neurobehavioral syndrome caused by dopaminergic neuron loss. *Brain Research, 823*(1–2), 1–10.

Brownell, A. L., Kuruppu, D., Kil, K. E., Jokivarsi, K., Poutiainen, P., Zhu, A., et al. (2015). PET imaging studies show enhanced expression of mGluR5 and inflammatory response during progressive degeneration in ALS mouse model expressing SOD1-G93A gene. *Journal of Neuroinflammation*. https://doi.org/10.1186/s12974-015-0439-9.

Bruijn, L. I., Miller, T. M., & Cleveland, D. W. (2004). Unraveling the mechanisms involved in motor neuron degeneration in ALS. *Annual Review of Neuroscience, 27*, 723–749.

Bryan, K. J., Lee, H., Perry, G., Smith, M. A., & Casadesus, G. (2009). Transgenic mouse models of Alzheimer's disease: Behavioral testing and considerations. In J. J. Buccafusco (Ed.), *Methods of behavior analysis in neuroscience, Chap. 1* (2nd edn.). Boca Raton: CRC Press/Taylor & Francis.

Buddeberg, B. S., Kerschensteiner, M., Merkler, D., Stadelmann, C., & Schwab, M. E. (2004). Behavioral testing strategies in a localized animal model of multiple sclerosis. *Journal of Neuroimmunology, 153*(1–2), 158–170.

Burgess, A., Dubey, S., Yeung, S., Hough, O., Eterman, N., Aubert, I., et al. (2014). Alzheimer disease in a mouse model: MR imaging-guided focused ultrasound targeted to the hippocampus opens the blood-brain barrier and improves pathologic abnormalities and behavior. *Radiology, 273*(3), 736–745.

Busche, M. A., Eichhoff, G., Adelsberger, H., Abramowski, D., Wiederhold, K. H., & Haass, C. (2008). Clusters of hyperactive neurons near amyloid plaques in a mouse model of Alzheimer's disease. *Science, 321*, 1686–1689. https://doi.org/10.1126/science.1162844.

Casteels, C., Vunckx, K., Aelvoet, S. A., Baekelandt, V., Bormans, G., Van Laere, K., et al. (2013). Construction and evaluation of quantitative small-animal PET probabilistic atlases for [^{18}F]FDG and [^{18}F]FECT functional mapping of the mouse brain. *PLoS One*. https://doi.org/10.1371/journal.pone.0065286.

Cepeda, C., Cummings, D. M., André, V. M., Holley, S. M., & Levine, M. S. (2010). Genetic mouse models of Huntington's disease:

focus on electrophysiological mechanisms. *ASN Neuro*. https://doi.org/10.1042/AN20090058.

Chamberlain, R., Reyes, D., Curran, G. L., Marjanska, M., Wengenack, T. M., Poduslo, J. F., et al. (2009). Comparison of amyloid plaque contrast generated by T2-weighted, T2*-weighted, and susceptibility-weighted imaging methods in transgenic mouse models of Alzheimer's disease. *Magnetic Resonance in Medicine, 61*(5), 1158–11564.

Chang, R., Liu, X., Li, S., & Li, X. J. (2015). Transgenic animal models for study of the pathogenesis of Huntington's disease and therapy. *Drug Design, Development and Therapy, 9*, 2179–2188.

Chen, L., Cagniard, B., Mathews, T., Jones, S., Koh, H. C., Ding, Y., et al. (2005). Age-dependent motor deficits and dopaminergic dysfunction in DJ-1 null mice. *The Journal of Biological Chemistry, 280*(22), 21418–21426.

Cheng, K. K., Chan, P. S., Fan, S., Kwan, S. M., Yeung, K. L., Wáng, Y. X., et al. (2015). Curcumin-conjugated magnetic nanoparticles for detecting amyloid plaques in Alzheimer's disease mice using magnetic resonance imaging (MRI). *Biomaterials, 44*, 155–172.

Cheng, Y., Peng, Q., Hou, Z., Aggarwal, M., Zhang, J., Mori, S., et al. (2011). Structural MRI detects progressive regional brain atrophy and neuroprotective effects in N171-82Q Huntington's disease mouse model. *NeuroImage, 56*(3), 1027–1034.

Choi, C. I., Lee, Y. D., Gwag, B. J., Cho, S.L., Kim, S. S., & Suh-Kim, H. (2008). Effects of estrogen on lifespan and motor functions in female hSOD1 G93A transgenic mice. *Journal of the Neurological Sciences, 268*(1–2), 40–47.

D'Hooge, R., & De Deyn, P. P. (2001). Applications of the Morris water maze in the study of learning and memory. *Brain Research Reviews, 36*(1), 60–90.

de Paula Faria, D., de Vries, E. F., Sijbesma, J. W., Dierckx, R. A., Buchpiguel, C. A., & Copray, S. (2014). PET imaging of demyelination and remyelination in the cuprizone mouse model for multiple sclerosis: a comparison between [11C]CIC and [11C] MeDAS. *NeuroImage, 87*, 395–402.

Deacon, R. M., Koros, E., Bornemann, K. D., & Rawlins, J. N. (2009). Aged Tg2576 mice are impaired on social memory and open field habituation tests. *Behavioural Brain Research, 197*(2), 466–468.

Dehghan, S., Mohajeri, M., & Javan, M. (2016). Animal models of multiple sclerosis. 5th Tehran IBRO School of Neuroscience, Chap. 1, pp. 3–16.

Denny, C. A., Desplats, P. A., Thomas, E. A., & Seyfried, T. N. (2010). Cerebellar lipid differences between R6/1 transgenic mice and humans with Huntington's disease. *Journal of Neurochemistry, 115*(3), 748–758.

Dewachter, I., van Dorpe, J., Spittaels, K., Tesseur, I., Van Den Haute, C., Moechars, D., et al. (2000). Modeling Alzheimer's disease in transgenic mice: effect of age and of presenilin1 on amyloid biochemistry and pathology in APP/London mice. *Experimental Gerontology, 35*(6–7), 831–841.

Dibaj, P., Steffens, H., Zschuntzsch, J., Nadrigny, F., Schomburg, E. D., Kirchhoff, F., et al. (2011). In vivo imaging reveals distinct inflammatory activity of CNS microglia versus PNS macrophages in a mouse model for ALS. *PLoS One*. https://doi.org/10.1371/journal.pone.0017910.

Diorio, D., Welner, S. A., Butterworth, R. F., Meaney, M. J., & Suranyi-Cadotte, B. E. (1991). Peripheral benzodiazepine binding sites in Alzheimer's disease frontal and temporal cortex. *Neurobiology of Aging, 12*(3), 255–258.

Dorr, A., Sahota, B., Chinta, L. V., Brown, M. E., Lai, A. Y., Ma, K., et al. (2012). Amyloid-β-dependent compromise of microvascular structure and function in a model of Alzheimer's disease. *Brain: a Journal of Neurology, 135*(Pt 10), 3039–3050.

Drouin-Ouellet, J., Sawiak, S. J., Cisbani, G., Lagacé, M., Kuan, W. L., Saint-Pierre, M., et al. (2015). Cerebrovascular and blood-brain barrier impairments in Huntington's disease: potential implications for its pathophysiology. *Annals of Neurology, 78*(2), 160–177.

Eaton, V. L., Vasquez, K. O., Goings, G. E., Hunter, Z. N., Peterson, J. D., & Miller, S. D. (2013). Optical tomographic imaging of near infrared imaging agents quantifies disease severity and immunomodulation of experimental autoimmune encephalomyelitis in vivo. *Journal of Neuroinflammation, 10*, 138.

Elder, G. A., Gama Sosa, M. A., & De Gasperi, R. (2010). Transgenic mouse models of Alzheimer's disease. *Mount Sinai Journal of Medicine: A Journal of Translational and Personalized Medicine, 77*(1), 69–81.

Evans, M. C., Serres, S., Khrapitchev, A. A., Stolp, H. B., Anthony, D. C., Talbot, K., et al. (2014). T_2-weighted MRI detects presymptomatic pathology in the SOD1 mouse model of ALS. *Journal of Cerebral Blood Flow & Metabolism, 34*(5), 785–793.

Faull, R. L., & Laverty, R. (1969). Changes in dopamine levels in the corpus striatum following lesions in the substantia nigra. *Experimental Neurology, 23*(3), 332–340.

Fernagut, P. O., & Chesselet, M. F. (2004). Alpha-synuclein and transgenic mouse models. *Neurobiology of Disease, 17*(2), 123–130.

Fernagut, P. O., Diguet, E., Stefanova, N., Biran, M., Wenning, G. K., & Canioni, P. (2002). Subacute systemic 3-nitropropionic acid intoxication induces a distinct motor disorder in adult C57Bl/6 mice: behavioural and histopathological characterisation. *Neuroscience, 114*(4), 1005–1014.

Fernagut, P. O., Hutson, C. B., Fleming, S. M., Tetreaut, N. A., Salcedo, J., Masliah, E., et al. (2007). Behavioral and histopathological consequences of paraquat intoxication in mice: effects of alpha-synuclein over-expression. *Synapse, 61*(12), 991–1001.

Fernandes, H. B., & Raymond, L. A. (2009). NMDA receptors and Huntington's disease. In A. M. Van Dongen (Ed), *Biology of the NMDA receptor*. Boca Raton: CRC Press/Taylor & Francis. Chapter 2.

Fjær, S., Bø, L., Myhr, K. M., Torkildsen, Ø., & Wergeland, S. (2015). Magnetization transfer ratio does not correlate to myelin content in the brain in the MOG-EAE mouse model. *Neurochemistry International, 83–84*, 28–40.

Fleming, S. M., Salcedo, J., Fernagut, P. O., Rockenstein, E., Masliah, E., Levine, M. S., et al. (2004). Early and progressive sensorimotor anomalies in mice overexpressing wild-type human alpha-synuclein. *The Journal of Neuroscience, 24*(42), 9434–9440.

Fleming, S. M., Tetreault, N. A., Mulligan, C. K., Hutson, C. B., Masliah, E., & Chesselet, M. F. (2008). Olfactory deficits in mice overexpressing human wildtype alpha-synuclein. *The European Journal of Neuroscience, 28*(2), 247–256.

Fleming, S. M., Ekhator, O. R., & Ghisays, V. (2013). Assessment of sensorimotor function in mouse models of Parkinson's disease. *Journal of Visualized Experiments, 76*, 50303, 2013.

Franciosi, S., Ryu, J. K., Shim, Y., Hill, A., Connolly, C., Hayden, M. R., et al. (2012). Age-dependent neurovascular abnormalities and altered microglial morphology in the YAC128 mouse model of Huntington disease. *Neurobiology of Disease, 45*(1), 438–439.

Furtado, J. C., & Mazurek, M. F. (1996). Behavioral characterization of quinolinate-induced lesions of the medial striatum: relevance for Huntington's disease. *Experimental Neurology, 138*(1), 158–168.

Gargiulo, S., Anzilotti, S., Coda, A. R. D., Gramanzini, M., Greco, A., Panico, M., et al. (2016). Imaging of brain TSPO expression in a mouse model of amyotrophic lateral sclerosis with 18F-DPA-714 and micro-PET/CT. *European Journal of Nuclear Medicine and Molecular Imaging*. https://doi.org/10.1007/S00259-016-3311-Y.

George, S., Rönnbäck, A., Gouras, G. K., Petit, G. H., Grueninger, F., Winblad, B., et al. (2014). Lesion of the subiculum reduces the spread of amyloid beta pathology to interconnected brain regions in a mouse model of Alzheimer's disease. *Acta Neuropatholica Communications, 2*, 17.

Gilli, F., Chen, X., Pachner, A. R., & Gimi, B. (2016). High-resolution diffusion tensor spinal cord MRI measures as biomarkers of disability progression in a rodent model of progressive multiple sclerosis. *PLoS One, 11*(7), e0160071.

Giménez-Llort, L., Blázquez, G., Cañete, T., Johansson, B., Oddo, S., Tobeña, A., et al. (2007). Modeling behavioral and neuronal symptoms of Alzheimer's disease in mice: a role for intraneuronal amyloid. *Neuroscience and Biobehavioral Review, 31*(1), 125–147.

Girard, S. D., Jacquet, M., Baranger, K., Migliorati, M., Escoffier, G., Bernard, A., et al. (2014). Onset of hippocampus-dependent memory impairments in 5XFAD transgenic mouse model of Alzheimer's disease. *Hippocampus, 24*(7), 762–772.

Glorioso, J. C., Cohen, J. B., Carlisle, D. L., Munoz-Sanjuan, I., & Friedlander, R. M. (2015). Moving toward a gene therapy for Huntington's disease. *Gene Therapy, 22*(12), 931–933.

Gorton, L. M., Vuckovic, M. G., Vertelkina, N., Petzinger, G. M., Jakowec, M. W., & Wood, R. I. (2010). Exercise effects on motor and affective behavior and catecholamine neurochemistry in the MPTP-lesioned mouse. *Behavioural Brain Research, 213*(2), 253–262.

Grandjean, J., Schroeter, A., He, P., Tanadini, M., Keist, R., Krstic, D., et al. (2014). Early alterations in functional connectivity and white matter structure in a transgenic mouse model of cerebral amyloidosis. *Journal of Neuroscience, 34*(41), 13780–11389.

Grant, R. A., Sharp, P. S., Kennerley, A. J., Berwick, J., Grierson, A., Ramesh, T., et al. (2014). Abnormalities in whisking behaviour are associated with lesions in brain stem nuclei in a mouse model of amyotrophic lateral sclerosis. *Behavioural Brain Research, 259*, 274–283.

Gu, H., Robison, G., Hong, L., Barrea, R., Wei, X., Farlow, M. R., et al. (2012). Increased β-amyloid deposition in Tg-SWDI transgenic mouse brain following in vivo lead exposure. *Toxicology Letters, 213*(2), 211–219.

Günther, R., Suhr, M., Koch, J. C., Bähr, M., Lingor, P., & Tönges, L. (2012). Clinical testing and spinal cord removal in a mouse model for amyotrophic lateral sclerosis (ALS). *Journal of Visualized Experiments*. https://doi.org/10.3791/3936.

Hall, A. M., & Roberson, E. D. (2012). Mouse Models of Alzheimer's Disease. *Brain Research Bulletin, 88*(1), 3–12.

Hanson, J. E., Orr, A. L., & Madison, D. V. (2010). Altered hippocampal synaptic physiology in aged parkin-deficient mice. *Neuromolecular Medicine, 12*(3), 270–276.

Hare, D., Ayton, S., Bush, A., & Lei, P. (2013). A delicate balance: iron metabolism and diseases of the brain. *Frontiers in Aging Neuroscience, 5*(34), 1–19. https://doi.org/10.3389/fnagi.2013.00034.

Havas, D., Hutter-Paier, B., Ubhi, K., Rockenstein, E., Crailsheim, K., Masliah, E., et al. (2012). A longitudinal study of behavioral deficits in an AβPP transgenic mouse model of Alzheimer's disease. *Journal of Alzheimer's Disease, 25*(2), 231–243.

Hawkes, C. A., & McLaurin, J. (2009). Selective targeting of perivascular macrophages for clearance of beta-amyloid in cerebral amyloid angiopathy. *Proceeding of the National Academy of Scinces of United States of America, 106*(4), 1261–1266.

Hébert, F., Grand'maison, M., Ho, M. K., Lerch, J. P., Hamel, E., & Bedell, B. J. (2013). Cortical atrophy and hypoperfusion in a transgenic mouse model of Alzheimer's disease. *Neurobiology of Aging, 34*(6), 1644–1652.

Helpern, J. A., Lee, S. P., Falangola, M. F., Dyakin, V. V., Bogart, A., Ardekani, B., et al. (2004). MRI assessment of neuropathology in a transgenic mouse model of Alzheimer's disease. *Magnetic Resonance in medicine, 51*(4), 794–798.

Heng, M. Y., Tallaksen-Greene, S. J., Detloff, P. J., & Albin, R. L. (2007). Longitudinal evaluation of the Hdh(CAG)150 knock-in murine model of Huntington's disease. *The Journal of Neuroscience, 27*(34), 8989–8998.

Heng, M. Y., Detloff, P. J., & Albin, R. L. (2008). Rodent genetic models of Huntington disease. *Neurobiology of Disease, 32*(1), 1–9.

Hickey, M. A., Zhu, C., Medvedeva, V., Lerner, R. P., Patassini, S., Franich, N. R., et al. (2012). Improvement of neuropathology and transcriptional deficits in CAG 140 knock-in mice supports a beneficial effect of dietary curcumin in Huntington's disease. *Molecular Neurodegeneration*. https://doi.org/10.1186/1750-1326-7-12.

Holcomb, L., Gordon, M. N., McGowan, E., Yu, X., Benkovic, S., Jantzen, P., et al. (1998). Accelerated Alzheimer-type phenotype in transgenic mice carrying both mutant amyloid precursor protein and presenilin 1 transgenes. *Nature Medicine, 4*(1), 97–100.

Honer, M., Hengerer, B., Blagoev, M., Hintermann, S., Waldmeier, P., & Schubiger, P. A. (2006). Comparison of [18F]FDOPA, [18F] FMT and [18F]FECNT for imaging dopaminergic neurotransmission in mice. *Nuclear Medicine and Biology, 33*(5), 607–614.

Hsiao, H. Y., Chen, Y. C., Huang, C. H., Chen, C. C., Hsu, Y. H., Chen, H. M., et al. (2015). Aberrant astrocytes impair vascular reactivity in Huntington disease. *Annals of Neurology, 78*(2), 178–192.

Hua, J., Unschuld, P. G., Margolis, R. L., van Zijl, P. C., & Ross, C. A. (2014). Elevated arteriolar cerebral blood volume in prodromal Huntington's disease. *Movementi Disorders, 29*(3), 396–401.

Iascone, D. M., Padidam, S., Pyfer, M. S., Zhang, X., Zhao, L., & Chin, J. (2013). Impairments in neurogenesis are not tightly linked to depressive behavior in a transgenic mouse model of Alzheimer's disease. *PLoS One*. https://doi.org/10.1371/journal.pone.0079651.

Jacobs, A. H., Tavitian, B., & INMiND Consortium. (2012). Noninvasive molecular imaging of neuroinflammation. *Journal of Cerebral Blood Flow and Metabolism, 32*(7), 1393–1415.

James, M. L., Belichenko, N. P., Nguyen, T. V., Andrews, L. E., Ding, Z., Liu, H., et al. (2015). PET imaging of translocator protein (18 kDa) in a mouse model of Alzheimer's disease using N-(2,5-dimethoxybenzyl)-2-18F-fluoro-N-(2-phenoxyphenyl)acetamide. *Journal of Nuclear Medicine, 56*(2), 311–316.

Jankowsky, J. L., Fadale, D. J., Anderson, J., Xu, G. M., Gonzales, V., Jenkins, N. A., et al. (2004). Mutant presenilins specifically elevate the levels of the 42 residue beta-amyloid peptide in vivo: evidence for augmentation of a 42-specific gamma secretase. *Human Molecular Genetics, 13*(2), 159–170.

Jaruszewski, K. M., Curran, G. L., Swaminathan, S. K., Rosenberg, J. T., Grant, S. C., Ramakrishnan, S., et al. (2014). Multimodal nanoprobes to target cerebrovascular amyloid in Alzheimer's disease brain. *Biomaterials, 35*(6), 1967–1976.

Jellinger, K. A. (2002). Alzheimer disease and cerebrovascular pathology: an update. *Journal of Neural Transmission Vienna, 109*(5–6), 813–836.

Joglar, B., Rodriguez-Pallares, J., Rodriguez-Perez, A. I., Rey, P., Guerra, M. J., & Labandeira-Garcia, J. L. (2009). The inflammatory response in the MPTP model of Parkinson's disease is mediated by brain angiotensin: relevance to progression of the disease. *Journal of Neurochemistry, 109*(2), 656–669.

Kandimalla, K. K., Wengenack, T. M., Curran, G. L., Gilles, E. J., & Poduslo, J. F. (2007). Pharmacokinetics and amyloid plaque targeting ability of a novel peptide-based magnetic resonance contrast agent in wild-type and Alzheimer's disease transgenic mice. *The Journal of Pharmacology and Experimental Therapy, 322*(2), 541–549.

Kane, A. D., Niu, Y., Herrera, E. A., Morton, A. J., & Giussani, D. A. (2016). Impaired nitric oxide mediated vasodilation in the peripheral circulation in the R6/2 mouse model of Huntington's disease. *Scientific Reports, 6*, 25979.

Kara, F., Dongen, E. S., Schliebs, R., Buchem, M. A., Groot, H. J., & Alia, A. (2012). Monitoring blood flow alterations in the Tg2576 mouse model of Alzheimer's disease by in vivo magnetic resonance angiography at 17.6 T. *NeuroImage, 60*(2), 958–966.

Keifer, O. P. Jr., O'Connor, D. M., & Boulis, N. M. (2014). Gene and protein therapies utilizing VEGF for ALS. *Pharmacology & Therapeutics, 141*(3), 261–271.

Keller, A. F., Gravel, M., & Kriz, J. (2009). Live imaging of amyotrophic lateral sclerosis pathogenesis: disease onset is characterized by marked induction of GFAP in Schwann cells. *Glia, 57*(10), 1130–1142.

Kennel, P., Revah, F., Bohme, G. A., Bejuit, R., Gallix, P., Stutzmann, J. M., et al. (2000). Riluzole prolongs survival and delays muscle strength deterioration in mice with progressive motor neuronopathy (pmn). *Journal of Neurolological Sciences, 180*(1–2), 55–61.

Khalil, M. M., Tremoleda, J. L., Bayomy, T. B., & Gsell, W. (2011). Molecular SPECT imaging: an overview. *International Journal of Molecular Imaging, 2011*, 796025.

Kikuta, S., Nakamura, Y., Yamamura, Y., Tamura, A., Homma, N., Yanagawa, Y., et al. (2015). Quantitative activation-induced manganese-enhanced MRI reveals severity of Parkinson's disease in mice. *Scientific Reports*. https://doi.org/10.1038/srep12800.

Kirkinezos, I. G., Hernandez, D., Bradley, W. G., & Moraes, C. T. (2003). Regular exercise is beneficial to a mouse model of amyotrophic lateral sclerosis. *Annals of Neurology, 53*(6), 804–807.

Kishimoto, Y., Higashihara, E., Fukuta, A., Nagao, A., & Kirino, Y. (2013). Early impairment in a water-finding test in a longitudinal study of the Tg2576 mouse model of Alzheimer's disease. *Brain Research, 1491*, 117–126.

Klein, C., Hain, E. G., Braun, J., Riek, K., Mueller, S., Steiner, B., et al. (2014). Enhanced adult neurogenesis increases brain stiffness: in vivo magnetic resonance elastography in a mouse model of dopamine depletion. *PLoS One*. https://doi.org/10.1371/journal.pone.0092582.

Klein, W. L. (2002). A toxicity in Alzheimer's disease: globular oligomers (ADDLs) as new vaccine and drug targets. *Neurochemistry International, 41*, 345–352.

Klohs, J., Politano, I. W., Deistung, A., Grandjean, J., Drewek, A., Dominietto, M., et al. (2013). Longitudinal assessment of amyloid pathology in transgenic ArcAβ mice using multi-parametric magnetic resonance imaging. *PLoS One, 8*(6), e66097.

Klohs, J., Rudin, M., Shimshek, D. R., & Beckmann, N. (2014). Imaging of cerebrovascular pathology in animal models of Alzheimer's disease. *Frontiers in Aging Neuroscience*. https://doi.org/10.3389/fnagi.2014.00032.

Knight, E. M., Williams, H. N., Stevens, A. C., Kim, S. H., Kottwitz, J. C., Morant, A. D., et al. (2015). Evidence that small molecule enhancement of β-hexosaminidase activity corrects the behavioral phenotype in Dutch APP(E693Q) mice through reduction of ganglioside-bound Aβ. *Molecular Psychiatry, 20*(1), 109–117.

Knippenberg, S., Thau, N., Dengler, R., & Petri, S. (2010). Significance of behavioural tests in a transgenic mouse model of amyotrophic lateral sclerosis (ALS). *Behavioural Brain Research, 213*(2), 82–87.

Knippenberg, S., Thau, N., Schwabe, K., Dengler, R., Schambach, A., Hass, R., et al. (2012). Intraspinal injection of human umbilical cord blood-derived cells is neuroprotective in a transgenic mouse model of amyotrophic lateral sclerosis. *Neurodegenerative Disease, 9*(3), 107–120.

Knobloch, M., Konietzko, U., Krebs, D. C., & Nitsch, R. M. (2007). Intracellular Ab and cognitive deficits precede b-amyloid deposition in transgenic arcAb mice. *Neurobiology of Aging, 28*(1), 1297–1306.

Kreiner, G. (2015). Compensatory mechanisms in genetic models of neurodegeneration: are the mice better than humans? *Frontiers in Cellular Neuroscience*. https://doi.org/10.3389/fncel.2015.00056.

Kudo, T., Loh, D. H., Tahara, Y., Truong, D., Hernández-Echeagaray, E., & Colwell, C. S. (2014). Circadian dysfunction in response to in vivo treatment with the mitochondrial toxin 3-nitropropionic acid. *ASN Neuro, 6*(1), e00133.

Kumar-Singh, S., Dewachter, I., Moechars, D., Lübke, U., De Jonghe, C., Ceuterick, C., et al. (2000). Behavioral disturbances without amyloid deposits in mice overexpressing human amyloid precursor protein with Flemish (A692G) or Dutch (E693Q) mutation. *Neurobiology of Disease, 7*(1), 9–22.

Kumar-Singh, S., Pirici, D., McGowan, E., Serneels, S., Ceuterick, C., Hardy, J., al (2005). Dense-core plaques in Tg2576 and PSAPP mouse models of Alzheimer's disease are centered on vessel walls. *The American Journal of Pathology, 167*(2), 527–543.

Lacor, P. N., Buniel, M. C., Chang, L., Fernandez, S. J., Gong, Y., Viola, K. L., et al. (2004). Synaptic targeting by Alzheimer's-related amyloid oligomers. *The Journal of Neuroscience, 24*(45), 10191–10200.

Lai, A. Y., Dorr, A., Thomason, L. A., Koletar, M. M., Sled, J. G., Stefanovic, B., et al. (2015). Venular degeneration leads to vascular dysfunction in a transgenic model of Alzheimer's disease. *Brain: a Journal of Neurology, 138*, 1046–1058.

Lee, J. D., Huang, C. H., Yang, S. T., Chu, Y. H., Shieh, Y. Y., Chen, J. W., et al. (2013). MRI/SPECT-based diagnosis and CT-guided high-intensity focused-ultrasound treatment system in MPTP mouse model of Parkinson's disease. *Medical Engineering & Physics, 35*(2), 222–230.

Lee, W. T., & Chang, C. (2004). Magnetic resonance imaging and spectroscopy in assessing 3-nitropropionic acid-induced brain lesions: an animal model of Huntington's disease. *Progress in Neurobiology, 72*(2), 87–110.

Lee, M.-J., Wang, K., Kim, I.-S., Lee, B.-H., & Han, H. S. (2012). Molecular imaging of cell death in an experimental model of Parkinson's disease with a novel apoptosis-targeting peptide. *Molecular Imaging and Biology, 14*(2), 147–155.

Lengfeld, J., Cutforth, T., & Agalliu, D. (2014). The role of angiogenesis in the pathology of multiple sclerosis. *Vascular Cell, 6*(1), 23.

Lerch, J. P., Carroll, J. B., Spring, S., Bertram, L. N., Schwab, C., Hayden, M. R., et al. (2008). Automated deformation analysis in the YAC128 Huntington disease mouse model. *NeuroImage, 39*(1), 32–39.

Lewandowski, N. M., Bordelon, Y., Brickman, A. M., Angulo, S., Khan, U., Muraskin, J., et al. (2013). Regional vulnerability in Huntington's disease: fMRI-guided molecular analysis in patients and a mouse model of disease. *Neurobiology of Disease, 52*, 84–93.

Li, H., Guo, Q., Inoue, T., Polito, V. A., Tabuchi, K., Hammer, R. E., et al. (2014). Vascular and parenchymal amyloid pathology in an Alzheimer disease knock-in mouse model: interplay with cerebral blood flow. *Molecular Neurodegeneration*. https://doi.org/10.1186/1750-1326-9-28.

Li, Y., Zhu, X., Wang, P., Wang, J., Liu, S., Li, F., et al. (2016). Detection of Aβ plaque deposition in MR images based on pixel feature selection and class information in image level. *BioMedical Engineering OnLine, 15*, 108.

Li-Chun, H. K., Schob, S., Zeller, M. W., Pulli, B., Ali, M., Wang, C., et al. (2015). Gelsolin decreases actin toxicity and inflammation in murine multiple sclerosis. *Journal of Neuroimmunology, 287*, 36–42.

Liebetanz, D., & Merkler, D. (2006). Effects of commissural de- and remyelination on motor skill behaviour in the cuprizone mouse model of multiple sclerosis. *Experimental Neurology, 202*(1), 217–224.

Lin, A. J., Liu, G., Castello, N. A., Yeh, J. J., Rahimian, R., Lee, G., et al. (2014). Optical imaging in an Alzheimer's mouse model reveals amyloid-β-dependent vascular impairment. *Neurophotonics, 1*(1), 011005.

Lin, C. Y., Hsu, Y. H., Lin, M. H., Yang, T. H., Chen, H. M., Chen, Y. C., et al. (2013). Neurovascular abnormalities in humans and

mice with Huntington's disease. *Experimental Neurology, 250*, 20–30.

Lin, W., Abendschein, D. R., Celik, A., Dolan, R. P., Lauffer, R. B., Walovitch, R. C., et al. (1997). Intravascular contrast agent improves magnetic resonance angiography of carotid areries in minipigs. *Journal of Magnetic Resonance Imaging, 7*, 963–971.

Lindenberg, K. S., Weydt, P., Müller, H. P., Bornstedt, A., Ludolph, A. C., Landwehrmeyer, G. B., et al. (2014). Two-point magnitude MRI for rapid mapping of brown adipose tissue and its application to the R6/2 mouse model of Huntington disease. *PLoS One*. https://doi.org/10.1371/journal.pone.0105556.

Litteljohn, D., Nelson, E., Bethune, C., & Hayley, S. (2011). The effects of paraquat on regional brain neurotransmitter activity, hippocampal BDNF and behavioural function in female mice. *Neuroscience Letters, 502*(3), 186–191.

Liu, Y., Sun, J. D., Song, L. K., Li, J., Chu, S. F., Yuan, Y. H., et al. (2015). Environment-contact administration of rotenone: a new rodent model of Parkinson's disease. *Behavioural Brain Research, 294*, 149–161.

Lockhart, A., Lamb, J. R., Osredkar, T., Sue, L., Joyce, J. N., Ye, L., et al. (2007). PIB is a non-specific imaging marker of amyloid-beta (Abeta) peptide-related cerebral amyloidosis. *Brain: a Journal of Neurology, 130*(Pt 10), 2607–2615.

Lowry, K. S., Murray, S. S., McLean, C. A., Talman, P., Mathers, S., Lopes, E. C., et al. (2001). A potential role for the p75 low-affinity neurotrophin receptor in spinal motor neuron degeneration in murine and human amyotrophic lateral sclerosis. *Amyotrophic Lateraleral Sclerosis and Other Motor Neuron Disorders, 2*(3), 127–134.

Lu, W., Yang, S., Zhang, L., Chen, L., Chao, F. L., Luo, Y. M., et al. (2016). Decreased myelinated fibers in the hippocampal dentate gyrus of the Tg2576 mouse model of Alzheimer's disease. *Current Alzheimer Research, 13*(9), 1040–1047.

Luchtman, D. W., Shao, D., & Song, C. (2009). Behavior, neurotransmitters and inflammation in three regimens of the MPTP mouse model of Parkinson's disease. *Phisiology and Behavior, 98*(1–2), 130–138.

Lunn, J. S., Sakowski, S. A., Kim, B., Rosenberg, A. A., & Feldman, E. L. (2009). Vascular endothelial growth factor prevents G93A-SOD1-induced motor neuron degeneration. *Developmental Neurobiology, 69*(13), 871–884.

Luo, F., Rustay, N. R., Ebert, U., Hradil, V. P., Cole, T. B., Llano, D. A., et al. (2012). Characterization of 7- and 19-month-old Tg2576 mice using multimodal in vivo imaging: limitations as a translatable model of Alzheimer's disease. *Neurobiology of Aging, 33*(5), 933–944.

Luo, F., Seifert, T. R., Edalji, R., Loebbert, R. W., Hradil, V. P., Harlan, J., et al. (2008). Non-invasive characterization of beta-amyloid(1–40) vasoactivity by functional magnetic resonance imaging in mice. *Neuroscience, 155*(1), 263–269.

Luo, J., Lee, S. H., VandeVrede, L., Qin, Z., Ben Aissa, M., Larson, J., et al. (2016). A multifunctional therapeutic approach to disease modification in multiple familial mouse models and a novel sporadic model of Alzheimer's disease. *Molecular Neurodegeneration, 11*, 35.

Luong, T. N., Carlisle, H. J., Southwell, A., & Patterson, P. H. (2011). Assessment of motor balance and coordination in mice using the balance beam. *Journal of Visualized Experiments, 49*, 2376. https://doi.org/10.3791/2376.

Lynch, J. L., Gallus, N. J., Ericson, M. E., & Beitz, A. J. (2008). Analysis of nociception, sex and peripheral nerve innervation in the TMEV animal model of multiple sclerosis. *Pain, 136*(3), 293–304.

Macdonald, I. R., DeBay, D. R., Reid, G. A., O'Leary, T. P., Jollymore, C. T., & Mawko, G. (2014). Early detection of cerebral glucose uptake changes in the 5XFAD mouse. *Current Alzheimer Research, 11*(5), 450–460.

Macmillan, C. J., Starkey, R. J., & Easton, A. S. (2011). Angiogenesis is regulated by angiopoietins during experimental autoimmune encephalomyelitis and is indirectly related to vascular permeability. *Journal of Neuropathology and Experimental Neurology, 70*(12), 1107–1123.

Mahler, J., Morales-Corraliza, J., Stolz, J., Skodras, A., Radde, R., Duma, C. C., et al. (2015). Endogenous murine Aβ increases amyloid deposition in APP23 but not in APPPS1 transgenic mice. *Neurobiology of Aging, 36*(7), 2241–2247.

Mancini, M., Greco, A., Tedeschi, E., Palma, G., Ragucci, M., Bruzzone, M. G., et al. (2015). Head and neck veins of the mouse. a magnetic resonance, micro computed tomography and high frequency color doppler ultrasound study. *PLoS One, 10*(6), e0129912.

Manook, A., Yousefi, B. H., Willuweit, A., Platzer, S., Reder, S., Voss, A., et al. (2012). Small-animal PET imaging of amyloid-beta plaques with [11C]PiB and its multi-modal validation in an APP/PS1 mouse model of Alzheimer's disease. *PLoS One*. https://doi.org/10.1371/journal.pone.0031310.

Mao, L., Nicolae, A., Oliveira, M. A., He, F., Hachi, S., & Fleming, R. M. (2015). A constraint-based modelling approach to metabolic dysfunction in Parkinson's disease. *Computational and Structural Biotechnology Journal, 13*, 484–491.

Martins, A. F., Morfin, J. F., Kubíčková, A., Kubíček, V., Buron, F., Suzenet, F., et al. (2013). PiB-conjugated, metal-based imaging probes: multimodal approaches for the visualization of β-amyloid plaques. *ACS Medicine Chemistry Letters, 4*(5), 436–440.

Mattner, F., Staykova, M., Berghofer, P., Wong, H. J., Fordham, S., Callaghan, P., et al. (2013). Central nervous system expression and PET imaging of the translocator protein in relapsing-remitting experimental autoimmune encephalomyelitis. *Journal of Nuclear Medicine, 54*(2), 291–298.

McCarthy, D. P., Richards, M. H., & Miller, S. D. (2012). Mouse models of multiple sclerosis: experimental autoimmune encephalomyelitis and Theiler's virus-induced demyelinating disease. *Methods in Molecual Biology, 900*, 381–401.

McLean, D., Cooke, M. J., Albay, R., Glabe, C., & Shoichet, M. S. (2013). Positron emission tomography imaging of fibrillar parenchymal and vascular amyloid-β in TgCRND8 mice. *ACS Chemical Neuroscience, 4*(4), 613–623.

Meadowcroft, M. D., Mutic, N. J., Bigler, D. C., Wang, J. L., Simmons, Z., Connor, J. R., et al. (2014). Histological–MRI correlation in the primary motor cortex of patients with amyotrophic lateral sclerosis. *Journal of Magnetic Resonance Imaging, 41*(3), 665–675.

Mellin, A. F., Cofer, G. P., Smith, B. R., Suddarth, S. A., Hedlund, L. W., & Johnson, G. A. (1994). Three dimensional magnetic resonance microangiography of rat neurovasculature. *Magnetic Resonance Medicine, 32*, 199–205.

Meredith, G. E., Totterdell, S., Potashkin, J. A., & Surmeier, D. J. (2008). Modeling PD pathogenesis in mice: advantages of a chronic MPTP protocol. *Parkinsonism Related Disorder, 14*(Suppl 2), S112-5.

Miller, S. D., Karpus, W. J., & Davidson, T. D. (2007). Experimental autoimmune encephalomyelitis in the mouse. *Current Protocols in Immunology*. Chapter 15, Unit–15.1. https://doi.org/10.1002/0471142735.im1501s77.

Milner, E., Zhou, M. L., Johnson, A. W., Vellimana, A. K., Greenberg, J. K., Holtzman, D. M., et al. (2014). Cerebral amyloid angiopathy increases susceptibility to infarction after focal cerebral ischemia in Tg2576 mice. *Stroke, 45*(10), 3064–3069.

Miyazaki, K., Ohta, Y., Nagai, M., Morimoto, N., Kurata, T., Takehisa, Y., et al. (2011). Disruption of neurovascular unit prior to motor

neuron degeneration in amyotrophic lateral sclerosis. *Journal of Neuroscience Research, 89*(5), 718–728.

Miyazaki, K., Masamoto, K., Morimoto, N., Kurata, T., Mimoto, T., Obata, T., et al. (2012). Early and progressive impairment of spinal blood flow-glucose metabolism coupling in motor neuron degeneration of ALS model mice. *Journal of Cerebral Blood Flow and Metabolism, 32*(3), 456–467.

Montgomery, K. S., Edwards, G. 3rd, Levites, Y., Kumar, A., Myers, C. E., Gluck, M. A., et al. (2016). Deficits in hippocampal-dependent transfer generalization learning accompany synaptic dysfunction in a mouse model of amyloidosis. *Hippocampus, 26*(4), 455–471.

Moser, J. M., Bigini, P., & Schmitt-John, T. (2013). The wobbler mouse, an ALS animal model. *Molecular Genetic and Genomics:MGG, 288*(5–6), 207–229.

Moussa, C. E., Rusnak, M., Hailu, A., Sidhu, A., & Fricke, S. T. (2008). Alterations of striatal glutamate transmission in rotenone-treated mice: MRI/MRS in vivo studies. *Experimental Neurology, 209*(1), 224–233.

Mucke, L., & Selkoe, D. J. (2012). Neurotoxicity of amyloid β-protein: synaptic and network dysfunction. *Cold Spring Harbor Perspectives in Medicine, 2*, a006338.

Muñoz-Manchado, A. B., Villadiego, J., Romo-Madero, S., Suárez-Luna, N., Bermejo-Navas, A., Rodríguez-Gómez, J. A., et al. (2016). Chronic and progressive Parkinson's disease MPTP model in adult and aged mice. *Journal of Neurochemistry, 136*(2), 373–387.

Muramatsu, R., Takahashi, C., Miyake, S., Fujimura, H., Mochizuki, H., & Yamashita, T. (2012). Angiogenesis induced by CNS inflammation promotes neuronal remodeling through vessel-derived prostacyclin. *Nature Medicine, 18*(11), 1658–1664.

Nathoo, N., Rogers, J. A., Yong, V. W., & Dunn, J. F. (2015). Detecting deoxyhemoglobin in spinal cord vasculature of the experimental autoimmune encephalomyelitis mouse model of multiple sclerosis using susceptibility MRI and hyperoxygenation. *PLoS One, 10*(5), e0127033.

Nathoo, N., Yong, V. W., & Dunn, J. F. (2014). Understanding disease processes in multiple sclerosis through magnetic resonance imaging studies in animal models. *Neuroimage: Clinical, 4*, 743–756.

Nessler, S., Boretius, S., Stadelmann, C., Bittner, A., Merkler, D., Hartung, H. P., et al. (2007). Early MRI changes in a mouse model of multiple sclerosis are predictive of severe inflammatory tissue damage. *Brain: a Journal of Neurology, 130*(Pt 8), 2186–2198.

Newbery, H. J., Gillingwater, T. H., Dharmasaroja, P., Peters, J., Wharton, S. B., Thomson, D., et al. (2005). Progressive loss of motor neuron function in wasted mice: effects of a spontaneous null mutation in the gene for the eEF1 A2 translation factor. *Journal of Neuropathology and Experimental Neurology, 64*(4), 295–303.

Nicholson, R. M., Kusne, Y., Nowak, L. A., LaFerla, F. M., Reiman, E. M., & Valla, J. (2010). Regional cerebral glucose uptake in the 3xTG model of Alzheimer's disease highlights common regional vulnerability across AD mouse models. *Brain Research, 1347*, 179–185.

Niessen, H. G., Angenstein, F., Sander, K., Kunz, W. S., Teuchert, M., Ludolph, A. C., et al. (2006). In vivo quantification of spinal and bulbar motor neuron degeneration in the G93A-SOD1 transgenic mouse model of ALS by T2 relaxation time and apparent diffusion coefficient. *Experimental Neurology, 201*(2), 293–300.

Oakley, H., Cole, S. L., Logan, S., Maus, E., Shao, P., Craft, J., et al. (2006). Intraneuronal β-amyloid aggregates, neurodegeneration, and neuron loss in transgenic mice with five familial Alzheimer's disease mutations: potential factors in amyloid plaque formation. *Journal of Neuroscience, 26*(40), 10129–10140.

Oddo, S., Caccamo, A., Kitazawa, M., Tseng, B. P., & LaFerla, F. M. (2003a). Amyloid deposition precedes tangle formation in a triple transgenic model of Alzheimer's disease. *Neurobiology of Aging, 24*(8), 1063–1070.

Oddo, S., Caccamo, A., Shepherd, J. D., Murphy, M. P., Golde, T. E., Kayed, R., et al. (2003b). Triple-transgenic model of Alzheimer's disease with plaques and tangles: intracellular Abeta and synaptic dysfunction. *Neuron, 39*(3), 409–421.

Oleszak, E. L., Chang, J. R., Friedman, H., Katsetos, C. D., & Platsoucas, C. D. (2004). Theiler's virus infection: a model for multiple sclerosis. *Clinical Microbiology Reviews, 17*(1), 174–207.

Oliván, S., Calvo, A. C., Rando, A., Muñoz, M. J., Zaragoza, P., & Osta, R. (2015). Comparative study of behavioural tests in the SOD1G93A mouse model of amyotrophic lateral sclerosis. *Experimental Animals, 64*(2), 147–153.

Onida, S., & Davies, A. H. (2014). The chronic cerebrospinal venous insufficiency debate. *European Journal of Vascular and Endovascular Surgery, 48*(1), 1–3.

Oosthuyse, B., Moons, L., Storkebaum, E., Beck, H., Nuyens, D., & Brusselmans, K. (2001). Deletion of the hypoxia-response element in the vascular endothelial growth factor promoter causes motor neuron degeneration. *Nature Genetetics, 28*(2), 131–138.

Ott, B., Dahlke, C., Meller, K., Napirei, M., Schmitt-John, T., Brand-Saberi, B., et al. (2015). Implementation of a manual for working with wobbler mice and criteria for discontinuation of the experiment. *Annals of Anatomy - Anatomischer Anzeiger, 200*, 118–124.

Parievsky, A., Cepeda, C., & Levine, M. S. (2012). Evidence from the R6/2 mouse model of Huntington's disease for using abnormal brain metabolism as a biomarker for evaluating therapeutic approaches for treatment. *Future Neurology, 7*(5), 527–530.

Passos, G. F., Medeiros, R., Cheng, D., Vasilevko, V., Laferla, F. M., & Cribbs, D. H. (2013). The bradykinin B1 receptor regulates Aβ deposition and neuroinflammation in Tg-SwDI mice. *The American Journal of Pathology, 182*(5), 1740–1749.

Patterson, A. P., Booth, S. A., & Saba, R. (2014). The emerging use of in vivo optical imaging in the study of neurodegenerative diseases. *Biomed Research Interntational*. https://doi.org/10.1155/2014/401306.

Paz Soldán, M. M., Raman, M. R., Gamez, J. D., Lohrey, A. K., Chen, Y., Pirko, I., et al. (2015). Correlation of brain atrophy, disability, and spinal cord atrophy in a murine model of multiple sclerosis. *Journal of Neuroimaging, 25*(4), 595–599.

Pépin, J., Francelle, L., Carrillo-de Sauvage, M. A., de Longprez, L., Gipchtein, P., Cambon, K., et al. (2016). In vivo imaging of brain glutamate defects in a knock-in mouse model of Huntington's disease. *NeuroImage, 139*, 53–64.

Peruga, I., Hartwig, S., Thöne, J., Hovemann, B., Gold, R., Juckel, G., et al. (2011). Inflammation modulates anxiety in an animal model of multiple sclerosis. *Behavioural Brain Research, 220*(1), 20–29.

Philipson, O., Lord, A., Gumucio, A., O'Callaghan, P., Lannfelt, L., & Nilsson, L. N. (2010). Animal models of amyloid-beta-related pathologies in Alzheimer's disease. *The FEBS Journal, 277*(6), 1389–1409.

Platt, B., Welch, A., & Riedel, G. (2011). FDG-PET imaging, EEG and sleep phenotypes as translational biomarkers for research in Alzheimer's disease. *Biochemical Society Transaction, 39*(4), 874–880.

Poduslo, J. F., Wengenack, T. M., Curran, G. L., Wisniewski, T., Sigurdsson, E. M., Macura, S. I., et al. (2002). Molecular targeting of Alzheimer's amyloid plaques for contrast-enhanced magnetic resonance imaging. *Neurobiology of Disease, 11*(2), 315–329.

Poesen, K., Lambrechts, D., Van Damme, P., Dhondt, J., Bender, F., Frank, N., et al. (2008). Novel role for vascular endothelial growth factor (VEGF) receptor-1 and its ligand VEGF-B in motor neuron degeneration. *Journal Neuroscience, 28*, 10451–10459.

Poisnel, G., Hérard, A. S., El Tannir El Tayara, N., Bourrin, E., Volk, A., Kober, F., et al. (2012). Increased regional cerebral glucose uptake in an APP/PS1 model of Alzheimer's disease. *Neurobiology of Aging, 33*(9), 1995–2005.

Poutiainen, P., Jaronen, M., Quintana, F. J., & Brownell, A. L. Precision medicine in multiple sclerosis: future of PET imaging of inflammation and reactive astrocytes. *Frontiers in Molecular Neurosciences, 9*(1), 85. https://doi.org/10.3389/fnmol.2016.00085.

Procaccini, C., De Rosa, V., Pucino, V., Formisano, L., & Matarese, G. (2015). Animal models of multiple sclerosis. *European Journal of Pharmacology, 759*, 182–191.

Radu, C. G., Shu, C. J., Shelly, S. M., Phelps, M. E., & Witte, O. N. (2007). Positron emission tomography with computed tomography imaging of neuroinflammation in experimental autoimmune encephalomyelitis. *Proceedings of the National Academy of Sciences of the United States of America, 104*(6),1937–1942.

Rahman, A., Ekman, M., Shakirova, Y., Andersson, K. E., Mörgelin, M., Erjefält, J. S., et al. (2013). Late onset vascular dysfunction in the R6/1 model of Huntington's disease. *European Journal of Pharmacology, 698*(1–3), 345–353.

Ramaswamy, S., McBride, J. L., & Kordower, J. H. (2007). Animal models of Huntington's disease. *ILAR Journal, 48*(4), 356–373.

Rattray, I., Smith, E., Gale, R., Matsumoto, K., Bates, G. P., & Modo, M. (2012). Correlations of behavioral deficits with brain pathology assessed through longitudinal MRI and histopathology in the R6/2 mouse model of HD. *PLoS One*. https://doi.org/10.1371/journal.pone.0060012.

Redwine, J. M., Kosofsky, B., Jacobs, R. E., Games, D., Reilly, J. F., Morrison, J. H., et al. (2003). Dentate gyrus volume is reduced before onset of plaque formation in PDAPP mice: a magnetic resonance microscopy and stereologic analysis. *Proceedings of National Academy of Science of the United States of America, 100*(3), 1381–1386.

Reilly, J. F., Games, D., Rydel, R. E., Freedman, S., Schenk, D., Young, W. G., et al. (2003). Amyloid deposition in the hippocampus and entorhinal cortex: quantitative analysis of a transgenic mouse model. *Proceedings of National Academy of Science of the United States of America, 100*(8), 4837–4842.

Rekha, K. R., & Selvakumar, G. P. (2014). Gene expression regulation of Bcl2, Bax and cytochrome-C by geraniol on chronic MPTP/probenecid induced C57BL/6 mice model of Parkinson's disease. *Chemico- Biological Interaction, 217*, 57–66.

Rial, D., Castro, A. A., Machado, N., Garção, P., Gonçalves, F. Q., Silva, H. B., et al. (2014). Behavioral phenotyping of Parkin-deficient mice: looking for early preclinical features of Parkinson's disease. *PLoS One*. https://doi.org/10.1371/journal.pone.0114216.

Robbins, E. M., Betensky, R. A., Domnitz, S. B., Purcell, S. M., Garcia-Alloza, M., Greenberg, C., et al. (2006). Kinetics of cerebral amyloid angiopathy progression in a transgenic mouse model of Alzheimer disease. *Journal of Neuroscience, 26*(2), 365–371.

Rockenstein, E., Mallory, M., Mante, M., Sisk, A., & Masliaha, E. (2001). Early formation of mature amyloid-beta protein deposits in a mutant APP transgenic model depends on levels of Abeta(1–42). *Journal of Neuroscience Research, 66*(4), 573–582.

Rojas, S., Herance, J. R., Gispert, J. D., Abad, S., Torrent, E., Jimenez, X., et al. (2013). In vivo evaluation of amyloid deposition and brain glucose me- tabolism of 5XFAD mice using positron emission tomography. *Neurobiology of Aging, 34*(7), 1790–1798.

Roman, F. S., Marchetti, E., Bouquerel, A., & Soumireu-Mourat, B. (2002). The olfactory tubing maze: a new apparatus for studying learning and memory processes in mice. *Journal of Neuroscience Method, 117*(2), 173–181.

Romberg, C., Horner, A. E., Bussey, T. J., & Saksida, L. M. (2013). A touch screen-automated cognitive test battery reveals impaired attention, memory abnormalities, and increased response inhibition in the TgCRND8 mouse model of Alzheimer's disease. *Neurobiology of Aging, 34*(3), 731–744.

Rönnbäck, A., Zhu, S., Dillner, K., Aoki, M., Lilius, L., Näslund, J., et al. (2011). Progressive neuropathology and cognitive decline in a single Arctic APP transgenic mouse model. *Neurobiology of Aging, 32*(2), 280–292.

Roscoe, W. A., Welsh, M. E., Carter, D. E., & Karlik, S. J. (2009). VEGF and angiogenesis in acute and chronic MOG((35–55)) peptide induced EAE. *Journal of Neuroimmunology, 209*(1–2), 6–15.

Rougon, G., Brasselet, S., & Debarbieux, F. (2016). Advances in intravital non-linear optical imaging of the central nervous system in rodents. *Brain Plasticity, 2*(1), 31–48.

Ryu, J. K., Petersen, M. A., Murray, S. G., Baeten, K. M., Meyer-Franke, A., Chan, J. P., et al. (2015). Blood coagulation protein fibrinogen promotes autoimmunity and demyelination via chemokine release and antigen presentation. *Nature Communications, 6*, 8164.

Santin, M. D., Vandenberghe, M. E., Herard, A.-S., Pradier, L., Cohen, C., Debeir, T., et al. (2016). In vivo detection of amyloid plaques by gadolinium-stained MRI can be used to demonstrate the efficacy of an anti-amyloid immunotherapy. *Frontiers in Aging Neuroscience, 8*, 55.

Sarkar, S., Raymick, J., Mann, D., Bowyer, J. F., Hanig, J. P., Schmued, L. C., et al. (2014). Neurovascular changes in acute, sub-acute and chronic mouse models of Parkinson's disease. *Current Neurovascolar Research, 11*(1), 48–61.

Sawiak, S. J., Wood, N. I., Williams, G. B., Morton, A. J., & Carpenter, T. A. (2009). Use of magnetic resonance imaging for anatomical phenotyping of the R6/2 mouse model of Huntington's disease. *Neurobiology of Disease, 33*(1), 12–19.

Schmalbruch, H., Jensen, H. J., Bjaerg, M., Kamieniecka, Z., & Kurland, L. (1991). A new mouse mutant with progressive motor neuronopathy. *Journal of Neuropathology and Experimental Neurology, 50*(3), 192–204.

Schwendele, B., Brawek, B., Hermes, M., & Garaschuk, O. (2012). High- resolution in vivo imaging of microglia using a versatile nongenetically encoded marker. *European Journal of Immunology, 42*, 2187–2196. https://doi.org/10.1002/eji.201242436.

Serres, S., Mardiguian, S., Campbell, S. J., McAteer, M. A., Akhtar, A., Krapitchev, A., et al. (2011). VCAM-1-targeted magnetic resonance imaging reveals subclinical disease in a mouse model of multiple sclerosis. *FASEB Journal, 25*(12), 4415–4422.

Sharma, S. K., Refaey, El, Ebadi, H., M (2006). Complex-1 activity and 18F-DOPA uptake in genetically engineered mouse model of Parkinson's disease and the neuroprotective role of coenzyme Q10. *Brain Research Bulletin, 70*(1), 22–32.

Shear, D. A., Dong, J., Haik-Creguer, K. L., Bazzett, T. J., Albin, R. L., & Dunbar, G. L. (1998). Chronic administration of quinolinic acid in the rat striatum causes spatial learning deficits in a radial arm water maze task. *Expental Neurology, 150*, 305–311.

Snellman, A., Rokka, J., López-Picón, F. R., Eskola, O., Salmona, M., Forloni, G., et al. (2013). In vivo PET imaging of beta-amyloid deposition in mouse models of Alzheimer's disease with a high specific activity PET imaging agent [(18)F]flutemetamol. *EJNMMI Research*. https://doi.org/10.1186/s13550-014-0037-3.

Southwell, A. L., Skotte, N. H., Villanueva, E. B., Østergaard, M. E., Gu, X., Kordasiewicz, H. B., et al. (2017). A novel humanized mouse model of Huntington disease for preclinical development of therapeutics targeting mutant huntingtin alleles. *Human Molecular Genetetic, 26*(6), 1115–1132.

Spencer, N. G., Bridges, L. R., Elderfield, K., Amir, K., Austen, B., & Howe, F. A. (2013). Quantitative evaluation of MRI and histological characteristics of the 5xFAD Alzheimer mouse brain. *NeuroImage, 76*, 108–115.

Spires-Jones, T., & Knafo, S. (2012). Spines, plasticity, and cognition in Alzheimer's model mice. *Neural Plasticity, 2012*, 319836.

Srivastava, A. K., Gross, S. K., Almad, A. A., Bulte, C. A., Maragakis, N. J., & Bulte, J. W. (2017). Serial in vivo imaging of transplanted allogeneic neural stem cell survival in a mouse model of amyotrophic lateral sclerosis. *Experimental Neurology, 289*, 96–102.

Stankoff, B., Freeman, L., Aigrot, M. S., Chardain, A., Dollé, F., Williams, A., et al. (2011). Imaging central nervous system myelin by positron emission tomography in multiple sclerosis using [methyl-^{11}C]-2-(4′-methylaminophenyl)- 6-hydroxybenzothiazole. *Annals of Neurology, 69*(4), 673–680.

Starkey, M. L., Barritt, A. W., Yip, P. K., Davies, M., Hamers, F. P., McMahon, S. B., et al. (2005). Assessing behavioural function following a pyramidotomy lesion of the corticospinal tract in adult mice. *Experimental Neurology, 195*(2), 524–539.

Steventon, J. J., Trueman, R. C., Ma, D., Yhnell, E., Bayram-Weston, Z., Modat, M., et al. (2016). Longitudinal in vivo MRI in a Huntington's disease mouse model: global atrophy in the absence of white matter microstructural damage. *Scientific Reports, 6*, 32423.

Storkebaum, E., Lambrechts, D., & Carmeliet, P. (2004). VEGF: once regarded as a specific angiogenic factor, now implicated in neuroprotection. *BioEssays, 26*(9), 934–954.

Stover, K. R., Campbell, M. A., Van Winssen, C. M., & Brown, R. E. (2015). Analysis of motor function in 6-month-old male and female 3xTg-AD mice. *Behavioural Brain Research, 281*, 16–23.

Suwijn, S. R., de Bruin, K., de Bie, R. M., & Booij, J. (2014). The role of SPECT imaging of the dopaminergic system in translational research on Parkinson's disease. *Parkinsonism and Related Disorders, 20*(Suppl 1), S184-6.

Switonski, P. M., Szlachcic, W. J., Gabka, A., Krzyzosiak, W. J., & Figiel, M. (2012). Mouse models of polyglutamine diseases in therapeutic approaches: review and data table. Part II. *Molecular Neurobiology, 46*(2), 430–466.

Takemiya, T., & Takeuchi, C. (2013). Traveled distance is a sensitive and accurate marker of motor dysfunction in a mouse model of multiple sclerosis. *ISRN Neuroscience, 170316*. https://doi.org/10.1155/2013/170316.

Taylor, T. N., Caudle, W. M., Shepherd, K. R., Noorian, A., Jackson, C. R., Iuvone, P. M., et al. (2009). Nonmotor symptoms of Parkinson's disease revealed in an animal model with reduced monoamine storage capacity. *The Journal of Neuroscience, 29*(25), 8103–8113.

Taylor, T. N., Greene, J. G., & Miller, G. W. (2010). Behavioral phenotyping of mouse models of Parkinson's disease. *Behavioural Brain Research, 211*(1), 1–10.

Teipel, S. J., Buchert, R., Thome, J., Hampel, H., & Pahnke, J. (2011). Development of Alzheimer-disease neuroimaging-biomarkers using mouse models with amyloid-precursor protein-transgene expression. *Progress in Neurobiology, 95*(4), 547–556.

Terzioglu, M., & Galter, D. (2008). Parkinson's disease: genetic versus toxin-induced rodent models. *The FEBS Journal, 275*(7), 1384–1391.

Thielsen, K. D., Moser, J. M., Schmitt-John, T., Jensen, M. S., Jensen, K., & Holm, M. M. (2013). The Wobbler mouse model of amyotrophic lateral sclerosis (ALS) displays hippocampal hyperexcitability, and reduced number of interneurons, but no presynaptic vesicle release impairments. *PLoS One, 8*(12), e82767.

Thomason, L. A., Stefanovic, B., & McLaurin, J. (2013). Cerebrovascular contributions to Alzheimer's disease pathophysiology and potential therapeutic interventions in mouse models. *The European Journal of Neuroscience, 37*(12), 1994–2004.

Toomey, J. S., Bhatia, S., Moon, L. T., Orchard, E. A., Tainter, K. H., Lokitz, S. J., et al. (2012). PET imaging a MPTP-induced mouse model of Parkinson's disease using the fluoropropyl-dihydrotetrabenazine analog [18F]-DTBZ (AV-133). *PLoS One*. https://doi.org/10.1371/journal.pone.0039041.

Tóth, M., Häggkvist, J., Stepanov, V., Takano, A., Nakao, R., Amini, N., et al. (2015). Molecular Imaging of PDE10A Knockout Mice with a novel PET Radiotracer: [(11)C]T-773. *Molecular Imaging and Biology, 17*(4), 445–449.

Tovar-y-Romo, L. B., Santa-Cruz, L. D., & Tapia, R. (2009). Experimental models for the study of neurodegeneration in amyotrophic lateral sclerosis. *Molecular Neurodegeneration*. https://doi.org/10.1186/1750-1326-4-31.

Turner, B. J., Cheah, I. K., Macfarlane, K. J., Lopes, E. C., Petratos, S., Langford, S. J., et al. (2003). Antisense peptide nucleic acid-mediated knockdown of the p75 neurotrophin receptor delays motor neuron disease in mutant SOD1 transgenic mice. *Journal of Neurochemistry, 87*(3), 752–763.

Van Cauwenberghe, C., Van Broeckhoven, C., & Sleegers, K. (2015). The genetic landscape of Alzheimer disease: clinical implications and perspectives. *Genetics in Medicine*. https://doi.org/10.1038/gim.2015.117.

Van Dam, D., D'Hooge, R., Staufenbiel, M., Van Ginneken, C., Van Meir, F., & De Deyn, P. P. (2003). Age-dependent cognitive decline in the APP23 model precedes amyloid deposition. *European Journal of Neuroscience, 17*, 388–396.

Van den Berg, R., Laman, J. D., van Meurs, M., Hintzen, R. Q., & Hoogenraad, C. C. (2016). Rotarod motor performance and advanced spinal cord lesion image analysis refine assessment of neurodegeneration in experimental autoimmune encephalomyelitis. *Journal of Neuroscience Methods, 262*, 66–76.

Van Dorpe, J., Smeijers, L., Dewachter, I., Nuyens, D., Spittaels, K., Van Den Haute, C., et al. (2000). Prominent cerebral amyloid angiopathy in transgenic mice overexpressing the london mutant of human APP in neurons. *The American Journal Pathology, 157*(4), 1283–1298.

Van Raamsdonk, J. M., Pearson, J., Slow, E. J., Hossain, S. M., Leavitt, B. R., & Hayden, M. R. (2005). Cognitive dysfunction precedes neuropathology and motor abnormalities in the YAC128 mouse model of Huntington's disease. *Journal of Neuroscience, 25*(16), 4169–4180.

Van Vickle, G. D., Esh, C. L., Daugs, I. D., Kokjohn, T. A., Kalback, W. M., Patton, R. L., et al. (2008). Tg-SwDI transgenic mice exhibit novel alterations in AbetaPP processing, Abeta degradation, and resilient amyloid angiopathy. *The American Journal of Pathology, 173*(2), 483–493.

Varma, A. R., Talbot, P. R., Snowden, J. S., Lloyd, J. J., Testa, H. J., & Neary, D. (1997). A 99mTc-HMPAO single-photon emission computed tomography study of Lewy body disease. *Journal of Neurology, 244*(6), 349–359.

Vastenhouw, B., van der Have, F., van der Linden, A., von Oerthel, L., Booij, J., Burbach, J. P., et al. (2007). Movies of dopamine transporter occupancy with ultra-high resolution focusing pinhole SPECT. *Molecular Psychiatry, 12*(11), 984–987.

Venneti, S., Lopresti, B. J., Wang, G., Hamilton, R. L., Mathis, C. A., Klunk, W. E., et al. (2009). PK11195 labels activated microglia in Alzheimer's disease and in vivo in a mouse model using PET. *Neurobiology of Aging, 30*(8), 1217–1226.

Vercelli, A., Mereuta, O. M., Garbossa, D., Muraca, G., Mareschi, K., Rustichelli, D., et al. (2008). Human mesenchymal stem cell transplantation extends survival, improves motor performance and decreases neuroinflammation in mouse model of amyotrophic lateral sclerosis. *Neurobiology of Disease, 31*, 395–405.

Vinters, H. V. (1987). Cerebral amyloid angiopathy. A critical review. *Stroke, 18*(2), 311–324.

Wadghiri, Y. Z., Hoang, D. M., Wisniewski, T., & Sigurdsson, E. M. (2012). In vivo magnetic resonance imaging of amyloid-β plaques in mice. *Methods in Molecular Biology, 849*, 435–451.

Wadghiri, Y. Z., Li, J., Wang, J., Hoang, D. M., Sun, Y., Xu, H., et al. (2013).). Detection of amyloid plaques targeted by bifunctional USPIO in Alzheimer's disease transgenic mice using magnetic resonance microimaging. *PLoS One*. https://doi.org/10.1371/journal.pone.0057097.

Waerzeggers, Y., Monfared, P., Viel, T., Winkeler, A., & Jacobs, A. H. (2010). Mouse models in neurological disorders: applications of non-invasive imaging. *Biochimica et Biophysica Acta, 1802*(10), 819–839.

Waldvogel, H. J., Dragunow, M., & Faull, R. L. (2015). Disrupted vasculature and blood-brain barrier in Huntington disease. *Annals of Neurology, 78*(2), 158–159.

Wang, L. H., & Qin, Z. H. (2006). Animal models of Huntington's disease: implications in uncovering pathogenic mechanisms and developing therapies. *Acta Pharmacologica Sinica, 27*(10), 1287–1302.

Wang, X., Sarkar, A., Cicchetti, F., Yu, M., Zhu, A., Jokivarsi, K., et al. (2005). Cerebral PET imaging and histological evidence of transglutaminase inhibitor cystamine induced neuroprotection in transgenic R6/2 mouse model of Huntington's disease. *Journal of Neurological Science, 231*(1–2), 57–66.

Webster, S. J., Bachstetter, A. D., & Van Eldik, L. J. (2013). Comprehensive behavioral characterization of an APP/PS-1 double knock-in mouse model of Alzheimer's disease. *Alzheimers Research and Therapy, 5*(3), 28.

Wei, Y. (2014). Autophagic induction of amyotrophic lateral sclerosis-linked Cu/Zn superoxide dismutase 1 G93A mutant in NSC34 cells. *Neural Regeneration Research, 9*(1), 16–24.

Woloschak, G. E., Rodriguez, M., & Krco, C. J. (1987). Characterization of immunologic and neuropathologic abnormalities in wasted mice. *Journal of Immunology, 138*(8), 2493–2499.

Xiong, H., Callaghan, D., Jones, A., Bai, J., Rasquinha, I., Smith, C., et al. (2009). ABCG2 is up-regulated in Alzheimer's brain with cerebral amyloid angiopathy and may act as a gatekeeper at the blood-brain barrier for Aβ1-40 peptides. *Journal of Neuroscience, 29*(17), 5463–5475.

Xu, W., Xu, F., Anderson, M. E., Kotarba, A. E., Davis, J., Robinson, J. K., et al. (2014). Cerebral microvascular rather than parenchymal amyloid-β protein pathology promotes early cognitive impairment in transgenic mice. *Journal of Alzheimers Disease, 38*(3), 621–632.

Yamasaki, T., Fujinaga, M., Yui, J., Ikoma, Y., Hatori, A., Xie, L., et al. (2014). Noninvasive quantification of metabotropic glutamate receptor type 1 with [^{11}C]ITDM: a small-animal PET study. *Journal of Cerebral Blood Flow & Metabolism, 34*(4), 606–612.

Yasuhara, T., Shingo, T., Kobayashi, K., Takeuchi, A., Yano, A., & Muraoka, K. (2004). Neuroprotective effects of vascular endothelial growth factor (VEGF) upon dopaminergic neurons in a rat model of Parkinson's disease. *The European Journal of Neuroscience, 19*(6), 1494–1504.

Zamboni, P. (2006). The big idea: iron-dependent inflammation in venous disease and proposed parallels in multiple sclerosis. *Journal of the Royal Society of Medicine, 99*, 589–593.

Zang, D. W., & Cheema, S. S. (2002). Degeneration of corticospinal and bulbospinal systems in the superoxide dismutase 1(G93A G1H) transgenic mouse model of familial amyotrophic lateral sclerosis. *Neuroscience Letters, 332*(2), 99–102.

Zang, D. W., Yang, Q., Wang, H. X., Egan, G., Lopes, E. C., & Cheema, S. S. (2004). Magnetic resonance imaging reveals neuronal degeneration in the brainstem of the superoxide dismutase 1 transgenic mouse model of amyotrophic lateral sclerosis. *The European Journal of Neuroscience, 20*(7), 1745–1751.

Zhang, J., Peng, Q., Li, Q., Jahanshad, N., Hou, Z., Jiang, M., et al. (2010). Longitudinal characterization of brain atrophy of a Huntington's disease mouse model by automated morphological analyses of magnetic resonance images. *NeuroImage, 49*(3), 2340–2351.

Zhang, R., Xue, G., Wang, S., Zhang, L., Shi, C., & Xie, X. (2012). Novel object recognition as a facile behavior test for evaluating drug effects in AβPP/PS1 Alzheimer's disease mouse model. *Journal of Alzheimer Disease, 31*(4), 801–812.

Zhao, Y., & Adjei, A. A. (2015). Targeting angiogenesis in cancer therapy: moving beyond vascular endothelial growth factor. *The Oncologist, 20*(6), 660–673.

Zhong, Z., Deane, R., Ali, Z., Parisi, M., Shapovalov, Y., O'Banion, M. K., et al. (2008). ALS-causing SOD1 mutants generate vascular changes prior to motor neuron degeneration. *Nature Neuroscience, 11*(4), 420–422.

Zhou, Y., Wang, Y., Kovacs, M., Jin, J. H., & Zhang, J. (2005). Microglial activation induced by neurodegeneration—a proteomic analysis. *Molecular Cell Proteomics, 4*, 1471–1479.

Ziebell, M., Andersen, B. B., Thomsen, G., Pinborg, L. H., Karlsborg, M., Hasselbalch, S. G., et al. (2012). Predictive value of dopamine transporter SPECT imaging with [123I]PE2I in patients with subtle parkinsonian symptoms. *European Journal of Nuclear Medicine Molecular Imaging, 39*, 242–250.